REPORT DOCUMENTATION PAGE

The public reporting burden for this collection of information is estimated to average 1 hour per response, including the time for reviewing instructions, searching existing data sources, gathering and maintaining the data needed, and completing and reviewing the collection of information. Send comments regarding this burden estimate or any other aspect of this collection of information, including suggesstions for reducing this burden, to Washington Headquarters Services, Directorate for Information Operations and Reports, 1215 Jefferson Davis Highway, Suite 1204, Arlington VA, 22202-4302. Respondents should be aware that notwithstanding any other provision of law, no person shall be subject to any oenalty for failing to comply with a collection of information if it does not display a currently valid OMB control number.
PLEASE DO NOT RETURN YOUR FORM TO THE ABOVE ADDRESS.

1. REPORT DATE (DD-MM-YYYY)	2. REPORT TYPE	3. DATES COVERED (From - To)
02-11-2012	Final Report	15-Aug-2006 - 14-Aug-2012

4. TITLE AND SUBTITLE	5a. CONTRACT NUMBER
Engineered Multifunctional Nanophotonic Materials for Ultrafast Optical Switching	W911NF-06-1-0283
	5b. GRANT NUMBER
	5c. PROGRAM ELEMENT NUMBER
	611103

6. AUTHORS	5d. PROJECT NUMBER
Eric Van Stryland, Seth Marder, Vladimir Drachev, Bernard Kippelen, Joe Perry, Pieter Kik, Robert Norwood, Vladimir Shalaev, David Hagan	
	5e. TASK NUMBER
	5f. WORK UNIT NUMBER

7. PERFORMING ORGANIZATION NAMES AND ADDRESSES	8. PERFORMING ORGANIZATION REPORT NUMBER
University of Central Florida Office of Research University of Central Florida Orlando, FL 32826 -0150	

9. SPONSORING/MONITORING AGENCY NAME(S) AND ADDRESS(ES)	10. SPONSOR/MONITOR'S ACRONYM(S)
U.S. Army Research Office P.O. Box 12211 Research Triangle Park, NC 27709-2211	ARO
	11. SPONSOR/MONITOR'S REPORT NUMBER(S)
	50372-CH-MUR.124

12. DISTRIBUTION AVAILIBILITY STATEMENT

Approved for Public Release; Distribution Unlimited

13. SUPPLEMENTARY NOTES

The views, opinions and/or findings contained in this report are those of the author(s) and should not contrued as an official Department of the Army position, policy or decision, unless so designated by other documentation.

14. ABSTRACT

This research was a comprehensive science and engineering program to develop a new generation of nanophotonic materials, structures, and devices exhibiting large, high-speed nonlinear optical (NLO) changes, as needed to enable new capabilities in all-optical switching for imaging applications. In particular, the problem of passive optical limiting and switching without using focusing optics is an extremely challenging task. The goal of this research was to tackle lensless optical limiting by determining the ultimate possibilities and limits on materials,

15. SUBJECT TERMS

nonlinear optics, nano-plasmonics, optical limiting, metal nonlinearities, semiconductor quantum dots, multiphoton absorption

16. SECURITY CLASSIFICATION OF:			17. LIMITATION OF ABSTRACT	15. NUMBER OF PAGES	19a. NAME OF RESPONSIBLE PERSON
a. REPORT	b. ABSTRACT	c. THIS PAGE			Eric Van Stryland
UU	UU	UU	UU		19b. TELEPHONE NUMBER
					407-823-6835

Report Title

Engineered Multifunctional Nanophotonic Materials for Ultrafast Optical Switching

ABSTRACT

This research was a comprehensive science and engineering program to develop a new generation of nanophotonic materials, structures, and devices exhibiting large, high-speed nonlinear optical (NLO) changes, as needed to enable new capabilities in all-optical switching for imaging applications. In particular, the problem of passive optical limiting and switching without using focusing optics is an extremely challenging task. The goal of this research was to tackle lensless optical limiting by determining the ultimate possibilities and limits on materials, materials structures, and device configurations. The approach we adopted combined three methodologies to achieve this goal: (1) to enhance the NLO response of the molecules through a variety of molecular engineering approaches, (2) to use surface plasmon field enhancements in nano-engineered clusters and arrays of metal and/or dielectric nanoparticles coupled to the organic NLO materials; and (3) to integrate the first two methodologies in systems having weakly resonant structures, including 3-D and/or 1-D photonic crystal structures (i.e. nonlinear Bragg mirrors). We made significant progress in all three areas and have observed orders of magnitude enhancement of NLO absorption; however, we have not been able to fully harness this enhancement for devices due to the transient nature of the effects.

Enter List of papers submitted or published that acknowledge ARO support from the start of the project to the date of this printing. List the papers, including journal references, in the following categories:

(a) Papers published in peer-reviewed journals (N/A for none)

Received	Paper	

08/20/2009   44.00   ChuanXiang Sheng, Robert A. Norwood, Jiafu Wang, Jayan Thomas, Yinglan Wu, Zhiping Zheng, N. Tabirian, Diane M. Steeves, Brian R. Kimball, N. Peyghambarian. Time-resolved studies of photoinduced birefringence in azobenzene dye-doped polymer films,
Applied Optics, (2008): . doi:

08/20/2009   57.00   Canek Fuentes-Hernandez, Lazaro A. Padilha, Daniel Owens, Shuo-Yen Tseng, Scott Webster, Jian-Yang Cho, David J. Hagan, Eric W. Van Stryland, Seth R. Marder, Bernard Kippelen. Linear and nonlinear optical properties of highly transmissive one dimensional metal-organic photonic bandgap structures,
Proceedings of SPIE, (2008): . doi:

08/20/2009   48.00   Amitabh Ghoshala, Pieter G. Kik. Excitation of propagating surface plasmons by a periodic nanoparticle array: Trade-off between particle-induced near-field excitation and damping,
Applied Physics Letters, (2009): . doi:

08/20/2009   47.00   Dana C. Kohlgraf-Owens, Pieter G. Kik. Linear and Nonlinear Effective Medium Properties of Metallodielectric Composites of Interacting Spheres and Isolated Spheroids,
Conference Proceeding: OSA, (2008): . doi:

08/20/2009   46.00   ChuanXiang Sheng, Robert A. Norwood, Jiafu Wang, Jayan Thomas, Diane Steeves, Brian Kimball, N. Peyghambarian. Nonlinear optical transmission of lead phthalocyanine-doped nematic liquid crystal composites for multiscale nonlinear switching from nanosecond to continuous wave,
Applied Optics, (2009): . doi:

08/20/2009   45.00   Dan T. Nguyen, Chuanxiang Sheng, Jayan Thomas, Robert Norwood, Brian Kimball, Diane M. Steeves, Nasser Peyghambarian. Observation of nonlinear transmission enhancement in cavities filled with nonlinear organic materials,
Applied Optics, (2008): . doi:

08/20/2009   37.00   Gero Nootz, Lazaro A. Padilha, Scott Webster, David J. Hagan, Eric W. Van Stryland, Larissa Levina, Vlad Sukhovatkin, Edward H. Sargent. Evidence of Symmetry Breaking in Lead Salt Quantum Dots,
Conference Proceeding: OSA, (2009): . doi:

08/20/2009   38.00   Honghua Hu, Lazaro A. Padilha, Scott Webster, Trenton R. Ensley, Davorin Peceli, Olga V. Przhonska, David J. Hagan, Eric W. Van Stryland, Mikhail V. Bondar, Yuriy L. Slominsky, Alexei D. Kachkovski, Andriy O. Gerasov, Mykola P. Shandura, Yuriy P. Kovtun. Comparison of Linear and Nonlinear Absorption in Three Series of Similar Cyanine Dyes: D-pi-D, A-pi-A and D-pi-A,
Conference Proceeding: OSA, (2009): . doi:

08/20/2009   43.00   Michaz Malicki, Zelei Guan, Sieu D. Ha, Georg Heimel, Stephen Barlow, Mariacristina Rumi, Antoine Kahn, Seth R. Marder. Preparation and Characterization of 40-Donor Substituted Stilbene-4-thiolate Monolayers and Their Influence on the Work Function of Gold,
Langmuir, (2009): . doi:

08/20/2009   36.00   Scott Webster, Susan A. Odom, Lazaro A. Padilha, Olga V. Przhonska, Davorin Peceli, Honghua Hu, Gero Nootz, Alexei D. Kachkovski, Jonathan Matichak. Nonlinear Absorption Spectroscopy of a Bis(Porphyrin)-Substituted Squaraine,
Conference Proceeding: OSA, (2009): . doi:

10/04/2012   2.00   S. Marder, M. Balu, E. Van Stryland, others, see report. Broadband Z-Scan Characterization Using a High Spectral Irradiance, High Quality, Supercontinuum,
J. Opt. Soc. Am. B, (02 2008): 159. doi:

10/05/2012   31.00   Scott Webster, Jie Fu, Lazaro A. Padilha, Olga V. Przhonska, David J. Hagan, Eric W. Van Stryland, Mikhail V. Bondar, Yuriy L. Slominsky, Alexei D. Kachkovski. Comparison of nonlinear absorption in three similar dyes: Polymethine, squaraine and tetraone,
Chemical Physics, (06 2008): 143. doi:

10/05/2012 20.00 Shino Ohira, Trenton Ensley, Chun Huang, Lazaro A. Padilha, Scott Webster, Veaceslav Coropceanu, Stephen Barlow, David J. Hagan, Eric W. Van Stryland, Jean-Luc Brédas, Harry L. Anderson, Michael R. Wasielewski, Seth R. Marder, Susan A. Odom, Richard F. Kelley. Synthesis and Photophysical Properties of an Alkyne-Bridged Bis(Zinc Porphyrin)–Perylene Diimide Derivative,
Journal of Physical Chemistry A, (09 2009): 10826. doi:

10/05/2012 39.00 Nasser Peyghambarian, Dan T. Nguyen, Robert A. Norwood. Multiple Spectral Window Mirrors Based on Fibonacci Chains of Dielectric Layers,
Optics Letters, (11 2009): 4199. doi:

10/08/2012 5.00 C. Sheng, N. Peyghambarian, others see report. Time Resolved Studies of Photoinduced Birefringence in Azobenzene Dye Doped Polymer Films,
Applied Optics, (09 2008): 5074. doi:

10/08/2012 99.00 X. Zhu, J. Wang, P. Lau, D. Nguyen, R. A. Norwood, N. Peyghambarian. Nonlinear optical performance of periodic structures made from composites of polymers and Co_3O_4 nanoparticles,
Applied Physics Letters, (08 2010): 93503. doi:

10/08/2012 83.00 Kuo-Ping Chen, Vladimir P. Drachev, Vladimir M. Shalaev, Joshua D. Borneman, Alexander V. Kildishev. Drude Relaxation Rate in Grained Gold Nanoantennas,
Nano Letters, (02 2010): 916. doi:

10/08/2012 27.00 Eric Van Stryland, David Hagan, Seth Marder. NONLINEAR OPTICS: The dream of a turnkey nonlinear spectrophotometer gets closer to reality,
Laser Focus World, (09 2008): 0. doi:

10/08/2012 41.00 Daniel Owens, Canek Fuentes-Hernandez, Bernard Kippelen. Optical properties of one-dimensional metal-dielectric photonic band-gap structures with low index dielectrics,
Thin Solid Films, (02 2009): 2736. doi:

10/08/2012 9.00 D.T. Nguyen, C. Sheng, J. Thomas, R. Norwood, B. Kimball, D.M. Steeves, N. Peyghambarian. Observation of Nonlinear Transmission Enhancement in Cavities Filled with Nonlinear Organic Materials,
Applied Optics, (10 2008): 5777. doi:

10/09/2012 14.00 Daniel T. Owens, Canek Fuentes-Hernandez, Joel M. Hales, Joseph W. Perry, Bernard Kippelen. A comprehensive analysis of the contributions to the nonlinear optical properties of thin Ag films,
Journal of Applied Physics, (06 2010): 1. doi:

10/09/2012 80.00 Vladimir P Drachev, Reuben M Bakker, Zhengtong Liu, Hsiao-Kuan Yuan, Rasmus H Pedersen, Alexandra. Nanoantenna array-induced fluorescence enhancement and reduced lifetimes,
New Journal of Physics, (12 2008): 1. doi:

10/09/2012 97.00 Scott Webster, Davorin Peceli, Honghua Hu, Lazaro A. Padilha, Olga V. Przhonska, Artem E. Masunov, Andriy O.Viniychuk, Emma Barrasso, Richard Lepkowicz, David J. Hagan, Eric W. Van Stryland. Near-Unity Quantum Yields for Intersystem Crossing and Singlet Oxygen Generation in Polymethine-like Molecules: Design and Experimental Realization,
Journal of Physical Chemistry Letters, (07 2010): 2354. doi:

10/09/2012 71.00 K. Chen, V. Drachev, J. Borneman, A. Kildishev, V. Shalaev. Drude Relaxation Rate in Grained Gold Nanoantennas,
Nano Letters, (02 2010): 916. doi:

10/09/2012 89.00 Francesca Terenziani, Olga V. Przhonska, Scott Webster, Lazaro A. Padilha, Yuriy L. Slominsky, Iryna G.. Essential-State Model for Polymethine Dyes: Symmetry Breaking and Optical Spectra,
Journal of Physical Chemistry Letters, (05 2010): 1800. doi:

10/10/2012 10.00 C. Sheng, R. Norwood, J. Wang, J. Thomas, D. Steeve, B. Kimball, N. Peyghambarian. Nonlinear optical transmission of lead phthalocyanine doped nematic liquid crystal composites for multi-scale nonlinear switching from nanosecond to continuous wave,
Applied Optics, (05 2009): 2731. doi:

10/10/2012 05.00 Susan A. Odom, Richard F. Kelley, Shino Ohira, Trenton R. Ensley, Chun Huang, Lazaro A. Padilha, Scott Webster, Veaceslav Coropceanu, Stephen Barlow, David J. Hagan, Eric W. Van Stryland, Jean-Luc Brdas, Harry L. Anderson, Michael R. Wasielewski, Seth R. Marder. Photophysical Properties of an Alkyne-Bridged Bis(zinc porphyrin)☐Perylene Bis(dicarboximide) Derivative,
Journal of Physical Chemistry A, (08 2009): 10826. doi:

10/10/2012 74.00 D. Owens, C. Fuentes-Hernandez, J. Hales, J. Perry, B. Kippelen. A comprehensive analysis of the contributions to the nonlinear optical properties of thin Ag films,
Journal of Applied Physics, (08 2010): 123114. doi:

10/10/2012 25.00 Zesheng An, Susan A. Odom, Richard F. Kelley, Chun Huang, Xuan Zhang, Stephen Barlow, Lazaro A. Padilha, Jie Fu, Scott Webster, David J. Hagan, Eric W. Van Stryland, Michael R. Wasielewski, Seth R. Marder. Synthesis and Photophysical Properties of Donor- and Acceptor-Substituted 1,7-Bis(arylalkynyl)perylene-3,4:9,10-bis(dicarboximide)s,
Journal of Physical Chemistry A, (04 2009): 5585. doi:

10/11/2012 30.00 Lazaro A. Padilha, Scott Webster, Honghua Hu, Olga V. Przhonska, David J. Hagan, Eric W. Van Stryland, Mikhail V. Bondar, Iryna G. Davydenko, Yuriy L. Slominsky, Alexei D. Kachkovski. Excited state absorption and decay kinetics of near IR polymethine dyes,
Chemical Physics, (09 2008): 97. doi:

10/11/2012 24.00 Susan A. Odom, Scott Webster, Lazaro A. Padilha, Davorin Peceli, Honghua Hu, Gero Nootz, Sung-Jae Chung, Shino Ohira, Jonathan D. Matichak, Olga V. Przhonska, Alexei D. Kachkovski, Stephen Barlow, Jean-Luc Bredas, Harry L. Anderson, David J. Hagan, Eric W. Van Stryland, Seth R. Marder. Synthesis and Two-Photon Spectrum of a Bis(Porphyrin)-Substituted Squaraine,
Journal of the American Chemical Society, (02 2009): 7510. doi:

10/11/2012 23.00 Honghua Hu, Davorin Peceli, Jonathan L. Rosch, Mikhail V. Bondar, Andriy O. Gerasov, Yuriy P. Kovtun, Mykola P. Shandura, Alexey D. Kachkovski, David J. Hagan, Eric W. Van Stryland, Lazaro A. Padilha, Scott Webster, Olga V. Przhonska. Nonlinear absorption in a series of Donor-pi-Acceptor cyanines with different
conjugation lengths,
Journal of Materials Chemistry, (06 2009): 7503. doi:

10/12/2012   8.00 S.V. Perminov, V.P. Drachev, S.G. Rautian. Optical Bistability Driven by the Light-Induced Forces Between Metal nanoparticles,
Optics Letters, (12 2008): 2998. doi:

10/12/2012 12.00 Seth R. Marder. Themed issue: nonlinear optics. The evolving field of nonlinear optics—a personal perspective,
Journal of Materials Chemistry, (08 2010): 7392. doi:

10/12/2012 06.00 Gero Nootz, Lazaro A. Padilha, Peter D. Olszak, Scott Webster, David J. Hagan, Eric W. Van Stryland, Larissa Levina, Vlad Sukhovatkin, Lukasz Brzozowski, Edward H. Sargent. Role of Symmetry Breaking on the Optical Transitions in Lead-Salt Quantum Dots,
Nano Letters, (05 2010): 3577. doi:

10/12/2012 82.00 Daniel T. Owens, Canek Fuentes-Hernandez, Joel M. Hales, Joseph W. Perry, Bernard Kippelen. A comprehensive analysis of the contributions to the nonlinear optical properties of thin Ag films,
J. Appl. Phys., (06 2010): 123114. doi:

10/12/2012 78.00 D. Owens, C. Fuentes-Hernandez, J. Hales, J. Perry, B. Kippelen. Nonlinear optical properties of induced transmission filters,
Optics Express, (08 2010): 19101. doi:

10/12/2012 84.00 X. Kong, Y. Wu, J. Wang, C. Sheng, R. Wang, N. Peyghambarian, R. A. Norwood, Z. Zheng. A dinuclear europium (III) complex with thenoyltrifluoracetonato and 1-(2-pyridylzao)-2-naphtholato ligands and its optical properties,
Chemistry of Materials, (08 2010): 346. doi:

10/12/2012 90.00 Micha⬚ Malicki, Joel M. Hales, Mariacristina Rumi, Stephen Barlow, LaKeisha McClary, Seth R. Marder and Joseph. Excited-state dynamics and dye–dye interactions in dye-coated gold nanoparticles with varying alkyl spacer lengths,
Physical Chemistry Chemical Physics, (04 2010): 6267. doi:

10/12/2012 92.00 U. K. Chettiar, P. Nyga, M. D. Thoreson, A. V. Kildishev, V. P. Drachev, V. M. Shalaev. FDTD modeling of realistic semicontinuous metal films,
Applied Physics B: Lasers and Optics, (03 2010): 159. doi:

10/12/2012 19.00 Scott Webster, Susan A. Odom, Lazaro A. Padilha, Olga V. Przhonska, Davorin Peceli, Honghua Hu, Gero Nootz, Alexei D. Kachkovski, Jonathan Matichak, Stephen Barlow, Harry L. Anderson, Seth R. Marder, David J. Hagan, Eric W. Van Stryland. Linear and Nonlinear Spectroscopy of a Porphyrin-Squaraine-Porphyrin Conjugated System,
Journal of Physical Chemistry, (10 2009): 14548. doi:

10/12/2012 29.00 Scott Webster, Lazaro A. Padilha, Honghua Hu, Olga V. Przhonska, David J. Hagan, Eric W. Van Stryland, Mikhail V. Bondar, Iryna G. Davydenko, Yuriy L. Slominsky, Alexei D. Kachkovski. Structure and linear spectroscopic properties of near IR polymethine dyes,
Journal of Luminescence, (12 2008): 1927. doi:

10/12/2012 42.00 Michal Malicki, Stephen Barlow, Joel M. Hales, LaKeisha McClary, Mariacristina Rumi, Seth R. Marder, Joseph W. Perry. Excited-State Dynamics and Dye–Dye Interactions in Chromophore-Coated Gold Nanoparticles with Varying Alkyl Spacer Lengths,
Journal of the American Chemical Society, (04 2009): 6267. doi:

10/12/2012 6.00 R.M. Bakker, Z. Liu, H.K. Yuan, R.H. Pedersen, A. Boltasseva, J. Chen, J. Irudayaraj, A. V. Kildishev, V.P. Drachev, V.M. Shalaev. Nanoantenna Array-Induced Fluorescence Enhancement and Reduced Lifetimes,
New Journal of Physics, (12 2008): 16. doi:

10/12/2012 1.00 L.A. Padilha, C.F. Hernandez, D. Owens, S.Y. Tseng, S. Webster, J.Y. Cho, D.J. Hagan, E.W. Van Stryland, S.R. Marder, B.Kippelen. Linear and Nonlinear Optical Properties of Highly Transmissive One-Dimensional Metal-Organic Photonic Bandgap Structures,
Linear and Nonlinear Optics of Organic Materials VIII, (08 2008): 1. doi:

10/15/2012 3.00 S.A. Odom, K. Lancaster, L. Beverina, K.M. Lefler, N.J. Thompson, V. Coropceanu, J.L. Bredas, S. R. Marder, Stephen Barlow. Bis[bis-(4-alkoxyphenyl)amino] Derivatives of Dithienylethene, Bithiophene, Dithienothiophene and Dithienopyrrole: Palladium-Catalysed Synthesis and Highly Delocalised Radical Cations,
Chem. Eur. J, (12 2007): 9637. doi:

10/15/2012 91.00 Claudiu M. Cirloganu, Lazaro A. Padilha, Scott Webster, David J. Hagan, Eric W. Van Stryland. Extreme Nondegenerate Two-photon Absorption in Semiconductors,
Nature Photonics, (08 2010): 0. doi:

10/22/2012 12.00 B. Kippelen, C. Fuentes-Hernandez. Nonlinear optical properties of copper-based photonic bandgap structures at the onset of interband transitions ,
Nonlinear Optics, Quantum Optics:Concepts in Modern Optics, (01 2010): 69. doi:

10/22/2012 22.00 Iam Choon Khoo, Scott Webster, Shoichi Kubo, W. Justin Youngblood, Justin D. Liou, Thomas E. Mallouk, Ping Lin, David J. Hagan, Eric W. Van Stryland. Synthesis and characterization of the multi-photon absorption and excited-state properties of a neat liquid 4-propyl 4 -butyl diphenyl acetylene,
Journal of Materials Chemistry, (07 2009): 7525. doi:

10/22/2012 98.00 Eric W. Van Stryland, David J. Hagan, Olga V. Przhonska, Seth R. Marder, Scott Webster, Lazaro A. Padilha. Nonlinear Absorption Spectroscopy of Organic Dyes,
Nonlinear Optics and Quantum Opitcs, (08 2010): 95. doi:

TOTAL: **50**

Number of Papers published in peer-reviewed journals:

(b) Papers published in non-peer-reviewed journals (N/A for none)

<u>Received</u>   <u>Paper</u>

10/22/2012 16.00 Dan T. Nguyen, Chuanxiang Sheng, Jayan Thomas, Robert Norwood. Observation of nonlinear
transmission enhancement in cavities filled with nonlinear organic materials,
Applied Optics, (10 2008): 5777. doi:

10/22/2012 15.00 ChuanXiang Sheng, Robert A. Norwood, Jiafu Wang, Jayan Thomas. Nonlinear optical transmission of
lead phthalocyaninedopednematic liquid crystal composites for multiscale nonlinearswitching from
nanosecond to continuous wave,
Applied Optics, (05 2009): 2731. doi:

10/22/2012 18.00 Sergey V. Perminov, Vladimir P. Drachev, Sergey G. Rautian. Optical bistability driven by the
light-induced forces betweenmetal nanoparticles,
Optics Letters, (12 2008): 2998. doi:

10/22/2012 17.00 Reuben M Bakker, Vladimir P Drachev, Zhengtong Liu, Hsiao-Kuan, Yuan, Rasmus H Pedersen,
Alexandra Boltasseva, Jiji Chen, Joseph Irudayaraj, Alexander V Kildishev, Vladimir M Shalaev.
Nanoantenna array-induced fluorescence enhancement andreduced lifetimes,
New Journal of Physics, (12 2008): 125022. doi:

10/22/2012 19.00 Eric W. Van Stryland, Sheng Yao, Kevin Belfield, Shijun Zheng, Stephen Barlow,, Seth Marder, Mihaela
Balu, Lazaro A. Padilha, David J. Hagan. Broadband Z-scan characterization using
ahigh-spectral-irradiance, high-quality supercontinuum,
Optical Society of America, (02 2008): 159. doi:

10/22/2012 20.00 Dana C. Kohlgraf-Owens, Pieter G. Kik. Structural control of nonlinear optical absorption and refractionin
dense metal nanoparticle arrays,
Optical Society of America, (08 2009): 15033. doi:

10/22/2012 21.00 Reuben M Bakker, , Vladimir P Drachev, Zhengtong Liu, Hsiao-Kuan Yuan, Rasmus H Pedersen,
Alexandra Boltasseva, Jiji Chen,, Joseph Irudayaraj, Alexander V Kildishev, Vladimir M Shalaev.
Nanoantenna array-induced fluorescence enhancement andreduced lifetimes,
New Journal of Physics, (12 2008): 125022. doi:

10/22/2012 22.00 Robert A. Norwood, Jiafu Wang, ChuanXiang Sheng, Jayan Thomas, Yinglan Wu. Time-resolved studies
of photoinduced birefringencein azobenzene dye-doped polymer films,
Applied Optics, (10 2008): 5074. doi:

10/23/2012 23.00 Huang, C., Sartin, M. M., Cozzuol, M., Siegel, N., Barlow, S., Perry, J. W., and Marder, S. R.
Photoinduced Electron Transfer and Nonlinear Absorption in Poly(carbazole-alt-2,7-fluorene)s Bearing
Perylene Diimides as Pendant Acceptors,
J. Phys. Chem. A, (04 2012): 4305. doi:

    TOTAL: **9**

Number of Papers published in non peer-reviewed journals:

(c) Presentations

Number of Presentations: 0.00

Non Peer-Reviewed Conference Proceeding publications (other than abstracts):

Received   Paper

   TOTAL:

Number of Non Peer-Reviewed Conference Proceeding publications (other than abstracts):

Peer-Reviewed Conference Proceeding publications (other than abstracts):

Received   Paper

   TOTAL:

Number of Peer-Reviewed Conference Proceeding publications (other than abstracts):

(d) Manuscripts

Received   Paper

   TOTAL:

Number of Manuscripts:

Books

Received   Paper

   TOTAL:

Patents Submitted

Patents Awarded

Awards

Eric Van Stryland - R.W. Wood Prize of the Optical Society of America, 2012

Graduate Students

NAME	PERCENT_SUPPORTED
FTE Equivalent:	
Total Number:	

Names of Post Doctorates

NAME	PERCENT_SUPPORTED
FTE Equivalent:	
Total Number:	

Names of Faculty Supported

NAME	PERCENT_SUPPORTED
FTE Equivalent:	
Total Number:	

Names of Under Graduate students supported

NAME	PERCENT_SUPPORTED
FTE Equivalent:	
Total Number:	

Student Metrics

This section only applies to graduating undergraduates supported by this agreement in this reporting period

The number of undergraduates funded by this agreement who graduated during this period: 0.00

The number of undergraduates funded by this agreement who graduated during this period with a degree in science, mathematics, engineering, or technology fields:...... 0.00

The number of undergraduates funded by your agreement who graduated during this period and will continue to pursue a graduate or Ph.D. degree in science, mathematics, engineering, or technology fields:...... 0.00

Number of graduating undergraduates who achieved a 3.5 GPA to 4.0 (4.0 max scale): 0.00

Number of graduating undergraduates funded by a DoD funded Center of Excellence grant for Education, Research and Engineering: 0.00

The number of undergraduates funded by your agreement who graduated during this period and intend to work for the Department of Defense 0.00

The number of undergraduates funded by your agreement who graduated during this period and will receive scholarships or fellowships for further studies in science, mathematics, engineering or technology fields: 0.00

Names of Personnel receiving masters degrees

NAME

Total Number:

Names of personnel receiving PHDs

NAME

Total Number:

Names of other research staff

NAME   PERCENT_SUPPORTED

FTE Equivalent:
Total Number:

Sub Contractors (DD882)

Inventions (DD882)

Scientific Progress

see attachment

Technology Transfer

Scientific Progress

Technology Transfer

Final Report ALR MURI-24:

Engineered Multifunctional Nanophotonic Materials for Ultrafast Optical Switching

P.I. Eric Van Stryland, CREOL - other co-PI's and report authors, CREOL, David Hagan; GeorgiaTech, Seth Marder, Joseph Perry, Bernard Kippelen; Arizona, Nasser Peyghambarian, Robert Norwood; Purdue, Vladimir Shalaev, Vladimir Drachev.

Table of Contents (if report is more than 10 pages)

Statement of the problem studied

This work was a comprehensive basic science and engineering research program to develop a new generation of nanophotonic materials, materials structures, and devices that exhibit large, high-speed nonlinear optical (NLO) absorption and index changes, as needed to enable powerful new capabilities in all-optical switching for imaging applications. In particular, the problem of passive optical limiting and switching without using focusing optics is an extremely challenging task. The goal of this research was to tackle lensless optical limiting by determining the ultimate possibilities and limits on materials, materials structures, and device configurations. The approach we adopted combined three methodologies to achieve this goal: (1) to enhance the NLO response of the molecules through a variety of molecular engineering approaches, (2) to use surface plasmon field enhancements in nano-engineered clusters and arrays of metal and/or dielectric nanoparticles coupled to the organic NLO materials; and (3) to integrate the first two methodologies in systems having weakly resonant structures, including 3-D and/or 1-D photonic crystal structures (i.e. nonlinear Bragg mirrors). The desire was that a combination of these three methodologies would provide the orders of magnitude enhancement in the NLO responses to realize optimized broadband device structures that demonstrate the ability to perform optical limiting in the nanosecond pulse regime suitable for DoD applications.

Summary of the most important result

The approach we adopted during the program to the problem summarized above combined three methodologies to achieve this goal: (1) to enhance the NLO response of the molecules through a variety of molecular engineering approaches – this was primarily tackled by the team at Georgia Tech led by Seth Marder – see attached report of Marder group (2) to use surface plasmon field enhancements in nano-engineered clusters and arrays of metal and/or dielectric nanoparticles coupled to the organic NLO materials – see report by the Purdue team led by Vladimir Shalaev and Vladimir Drachev, the Georgia Tech groups led by Joeseph Perry and the report of Bernard Kippelen; and also see the report from CREOL led by Eric Van Stryland and David Hagan - and (3) to integrate the first two methodologies in systems having weakly resonant structures, including 3-D and/or 1-D photonic crystal structures (i.e. nonlinear Bragg mirrors) – see the report by the group at the University of Arizona led by Nasser Peyghambarian and Robert Norwood. Aspects of this task are also included in the report by Bernard Kippelen.

We focused our efforts primarily on using nonlinear absorption (NLA) as opposed to nonlinear refraction (NLR) for the following reasons. The primary advantage of nonlinear refractive effects in focusing geometries comes from the beam propagation changing phase distortion into amplitude distortions. This is the same reason that the Z-scan has interferometric sensitivity (the center of the beam interferes with the wings of the beam through propagation). Loss of propagation in lensless systems makes NLR effects much less effective.

The results of this research are mixed. While the ultimate goal of an effective optical limiting device without lenses remains a challenging problem there are several avenues of continued research that look very promising and a number of device geometries have been pointed out for optical limiting and switching using lenses in the systems. Additionally, plasmonic enhancement has been measured and verified in both thin film and bulk materials; however, these enhancements have still not been harnessed for devices. In thin films this is due to the fact that even with the approximately order of magnitude enhancement the observed effects are still relatively small. In bulk, this is due to the fact that we have so far only been able to obtain the proper nanoparticle geometry (probably a fractal geometry) in a liquid suspension, and the two to three orders of magnitude enhancement occurs on a time scale of ~20 minutes and then disappears on the same time scale in solution chemistry. So far, efforts to stabilize this transient enhancement have failed. However, pathways toward stabilization are defined and researchers from this program are looking for funding to continue these efforts.

A large number of publications resulted from this research, several PhD degrees were awarded and many invited, refereed and contributed talks were presented at international and national conferences. Patents were also developed under this program. These are all reported in the interim reports.

The individual reports of the groups follow. However, this was a very collaborative effort with samples traversing the United States for development and characterization from one group to the next, monthly conference calls and individual calls and e-mails when needed.

Bibliography is included at the end of each section

Georgia Tech: Seth Marder Research Group

Interactions between Conjugated Ligands and Noble Metals

Interactions between nonlinear optical organic dyes and assmblies of noble-metal nanostructures may potentially be exploited for optical-switching applications. Our focus has been on studying fundamental aspects of the interactions between conjugated molecules and noble metals.

Aus nanoparticles (ca. 3 nm in diameter) coated with bis(diarylamino)biphenyl-based thiols with two different alkyl spacers (propyl and dodecyl) between the chromophore and the surface-anchoring thiol group have been prepared and were characterized (collaboration with **Perry**) with a variety of techniques. The excited-state dynamics of the dyes in close proximity to the nanoparticle surface were studied using the time-correlated single-photon counting technique and near-IR fs transient absorption spectroscopy. The excited states of the dyes in the hybrid metal/organic systems exhibit ultrafast (<5 ps) deactivation, the length of the alkyl spacer between the dye and the thiol group having a profound effect on the ultrafast dynamics. Ultrafast formation (ca. 0.5 ps) of a cation-like species was seen for the propyl system but not for the

dodecyl-linker system, and was attributed to dye–dye interactions leading to the formation of a charge-transfer species involving two or more dye molecules.[1]

We have also, in collaboration with Antoine Kahn (Princeton) and Georg Heimel (Humboldt, Berlin), investigated the electronic structure of planar Au surfaces coated with variously substituted stilbene thiolates using photoelectron spectroscopy and comparison with theory. In particular, we confirmed for the first time theoretical predictions that π-donors in self-assembled monolayers have only a minor influence on the hole injection barrier from the metal to the organic, despite significantly affecting the molecular ionization potential.[2,3]

We have also supplied thiol lignads to other groups in the program for nonlinear optical measurements.

Heavy-Metal Phthalocyanines with Reduced Aggregation

Phthalocyanines (Pc) are attractive candidates for optical limiting in the vicinity of 500 nm since they have weak ground-state absorption and strong excited-state triplet absorption at this wavelength. However, it is necessary that the Pc derivative exhibits rapid intersystem crossing and, that the Pcs do not aggregate at high chromophore densities since aggregation leads to deleterious changes to the absorption characteristics. We investigated several approaches to developing non-aggregating metal-Pcs with high ISC rates by axially coordination of the central metal atom with dendrimeric species. The use of iodine substituents on the dendrimer has relatively minor effects on the triplet yield. Another approach investigated involved appending heavy-metal acetylides to Pc cores, but this also led to limited success. Another, more successful approach involves incorporation of heavy group 8 metals into the Pc (Fig 1), these being attractive due to their preference for 6-fold coordination, allowing for attachment of dendrimers above and below the Pc plane. We have synthesized a range of such species and investigated their optical properties in collaboration with **Hagan**, **Van Styland**, and **Perry**. While the spectral peculiarities of RuPc and Nc derivatives, notably the hypsochromic shifts of the Q bands relative to those of, for example, Zn^{II} and In^{III} analogues, will likely somewhat restrict the wavelength range over which effective OL can be achieved, we have shown the combination of a heavy central atom to promote rapid intersystem crossing and the suppression of solid-state aggregation effects via axially coordinated dendrimers, leads to examples that exhibit strong nonlinear absorption at 475 nm in both solution and neat films.[4]
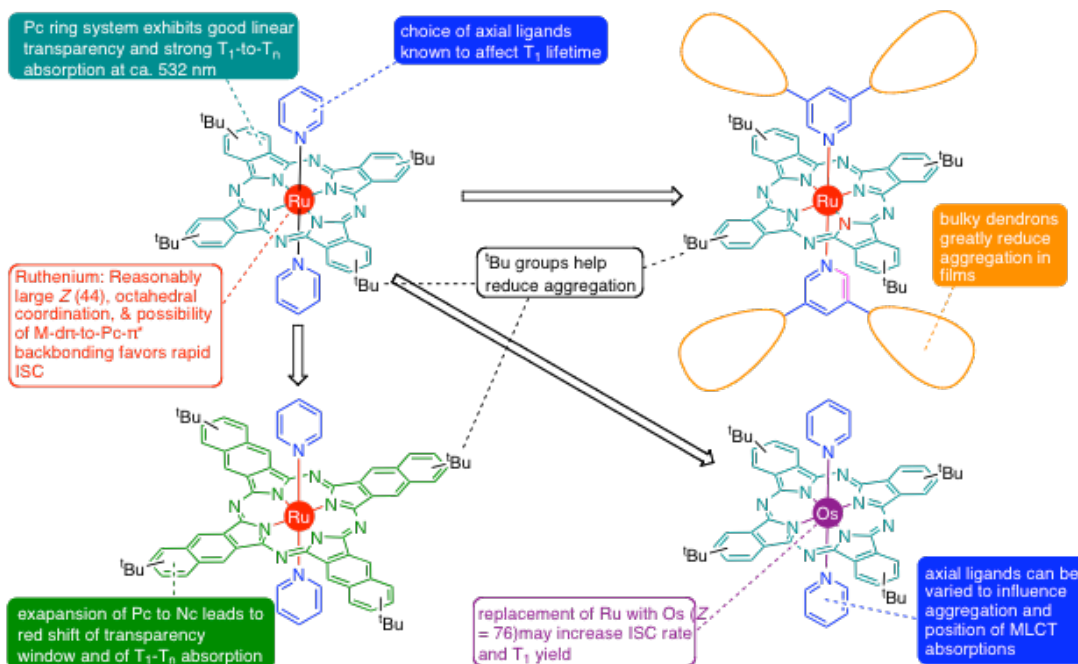
Figure 1. General Approach to Ru / Os Pc / Nc derivatives for vis. OL applications.

Polymethines and Squaraines with Heavy-Metal Functionalization

Polymethines (such as cyanines) exhibit windows of high linear transparency on the high-energy side of the their relatively narrow and strong low-energy optical transitions. If strong excited-state absorptions can be obtained at wavelengths corresponding to these windows of near-transparency and if the excited state in question is long-lived, optical pulse suppression based on reverse saturable absorption is feasible at these wavelengths. We have previously found that some polymethines do indeed exhibit excited-state absorptions in this region. Another attractive feature of polymethines is that the absorption maxima, and, therefore, also the windows of transparency, can be varied over a wide range of visible and near-IR wavelengths by varying the chain length and the end groups, allowing development of dyes for the applications at different wavelengths. In order to achieve long-lived excited states we have
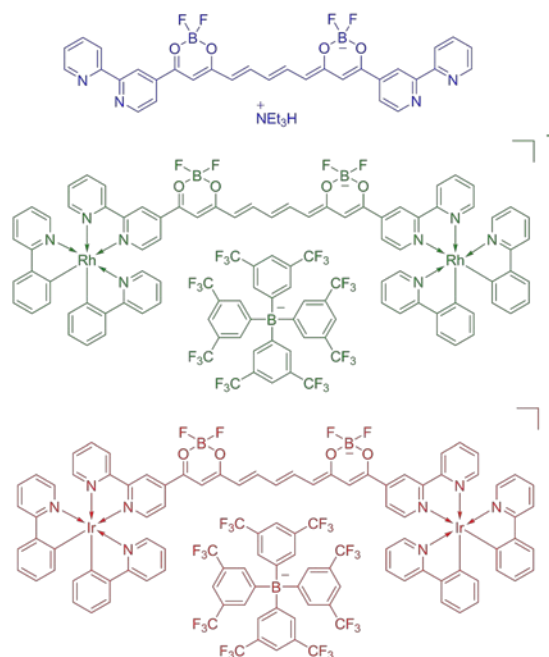
Fig. 2. Structure of bis(dioxaborine)-terminated pentamethines functionalized with bipyridine ligands (top) and with Rh and Ir complexes.

been working on incorporating heavy atoms into cyanine-type structures; the strong spin-orbit coupling associated with heavy atoms is hoped to lead to rapid intersystem crossing to afford strong-absorbing long-lived triplet states. We have investigated a number of different synthetic approaches. One such class of metal-functionalized polymethines, studied in collaboration with **Perry** and the **UCF** groups, is shown in Fig. 2. These Rh and Ir-coordinated bipyridine-functionalized bis(dioxaborine) heptamethines open the possibility of postterminal-group metal complexation as a means of modifying the properties of polymethines. Functionalization of this type can also modify the third-order nonlinear optical properties and, at least for the particular counterions used here, potentially mitigate the adverse effects of solid-state aggregation on linear transparency. Metallation results in small increases in the magnitude of Re(g) at 1.55 mm, with comparable Im(g) associated with 2PA at the same wavelength. In the context of this program, these dyes may be useful for optical pulse suppression based on two-photon absorption.[5]

Squaraines are closely related to polymethines and share a number of spectral characteristics. Accordingly, we have also synthesized a range of new squaraine-based architectures in which multiple squaraines are connected to one another and / or functionalized with heavy-metal acetylides and some of these materials have been studied at **UCF**.

Porphyrin / Squaraine and Porphyrin / Perylene Diimide Triads

Here we investigated (with **Hagan** and **Van Stryland** and with Jean-Luc Brédas at GIT and Harry Anderson at Oxford) the electronic and optical consequences of coupling porphyrin and squaraine or perylene diimide (PDI) moieties in ethynylene-bridged triads. This work was motivated by the observation that squaraines and PDIs have been found to exhibit large 2PA cross-sections at wavelengths close to their one-photon absorption (1PA) edges, while dimers and oligomers of conjugated zinc porphyrins have also been shown to exhibit very strong 2PA, with maximum cross-sections up to 500 times those of monomeric analogues. Moreover, linear absorption spectra of all three classes of compound exhibit bands characterized by large transition dipole moments, a key prerequisite for obtaining strong 2PA. In addition, the S0-S1 transition energies of bis(indolinylidenemethyl) squaraines closely match those of porphyrins, suggesting the possibility of substantial excitonic electronic coupling in a π-conjugated hybrid of these two components. On the basis of these observations, we were interested in investigating whether the electronic coupling between the constituent subunits of these triads could be sufficiently strong to result in enhanced 2PA.

The maximum 2PA cross-section of 11 000 GM measured for the porphyrin-squaraine triad (Fig 3) is much larger than that for either model compound but is similar in magnitude to those measured for several other porphyrin dimers with conjugated bridges, for which, however, the maxima are observed at somewhat shorter wavelengths. More unusually, and in contrast to the 2PA spectra of model compounds and other porphyrin dimers, the 2PA absorption of **1** is very broad, with $\delta > 780$ GM over the entire measurable region, which includes the

telecommunications range (1300-1550 nm),[6,7] The enhancement of cross-section suggests substantial electronic coupling between the porphyrin and squaraine moieties; this idea is confirmed by the DFT frontier orbitals. The complexity of this compound and the porphyrin-squaraine coupling are anticipated to lead to a large number of low-lying excited states. Therefore, the broad 2PA spectrum is likely to arise from overlap of several transitions. The calculations support this idea, as they reproduce the main features of the experimental spectrum, indicating peaks with δ) ~6900 and 9700 GM at transition energies between those of the two strong 1PA states. The observation of large δ over a 750 nm-wide wavelength range suggests applications in broadband NIR pulse suppression.
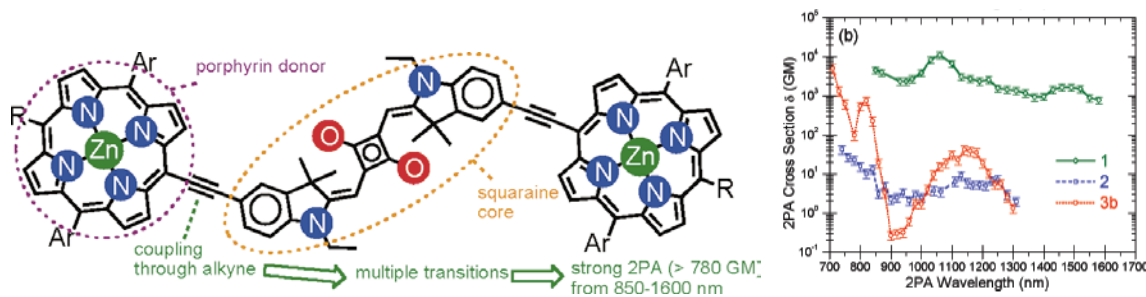
Figure 3. Structure of a porphyrin-squaraine triad (left) and 2PA spectra of the triad (**1**) and porphyrin (**2**) and squaraine (**3**) model compounds.

In contrast to that of a related *p*-phenylene-bridgedsystem, the UV-vis-NIR absorption spectrum of the porphyrin-PDI triad deviates significantly from the sum of spectra of isolated porphyrin and PDI units, demonstrating more extensive donor-acceptor interaction. This finding is consistent with quantum-chemical calculations showing more extensive delocalization of frontier orbitals over both the donor and acceptor, and with electrochemical data. The transient absorption behavior has been investigated in collaboration with M. Wasielewski at Northwestern and is consistent with strong porphyrin-PDI coupling than in the phenylene-bridged analogue. Large 2PA cross sections are found at wavelengths of ca. 1.06-1.20 μm, at which isolated porphyrin and PDI chromophores do not absorb. Quantum-chemical calculations indicate that this 2PA can be attributed to the presence of frontier molecular orbitals with mixed poprhyrin and PDI character and that comparably long-wavelength strong 2PA is not expected for the more weakly coupled compound phenyl-bridged analogue.[8]

Charge-Transfer Optical-Limiting in Donor / Perylene Diimide Assemblies

We have designed and studied systems for optical limiting in which one- or two-photon absorption is followed by formation of strongly absorbing radical ions. We have synthesized and studied two molecular dyads consisting of a 2,7-bis(4-(diarylamino)styryl)carbazole two-photon (2P) absorbing donor, connected by different linkers to a perylene diimide (PDI) acceptor (Figure 4).[9] Photo-induced charge transfer (CT) was characterized using transient absorption measurements. Because of spectral overlap between the donor 2P band and the 1P absorption

band of the PDI radical anion the dyads exhibit enhanced nonlinear absorption at 700-800 nm relative to that seen for the 2P donor chromophore. These systems, therefore, represent an example of a 2P charge-transfer approach to optical power limiting. We have also studied related systems based on poly(carbazole-*alt*-fluorene)s with pendant PDI groups. The PDI pendants are aggregated, even in dilute solution, extendingthe onset of linear PDI absorption into the NIR. Transient-absorption spectra provide evidence for efficient CT following either donor or acceptor photo-excitation to form long-lived charge-separated species, which exhibit strong absorption in the NIR. The spectral overlap between the transient species and the long-wavelength-edge absorption of the aggregated PDI leads to reverse saturable absorption at 680 nm that can be used for optical-pulse suppression. Additionally, at high input energies, 2P mechanisms may also contribute to the suppression. These PDI-grafted polymers exhibit enhanced optical-pulse suppression compared with blends of model materials comprised of unfunctionalized poly(carbazole-*alt*-fluorene)s and PDI small molecules.[10]
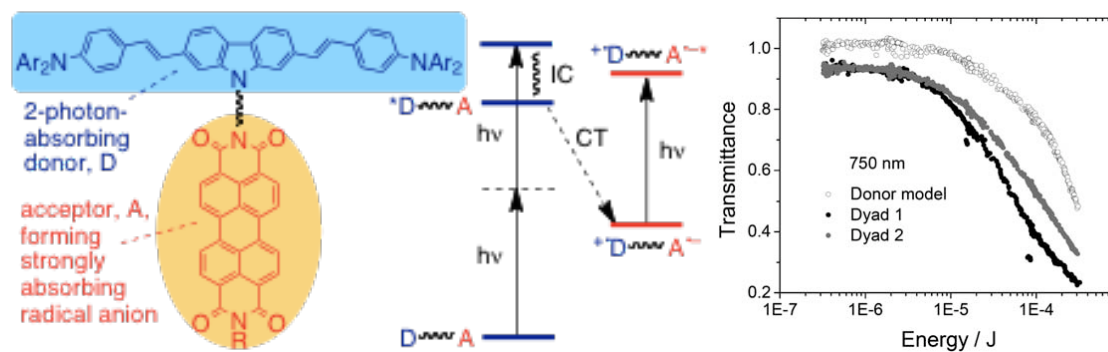
Figure 4. Schematic for 2PA-induced CT optical limiting in donor-PDI dyads (left) and non-linear transmission behavior in toluene at 750 nm (2 mM, 6 ns pulses, f/5 geometry focussed in center of 1 cm cell) (right). The two dyads differ in the structure of the linker.

1. Malicki, M.; Hales, J. M.; Rumi, M.; Stephen Barlow; McClary, L.; Marder, S. R.; and Perry, J. W., Phys. Chem. Chem. Phys. 2010, 12, 6267-6277.
2. Malicki, M.; Guan, Z.; Ha, S. D.; Heimel, G.; Barlow, S.; Rumi, M.; Kahn, A.; and Marder, S. R., "Preparation and Characterization of 4′-Donor Substituted Stilbene-4-thiolate Monolayers and Their Influence on the Work Function of Gold", Langmuir 2009, 25, 7967–7975.
3. Malicki, M.; Heimel, G.; Guan, Z.-L.; Ha, S. D.; Barlow, S.; Kahn, A.; and Marder, S. R., "Energy-Level Alignment in 4'-Substituted Stilbene-4-thiolate Self-Assembled Monolayers on Gold", J. Phys. Chem. C 2011, 115, 7487–7495.
4. Dasari, R. R.; Sartin, M. M.; Cozzuol, M.; Barlow, S.; Perry, J. W.; and Marder, S. R., "Synthesis and linear and nonlinear absorption properties of dendronised ruthenium(II) phthalocyanine and naphthalocyaninew", Chem. Commun. 2011, 47, 4547-4549.

5.   Lin, H.-C.; Kim, H.; Barlow, S.; Hales, J. M.; Perry, J. W.; and Marder, S. R., "Synthesis and linear and nonlinear optical properties of metal-terminated bis(dioxaborine) polymethines", Chem. Commun. 2011, 47, 782-784.

6.   Odom, S. A.; Webster, S.; Padilha, L. A.; Peceli, D.; Hu, H.; Nootz, G.; Chung, S.-J.; Ohira, S.; Matichak, J. D.; Przhonska, O. V.; Kachkovski, A. D.; Barlow, S.; Brédas, J.-L.; Anderson, H. L.; Hagan, D. J.; Stryland, E. W. V.; and Marder, S. R., "Synthesis and Two-Photon Spectrum of a Bis(Porphyrin)-Substituted Squaraine", J. Am. Chem. Soc. 2009, 131, 7510–7511.

7.   Webster, S.; Odom, S. A.; Padilha, L. A.; Przhonska, O. V.; Peceli, D.; Hu, H.; Nootz, G.; Kachkovski, A. D.; Matichak, J.; Barlow, S.; Anderson, H. L.; Marder, S. R.; Hagan, D. J.; and Stryland, E. W. V., "Linear and Nonlinear Spectroscopy of a Porphyrin-Squaraine-Porphyrin Conjugated System", J. Phys. Chem. B 2009, 113, 14854–14867.

8.   Odom, S. A.; Kelley, R. F.; Ohira, S.; Ensley, T. R.; Huang, C.; Padilha, L. A.; Webster, S.; Coropceanu, V.; Barlow, S.; Hagan, D. J.; Van Stryland, E. W.; Brédas, J. L.; Anderson, H. L.; Wasielewski, M. R.; and Marder, S. R., "Photophysical Properties of an Alkyne-Bridged Bis(zinc porphyrin)-Perylene Bis(dicarboximide) Derivative", J. Phys. Chem. A 2009, 113, 10826-10832.

9.   Huang, C.; Sartin, M. M.; Siegel, N.; Cozzuol, M.; Zhang, Y.; Hales, J. M.; Barlow, S.; Perry, J. W.; and Marder, S. R., "Photo-induced charge transfer and nonlinear absorption in dyads composed of a two-photon-absorbing donor and a perylene diimide acceptor", J. Mater. Chem. 2011, 21, 16119-16128.

10.   Huang, C.; Sartin, M. M.; Cozzuol, M.; Siegel, N.; Barlow, S.; Perry, J. W.; and Marder, S. R., "Photoinduced Electron Transfer and Nonlinear Absorption in Poly(carbazole-alt-2,7-fluorene)s Bearing Perylene Diimides as Pendant Acceptors", J. Phys. Chem. A submitted.

Georgia Tech: Bernard Kippelen Research Group
Scientific Progress and Accomplishments

The main goal of the Kippelen group during this project was to **study the potential of using metals and metallic nanostructures for optical limiting applications**. Our initial objective was to study the linear and nonlinear optical (NLO) properties of metal-dielectric multilayer stacks, also known as metal-dielectric photonic bandgap structures (MDPBGs). MDPBGs are attractive passband optical filters because they can be designed to yield optical transmittance windows with large transparency and large field-of-view despite containing large total metal thickness in their structure. In addition, univalent noble metals such as Au, Ag and Cu were also reported to yield an extremely large nonlinear optical (NLO) response in the fs and ps temporal ranges [1-4]. Third order nonlinear susceptibilities, $|\chi^{(3)}|$, as large as 1×10^{-6} esu were estimated for bulk Cu from the NLO response of Cu nanoparticle-doped glasses [4]. Indeed, theoretical studies using such large values of $\chi^{(3)}$ suggested the possibility of ultrabroadband optical limiting MDPBG filters [5]; although the few experimental realizations suggested much more modest performance [6-8] it was not clear if this modest NLO behavior was due to an unoptimized device geometry or to intrinsic limitations of this approach.

A first accomplishment of the Kippelen group during this program was the optimization and experimental demonstration of highly transparent MDPBG filters with large spectral and angular bandwidths [9]. The consequences of using lower index dielectric materials in MDPBG structures were studied. We also described design techniques to minimize some of the detrimental effects that arose from using these low index dielectrics and demonstrated the flexibility of these structures by demonstrating a method for producing 1D MDPBG structures containing Ag and relatively low refractive index dielectric layers which show the characteristics of a flat-passband optical filter. Such a structure had a transmission comparable to that of a periodic structure but would minimize the effects of the individual resonance peaks that are characteristic of MDPBGs using moderate refractive index dielectrics, and lead to transparent optical filters with a large field-of-view (FOV) that were capable of broadband applications within the visible spectrum. To validate this approach we fabricated an MDPBG using Al_2O_3 as the dielectric. The fabricated structure shows 53%±3% transmission over a 150 nm bandwidth between 475 nm and 625 nm, with an angular change of less than 5% when the angle of incidence is varied by ±30° with respect to normal incidence. We also showed that the optical properties of such devices are insensitive to temperature changes up to 150 °C and demonstrated environmental stability over a period of ten months. The properties of these filters are attractive as hot-mirrors due to their very high out-of-band rejection, particularly in the infrared (IR) and give rise to a separate program on funded under the Applied Metamaterials Program by the Air Force Research Laboratory.

As the nonlinear of neat noble metal layers and MDPBGs were studied using Z-scan measurements, it became clear that the interpretation of the NLO response of the metals has a third-order NLO process was not adequate. Intensity dependent $\chi^{(3)}$ values, which changed with pulsewidth rise serious concerns about the validity of interpreting Z-scan measurements in light of a third order NLO process. In addition, $\chi^{(3)}$ values derived through these measurements prove of little use to predict the NLO behavior of complex metal-dielectric multilayer structures [10-16]. In hence it became clear that an alternative description of the NLO response of noble metals was needed. It was found that a description of the NLO response of bulk metals could be found in the context of thermoreflectance measurements, known since mid-seventies [17].

The NLO properties of Ag, Au and Cu were studied by the Kippelen group using white-light continuum (WLC) pump-probe spectroscopy. An accurate characterization of the linear optical properties of thin metal films (on the order of their skin depth) was conducted by spectroscopic ellipsometry. Complex refractive index values and surface morphology were extracted from such measurements. These measurements enable the optimization of the conditions for the deposition of high quality metallic films on a variety of organic and inorganic substrates using an e-beam deposition system. Physical models were then derived to describe the measured refractive index (or alternatively the dielectric permittivity) of Ag, Au and Cu films by considering contributions arising from interband electronic transitions and intraband (Drude type) electronic transitions. Electronic interband transitions in the visible or ultraviolet (UV) spectral region arise from bound electrons excited from fully occupied electronic states within the d-band, below the Fermi

energy level, to the half filled s-p electronic bands in the conduction band. In this spectral region, metals are opaque because optical fields are strongly absorbed. At lower energies, electronic intraband transitions occur from free electrons stimulated within the conduction band. In this spectral region, metals are opaque mainly because the optical fields are reflected off its surface, rather than absorbed in the bulk.

The dielectric permittivity can be expressed as a function of temperature as,

$$\varepsilon(\omega,T_e,T_L) = \varepsilon_{\text{inter}}(\omega,T_e,T_L) + \varepsilon_{\text{intra}}(\omega,T_e,T_L) \tag{1}$$

where ω is the free space optical frequency, T_l and T_e are the lattice and electron temperatures, respectively, and for our purposes should be considered time dependent quantities.

The first term in Eq.1 is typically modeled as,

$$\varepsilon_{\text{inter}}\left(\omega,T_e(t)\right) = \sum_{j=1}^{M} \kappa_{(j)} \int_0^\infty dx \frac{\sqrt{x-E_{g(j)}}}{x^2} \left[1-F_{(j)}\left(x,T_e(t)\right)\right] \frac{\hbar^2\omega^2 - x^2 - \gamma_{ee(j)}^2 - 2i\hbar\omega\gamma_{ee(j)}}{(\hbar^2\omega^2 - x^2 - \gamma_{ee(j)}^2)^2 + 4\hbar^2\omega^2\gamma_{ee(j)}^2}$$

with parameters,

$$F_{(j)}(x,T_e(t)) = \left(1+\exp\left(\frac{x-E_{f(j)}}{k_B T_e(t)}\right)\right)^{-1}, \quad E_{f(j)} = E_{fd(j)}\left(1-\frac{\pi^2}{12}\left(\frac{k_B T_e(t)}{E_{fd(j)}}\right)^2\right),$$

and $\gamma_{ee(j)}[T_e(t)] = \hbar(\gamma_{a(j)} T_e^2(t) + \gamma_{b(j)}\omega^2)$

$$\tag{2}$$

where the summation is composed of M interband terms and each contribution term is denoted by the subscript j, x is the electron energy, κ is a constant related to effective electron mass, E_g is the minimum transition energy from a valence band to an ideal parabolic conduction band, γ_{ee} is the inverse scattering time, $F(x,T_e(t))$ is the electron occupation number, E_f is the electron distribution function, E_{fd} is the transition energy from the band to the Fermi level, k_B is the Boltzman constant, $\hbar$ is the plank constant, and γ_a and γ_b are constant coefficients [18].

The second term in Eq. 1 is a Drude term typically given as

$$\varepsilon_{\text{intra}}\left(\omega,T_l(t),T_e(t)\right) = 1 + \varepsilon_b - \frac{\omega_p^2}{\omega^2 + i\gamma\omega}$$

with parameters,

$$\gamma[T_l(t),T_e(t)] = \gamma_0 + \gamma_1 \times T_l(t) + \gamma_2 \times T_e^2(t) + \gamma_3 \times \omega^2 \tag{3}$$

where, ε_b is the background dielectric constant, γ is the damping constant, ω_p is the bulk plasma frequency, and γ_0, γ_1, γ_2, and γ_3 are constant coefficients [19].

Eqs. 1-3 provide a physical model allowing the calculation of the NLO changes of refractive index that occur in a metal when excited by an ultrafast optical pulse. When energy from the

11

optical pulse is absorbed by the electron gas raises its temperature and smears the electronic distribution around the Fermi energy (Fermi-smearing), causing a very strong change of the dielectric permittivity of the metal around the onset of interband region [20]. In the intraband region, an increased electron temperature increases electron scattering processes which change the dielectric permittivity, albeit these changes are of smaller magnitude than the ones produced in the onset of the interband region [21].

The temporal evolution of the electron and lattice temperatures can themselves be modeled by using the so-called two-temperature model. The two-temperature model describe the heat exchange from a thermalized of electron gas to the lattice [20, 21].

$$C_e\left(T_e\right)\frac{dT_e}{dt} = -G(T_e - T_l) + P(t)$$

$$C_l\frac{dT_l}{dt} = G(T_e - T_l)$$

(4)

The changes in electron and lattice temperatures calculated through the two temperature model depend upon intrinsic material properties such as the electron and lattice specific heats, C_e and C_l, respectively, and the electron phonon coupling constant, G, and are driven by the density of absorbed power within each individual layer $P(t)$ estimated as $P(t) = I(t)A/d\left[W/m^3\right]$, where $I(t)$ is the pump irradiance, assumed to have a Gaussian temporal, A is the linear absorptance in the metal layer, calculated using the transfer matrix method, and d is the thickness of the metal layer. As others, we found that the linear approximation of $C_e(T_e)$ and a temperature independent value of G are valid only in the low-fluence regime; i.e. for electron temperatures smaller than around 3000 K for Au [22].

Using the described theoretical formalism, the spectroscopic ellipsometry and pump-probe data can be modeled to provide an excellent description of the linear and NLO properties of noble metals, fully explaining the intensity and pulse-width dependence of the metal's NLO response previously observed. As an example, the value of the constant coefficients used to describe the permittivity of a 23 nm-thick Au film deposited by an e-beam are listed in Table 1 and 2.

Table 1 Constant coefficients of a Au dielectric permittivity model for intraband transition term.

ε_{intra}	ε_b	$\gamma_0(s^{-1})$	$\gamma_1(s^{-1}k^{-1})$	$\gamma_2(s^{-1}k^{-2})$	$\gamma_3(s^{-3})$	$\omega_p(s^{-1})$
	3.5	1.2×10^{14}	1×10^{10}	2.5×10^{7}	2.1×10^{-18}	1.3×10^{16}

Table 2 Constant coefficients of a Au dielectric permittivity model of the first and second interband transition term, respectively.

$\varepsilon_{inter(1)}$	$\kappa_{(1)}$	$E_{fd(1)}(eV)$	$E_{f(1)}(eV)$	$\gamma_{a(1)}(s^{-1}k^{-2})$	$\gamma_{b(1)}(s^{-3})$
	100	2.59	1.44	1.2×10^{-4}	1.6×10^{-16}
$\varepsilon_{inter(2)}$	$\kappa_{(2)}$	$E_{fd(2)}(eV)$	$E_{f(2)}(eV)$	$\gamma_{a(2)}(s^{-1}k^{-2})$	$\gamma_{b(2)}(s^{-3})$
	20	3.1	0.5	5.4×10^{-4}	7×10^{-17}

Figure 1 shows the comparison between simulated Au permittivity and that obtained by spectroscopic ellipsometry. Fig. 2 shows a comparison between the measured changes in transmittance and reflectance and the values predicted by the model here described. As can be seen, the model provides very good spectral and temporal agreement with respect to the measured NLO response of Au (23 nm thick).
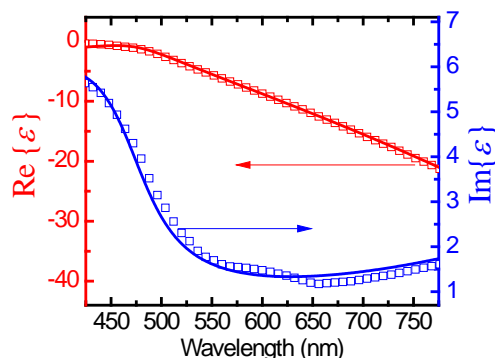
Fig. 1 Comparison of measured (symbols) and simulated (solid lines) complex dielectric permittivity spectra in visible range for fabricated samples **R1.** The dielectric permittivity of Au was modeled as a set of explicit equations (Eqs. 2-4) and compared with measured ellipsometric data.
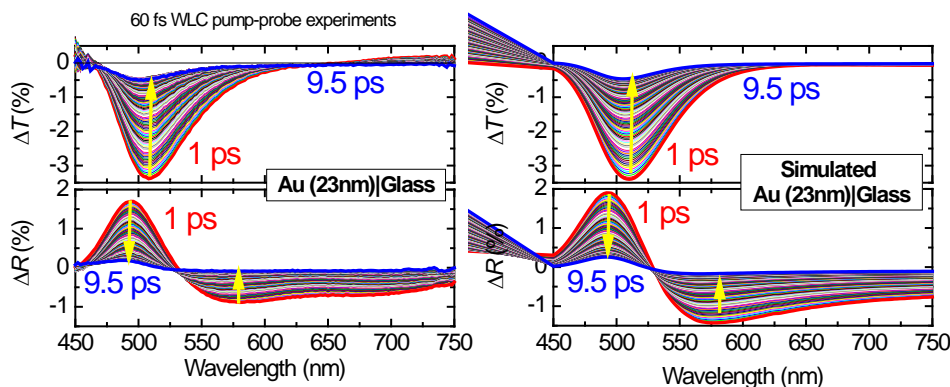
Fig. 2 Comparison of measured (left) and simulated (right) changes of transmittance and reflectance in Au.

Through this program, the Kippelen group developed comprehensive models to describe the linear and nonlinear optical properties of thin films of Au, Cg and Cu.

An important test for the validity of these models, and their broader impact, is to confirm their ability to predict the linear and NLO properties of complex metal-dielectric multilayer structures. Indeed, the Kippelen group used these models to study theoretically and experimentally the

13

properties of MDPBGs (Fig. 3), induced transmission filters (Fig. 4), bilayer metal layers (Fig. 5), and more recently of novel nonlinear mirror structures. The details of these studies and a full discussion of the limitations of the model and of metal dielectric multilayer structures have been published by the Kippelen group[15, 16, 23-25]. The work conducted by the Kippelen group therefore validates the idea that the NLO response of metals is better described as a $\chi^{(1)}$ process caused by electron and lattice heating.[1, 21] Furthermore, that this description can be used to realistically predict the NLO response of complex metal-dielectric structures.
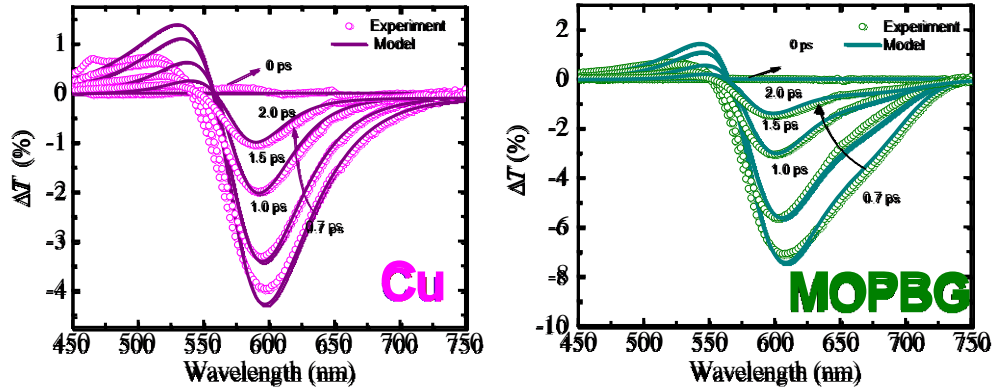
Fig. 3. Comparison between experimental and modeled spectral and temporal evolution of the transmittance change measured by WLC pump-probe in a) a **Cu** reference sample; and b) a Metal-organic photonic bandgap (MOPBG) structure comprising three Cu layers.
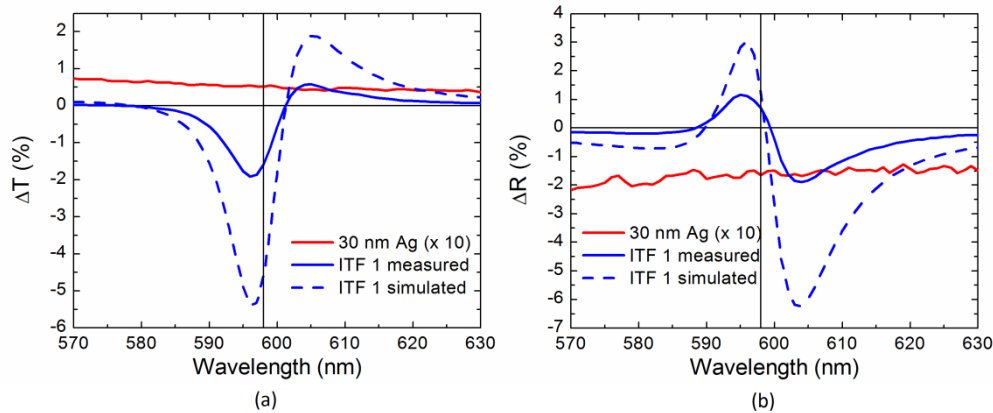
Fig 4. Measured spectral changes in (a) transmittance and (b) reflectance of 30 nm Ag film and and induced transmission filter (ITF) and simulated changes in ITF at $t = 0.8$ ps due to 32 J/m^2 pump pulse at 600 nm

As shown by these studies, noble metals offer a great opportunity to tune the linear optical properties of optical filters to meet a very wide range of different applications and functionalities. Although the modulations of the transmittance obtained by the use of metal-

14

dielectric multilayer structures are smaller than what will be needed for optical limiting applications, the combination of linear and nonlinear optical properties offer interesting possibilities for the realization of novel nonlinear optical devices in the visible spectral range, where no other class of nonlinear optical materials offers similar NLO response as metals. Furthermore, recent developments on the design and demonstration of novel nonlinear mirror structures, open very interesting possibilities for the control of ultrafast optical pulses because changes in reflectance can be amplified while preserving little optical loss. We expect that this realization will have a broad impact well beyond the original goals proposed under this program.
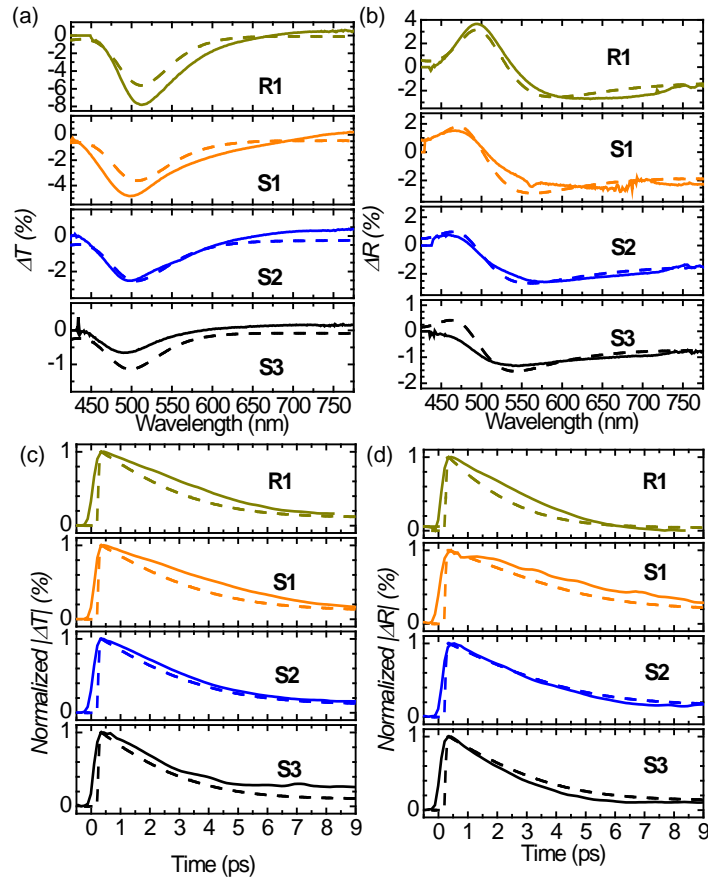
Fig. 5(a), (b) Spectral dependence of transmittance and reflectance changes measured from WLC pump probe experiment (solid line) and simulation by two-temperature model (dashed line) of samples **R1 (Au film)**, **S1 (Au(15nm)/Ag(5nm))**, **S2 (Au(10nm)/Ag(10nm))** and **S3 (Au(5nm)/Ag(15nm)** with a pump fluence of 25 J/m^2; (c), (d) experimental (solid line) and simulated (dashed line) temporal dependence of the normalized absolute transmittance and reflectance changes probed at 520 nm. The excitation wavelength in all cases was 560 nm.

Finally, an important realization from our detailed investigations conducted through this program, is that the success of the theoretical formalism derived to physically interpret data derived from Z-scan measurements on dielectrics and semiconductors has led the community to

often apply it to metallic materials without considering the strong optical reflection that metallic structures can have. As clearly stated by Sheik-Bahae M., et.al. (IEEE Journal of Quantum Electronics, 26, 760, 1990), the interpretation of Z-scan experiments was developed upon the approximation of negligible NLO changes in the sample's reflectance, ΔR. This key approximation in the original formalism, has been often overlooked by the community when analyzing data derived from Z-scan measurements on thin metal films, metal-dielectric structures, and metallic nanostructures. In this class of materials, our studies and those of others, have clearly shown that $|\Delta R|\sim|\Delta T|$. This implies that the NLO changes in transmittance, ΔT, measured in open-aperture Z-scan experiments cannot be directly correlated directly with the NLO changes in absorptance, ΔA, such that $\Delta A = -\Delta T$. Instead changes in absorptance must be related to both NLO changes in transmittance and reflectance, such that $\Delta A = -(\Delta T + \Delta R)$. A consequence of the adoption of the original formalism that neglects effects from reflection, is that not only the magnitude, but even the sign of the nonlinearity, can completely be mischaracterized.

[1] N. Rotenberg, A.D. Bristow, M. Pfeiffer, M. Betz, H.M. van Driel, Phys. Rev. B, 75 (2007) 155426.

[2] D.D. Smith, Y. Yoon, R.W. Boyd, J.K. Campbell, L.A. Baker, R.M. Crooks, M. George, J. Appl. Phys., 86 (1999) 6200-6205.

[3] G. Yang, D.Y. Guan, W.T. Wang, W.D. Wu, Z.H. Chen, Optical Materials, 25 (2004) 439-443.

[4] K. Uchida, S. Kaneko, S. Omi, C. Hata, H. Tanji, Y. Asahara, A.J. Ikushima, T. Tokizaki, A. Nakamura, Journal of the Optical Society of America B, 11 (1994) 1236-1243.

[5] M. Scalora, N. Mattiucci, G. D'Auguanno, M. Larciprete, M.J. Bloember, Physical Review E, 73 (2006) 016603.

[6] R.S. Bennink, Y.K. Yoon, R.W. Boyd, J.E. Sipe, Optics Letters, 24 (1999) 1416-1418.

[7] N.N. Lepeshkin, A. Schweinsberg, G. Piredda, R.S. Bennink, R.W. Boyd, Physical Review Letters, 93 (2004) 123902.

[8] M.C. Larciprete, C. Sibilia, S. Paoloni, M. Bertolotti, F. Sarto, M. Scalora, J. Appl. Phys., 93 (2003) 5013-5017.

[9] D. Owens, C. Fuentes-Hernandez, B. Kippelen, Thin Solid Films, 517 (2009) 27736-22741.

[10] C. Fuentes-Hernandez, L.A. Padilha, D. Owens, S.-Y. Tseng, S. Webster, J.-Y. Cho, D.J. Hagan, E.W. Van Stryland, S.R. Marder, B. Kippelen, Linear and nonlinear optical properties of highly transmissive one-dimensional metal-organic photonic bandgap structures, in: Linear and Nonlinear Optics of Organic Materials VIII, SPIE, San Diego, CA, USA, 2008, pp. 70490O-70499.

[11] C. Fuentes-Hernandez, L.A. Padilha, D. Owens, S.-Y. Tseng, S. Webster, J.-Y. Cho, D.J. Hagan, E.W. VanStryland, S.R. Marder, B. Kippelen, Nonlinear Refraction and Absorption in Highly Transmissive One-Dimensional Metal-Organic Photonic Bandgap Structures, in: Conference on Lasers and Electro-Optics/Quantum Electronics and Laser Science Conference and Photonic Applications Systems Technologies, Optical Society of America, San Jose, CA, 2008, pp. CThI6.

[12] C. Fuentes-Hernandez, L.A. Padilha, J.M. Hales, D. Owens, J. Kim, S. Webster, J.W. Perry, D.J. Hagan, E.W. VanStryland, B. Kippelen, Enhanced Nonlinear Absorption in Low-Finesse Metal-Dielectric Fabry-Perot Resonators, in: Conference on Lasers and Electro-Optics/International Quantum Electronics Conference, Optical Society of America, Baltimore, MD, 2009, pp. IThD5.

[13] C. Fuentes-Hernandez, L.A. Padilha, J.M. Hales, D. Owens, J. Kim, S. Webster, J.W. Perry, D.J. Hagan, E.W. VanStryland, B. Kippelen, The Nonlinear Optical Response of Transparent Metal-Dielectric Multilayer Structures, in: Integrated Photonics and Nanophotonics Research and Applications, Optical Society of America, Honolulu, Hawaii, 2009, pp. JTuA2.

[14] C. Fuentes-Hernandez, L.A. Padilha, J.M. Hales, D.T. Owens, J. Kim, S. Webster, J.W. Perry, D.J. Hagan, E.W. VanStryland, B. Kippelen, The Nonlinear Optical Response of Transparent Metal-Dielectric Multilayer Structures, in: Nonlinear Optics: Materials, Fundamentals and Applications, Optical Society of America, Honolulu, Hawaii, 2009, pp. JTuA2.

[15] C. Fuentes-Hernandez, B. Kippelen, Nonlinear Optics and Quantum Optics,, 40 (2010) 69-82.

[16] C. Fuentes-Hernandez, D. Owens, J.M. Hales, J.W. Perry, B. Kippelen, Nonlinear Optical Properties of Layered Multi-Metal Nanostructures, in: Quantum Electronics and Laser Science Conference, Optical Society of America, San Jose, CA, 2010, pp. JWA4.

[17] R. Rosei, D.W. Lynch, Phys. Rev. B, 5 (1972) 3883-3894.

[18] J.Y. Bigot, J.Y. Merle, O. Cregut, A. Daunois, Physical Review Letters, 75 (1995) 4702-4705.

[19] D. Owens, C. Fuentes-Hernandez, J.M. Hales, J.W. Perry, B. Kippelen, A comprehensive study of the contributions to the nonlinear optical properties of thin Ag films, in: G.S. Subramania, S. Foteinopoulou (Eds.) SPIE Optics and Photonics, SPIE, San Diego, California, USA, 2010, pp. 77560K-77511.

[20] C. Voisin, N. Del Fatti, D. Christofilos, F. Vallee, J. Phys. Chem. B, 105 (2001) 2264-2280.

[21] D.T. Owens, C. Fuentes-Hernandez, J.M. Hales, J.W. Perry, B. Kippelen, J. Appl. Phys., 107 (2010) 123114-123118.

[22] Z. Lin, L.V. Zhigilei, V. Celli, Phys. Rev. B, 77 (2008) 075133.

[23] C. Fuentes-Hernandez, T.D. Owens, J. Hsu, R.A. Ernst, M.J. Hales, W.J. Perry, B. Kippelen, The nonlinear optical response of transparent silver/gold multimetal layers, in: S.G. Subramania, F. Stravroula (Eds.) SPIE Optics and Photonics San Diego, CA, 2010, pp. 77560G.

[24] D.T. Owens, C. Fuentes-Hernandez, J.M. Hales, J.W. Perry, B. Kippelen, Optics Express, 18 (2010) 19101-19113.

[25] J. Hsu, C. Fuentes-Hernandez, A.R. Ernst, J.M. Hales, J.W. Perry, B. Kippelen, Opt. Express, 20 (2012) 8629-8640.

Georgia Tech: Joseph W. Perry Research Group

Synthesis and optical properties of silver and gold nanoparticles and their aggregates

The plasmonic enhancement of nonlinear absorption properties of chromophores in proximity to metal nanoparticles or nanoparticle aggregates is of interest for potential use in ultrafast optical switching and in optical limiting. While the enhancement of two-photon excited fluorescence of molecules bound to and chromophoric polymer thin films deposited on fractal clusters of silver nanoparticles has been reported, convincing evidence of plasmonic enhancement of nonlinear absorption as opposed to irreversible laser induced processes such as photomodification of metal nanoparticles or aggregates is lacking. Thin films of fractal aggregates do not appear to be suitable systems for achieving clearly measureable nonlinear

absorption enhancement, because of the limited interaction length and range of the enhanced field distribution around the particles and because of extreme localized heating in such films under excitation with energetic nanosecond laser pulses. It is our hypothesis that small sized metal nanoparticle aggregates dispersed at moderate concentration (~10% by volume and with an interaction length that provides a reasonable transmission say ~ 70%) in a concentrated chromophoric liquid phase or polymer solid solution could allow for both significant enhancement of nonlinear absorption of laser pulses and dissipation of absorbed energy without major irreversible changes. To investigate this possibility, it is necessary to develop methods for the preparation or organic soluble and reasonably robust aggregates of metal nanoparticles.

1.   Synthesis of nanoparticles

Preparation of fractal clusters in organic medium requires a synthetic method, which produces homogenous nanoparticles on a large scale with weakly bound protecting ligands. Synthesis of silver and gold nanoparticles is done in organic solvent at reflux conditions (Figure 1). This method produces silver and gold nanoparticles with narrow size distribution (Figure 2), where primary amines serve as reducing agent and as capping ligands. Due to the weak binding of primary amines to silver or gold surface they can be quickly replaced by strongly binding thiolated ligands. Quick replacement of ligands allows for attachment of e.g. chromophoric ligands or ligands that promote aggregation of the particles. Amine modified silver nanoparticles also show less plasmon resonance damping then thiol modified particles, which can have significant impact on local field enhancements and thus nonlinear properties of nanocomposites.
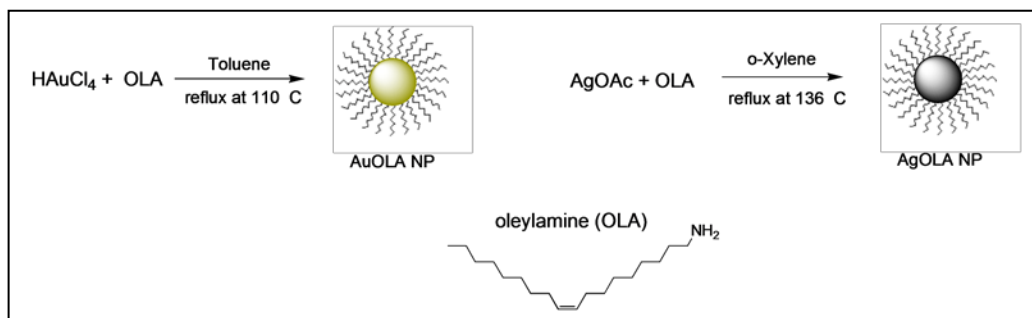
Figure 1. Synthesis of gold and silver nanoparticles in presence of oleylamine under reflux conditions.
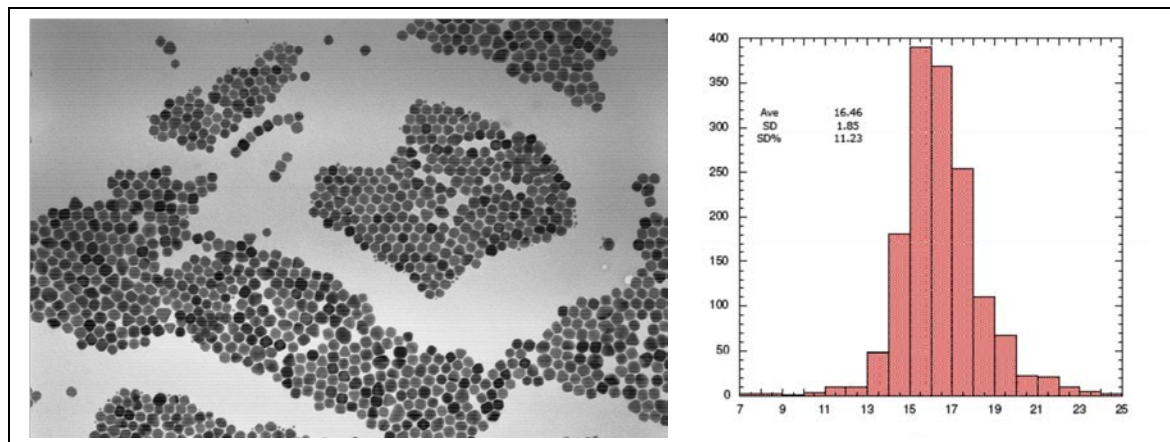
Figure 2. TEM image of silver nanoparticles and histogram of measured diameters in nm.

2. Exchange of ligands

The exchange of the ligands has been shown by monitoring changes in fluorescence intensity of chromophoric ligands in time after addition of gold or silver nanoparticle. The change in the fluorescence intensity is attributed to the strong fluorescence quenching effects of chromophores in the proximity to the metal surface. The time domain vs. fluorescence intensity changes (Figure 3) could be very well fitted with double exponentials. The fast component of the rate constant seems to be almost independent on the reactants concentration, and the slow component is almost linearly dependent on the concentration of both the ligands and the nanoparticles. Thus, first stage of the reaction is semi-zero order and it is a first order reaction with respect to the ligand and the nanoparticles.
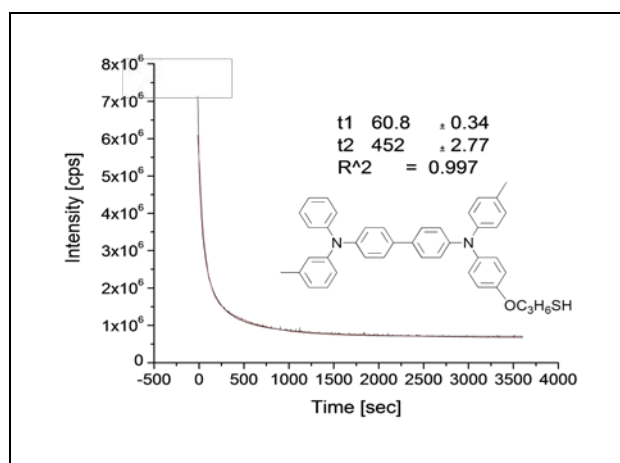
Figure 3. Fluorescence intensity change after addition of AuNP functionalized with oleylamine. The adsorption of the chromophore can be monitored this way due to the strong quenching in the proximity of the metal surface.

3. Aggregation of nanoparticles

Three approaches (Figure 4) to aggregate silver and gold nanoparticles in organic solvents have been studied. All three approaches involve exchanging ligands from weakly bound oleylamine (OLA) to either mercaptoundecanoic acid (MUA) or 1,4 benzene dithiol (BDT) or 2-naphthalene thiol (NT). The aggregation trends are similar for both gold and silver nanoparticles. In the first approach, solubility of nanoparticles changes upon exchange of ligands from (OLA) to ligands with carboxylic group at the end (MUA). The exchange is fast and leads to aggregation of the particles in nonpolar solvents such as toluene. The morphology of such aggregates is branched out and provides large surface area with respect to the structure volume (Figure 5).
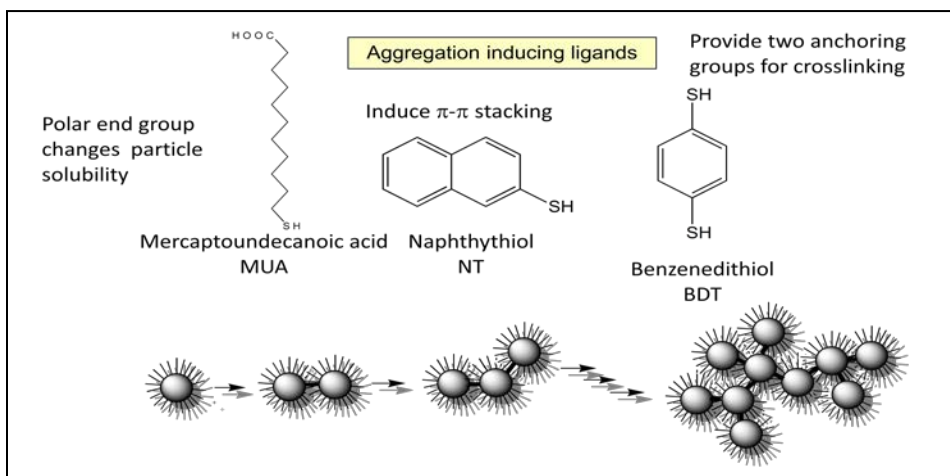
Figure 4. Ligands used in the aggregation methods. MUA – changes solubility of nanoparticles, NT – introduces strong pi-pi interaction between ligands, and BDT – provides two binding sides to keep the particles together.
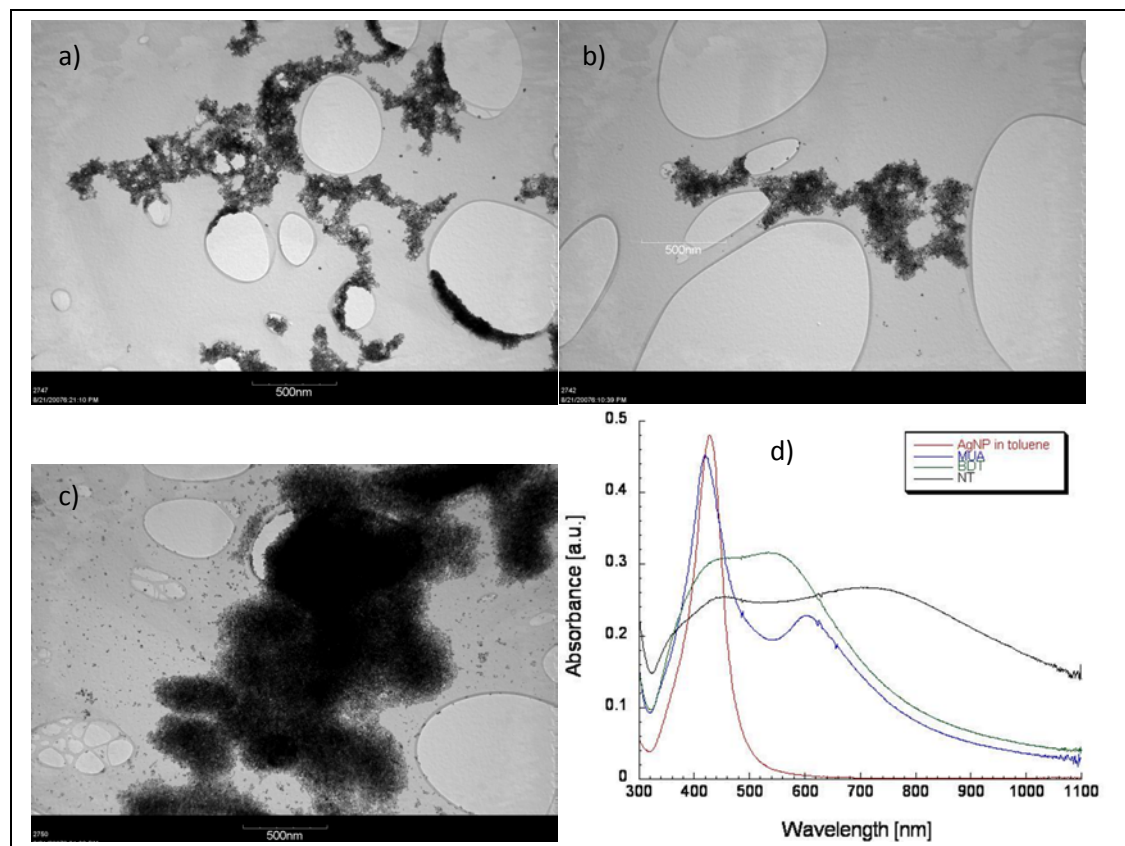
Figure 5. TEM images of a) MUA induced aggregates, b) BDT induced aggregates and c) NT induced aggregates. UV-vis absorption of the above aggregates is shown in d).

In the second approach, BDT is providing two strongly binding sides, which forms similar aggregates as in the former approach. The third approach uses π-π stacking interaction between NT ligands, which also readily exchanges OLA. This aggregation on the other hand leads to bulky almost spherical structures that tend to further aggregate with each other. The aggregates produced by the 3 methods can be sedimented by centrifugation and cleaned by disposing the supernatant and then redispersed in a solvent of choice. They were also proven to be able to form good optical quality films when embedded in PMMA matrix. The extinction spectra of the aggregates are red-shifted with respect to the spectra of the free nanoparticles and the shift is more significant for the more bulky morphologies.

4. Optical limiting

   The influence of silver nanoparticle aggregates on optical limiting of nonlinear medium has been studied using nanosecond laser at 532nm in f/5 geometry with the beam focused inside 1 cm cuvette. The nonlinear medium was 0.12M solution of TPD in toluene. Ag nanoparticle aggregates has been prepared using BDT as the aggregating agent and dispersed in toluene and the concentration has been chosen to obtain 60-70% transmittance.
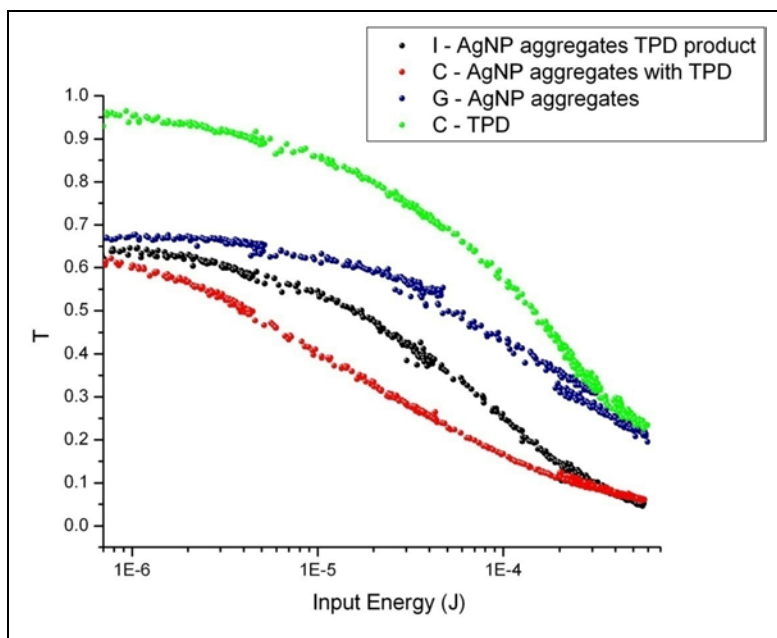
Figure 6. Optical limiting of 0.12M solution of TPD (green), silver nanoparticle aggregates (blue), the mixture of 0.12M solution of TPD and silver nanoparticle aggregates (red) and product of TPD solution with suspension of silver nanoparticle aggregates – green * blue = (black)

The focus of the experiment was to look at differences in nonlinear response of the TPD solution mixed with nanoparticle aggregates with the product of the optical limiting responses of TPD and AgNP aggregates measured separately. The optical limiting responses are shown in Figure 6. TPD – green, the nanoparticle aggregates in toluene – blue, the mixture of the TPD with AgNP aggregates – red, and multiplied transmittance of TPD solution with suspension of silver nanoparticle aggregates – green * blue = black. The last two curves (red and black) should be overlapping or be close to each other assuming no interaction or enhancements taking place. However, what has been observed is faster turn on of the mixture (red) with respect to the product (black). The results have been reproduced and the difference is considerable taking into account very low concentration of the AgNP aggregates (<0.1 w %). Going further into the higher energies (10^{-4} J) the difference in the response of these two samples decreases and finally overlaps at even higher energies. The decrease in this enhancement is most likely due to loss of the aggregates at those high intensities, which has been observed by drastically decreasing plasmon absorption at the pump wavelength after the measurement.

5. Femtosecond Z-scans

In order to further investigate the nonlinear behavior of the TPD-AgNP mixture a series of femtosecond z-scans at 535 nm have been done. In a similar fashion to the nanosecond optical limiting experiments, z-scans of three samples were compared to each other (Figure 7). First sample contains AgNP aggregates suspension in toluene / DMF mixture. The aggregates in this

case have been prepared by aggregation of silver nanoparticles functionalized with TPD($C_8H_{16}SH$) by dispersing of the nanoparticles in 1:1 mixture of toluene / DMF. The z-scan (a) show only saturable absorption by the AgNP aggregates, which is much stronger than the nonlinear absorption by the TPD ligand due to the very low concentration of the TPD ligands. The second sample (b) is a 0.11M TPD solution in 1:1 toluene / DMF mixture.
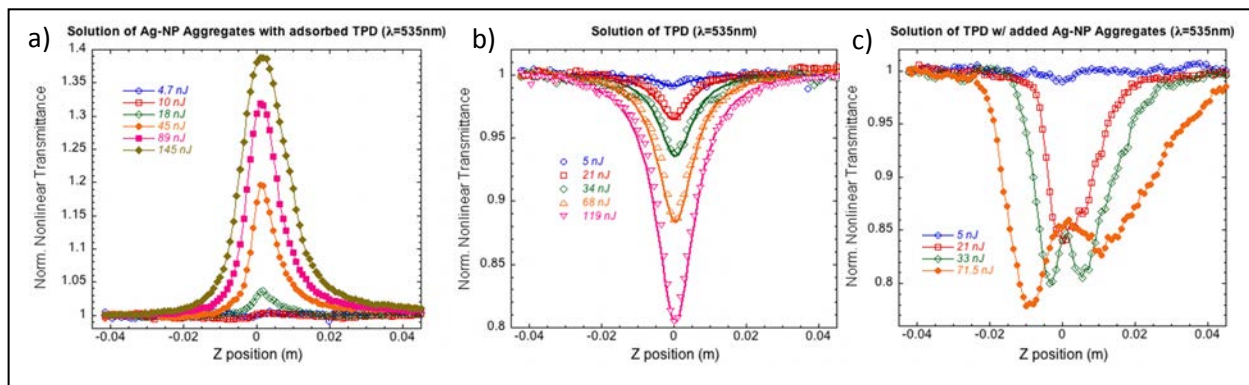
Figure 7. z-scan measurements of a) AgNP functionalized with TPD($C_8H_{16}SH$) aggregates in 1:1 toluene / DMF mixture, b) 0.11M TPD solution in 1:1 toluene / DMF mixture, c) AgNP in 0.11M TPD solution in 1:1 toluene / DMF mixture. All z-scans have been done in 1mm cuvettes.

The response of this sample is slightly dependant on the irradiance and it can be very well fitted using two-photon plus excited state absorption. In the third case (c) the same procedure to prepare AgNP aggregates in 0.11M TPD solution in 1:1 toluene / DMF mixture results in much smaller or no aggregation of the particles. High concentration of TPD changes solubility of the nanoparticles, which prevents the aggregation. The z-scan measurement of this sample is surprisingly different from both a) and b). The curves are asymmetric, which could be attributed to formation of some longer living transient species or permanent change of the material e.g. formation of TPD cationic species. A control sample of TPD in a 1:1 mixture of toluene / DCM has been prepared, since DCM is known to promote cationic species formation at high excitation intensities.

In order to refresh the spot at which the sample was excited it was translated vertically during the z-scan. The comparisons of the z-scan measurement with and without vertical scanning (Y-scan) are shown in Figure 8a. There is no difference in z-scan profile and intensity in case of the TPD solution in toluene / DMF mixture. A large difference is observed for TPD in presence of AgNP, where the z-scan profile is more symmetric and much smaller in amplitude when the sample is Y-scanned. A difference is also quite large for TPD in toluene / DCM mixture. Series of z-scans with Y-scanning has been measured for TPD in presence of AgNP (c), and TPD in toluene / DCM mixture (d). The z-scan data have been fitted for TPD in toluene / DMF and for the series (c) and (d). The extracted two-photon cross-sections vs. irradiance are shown in Figure 9.

23
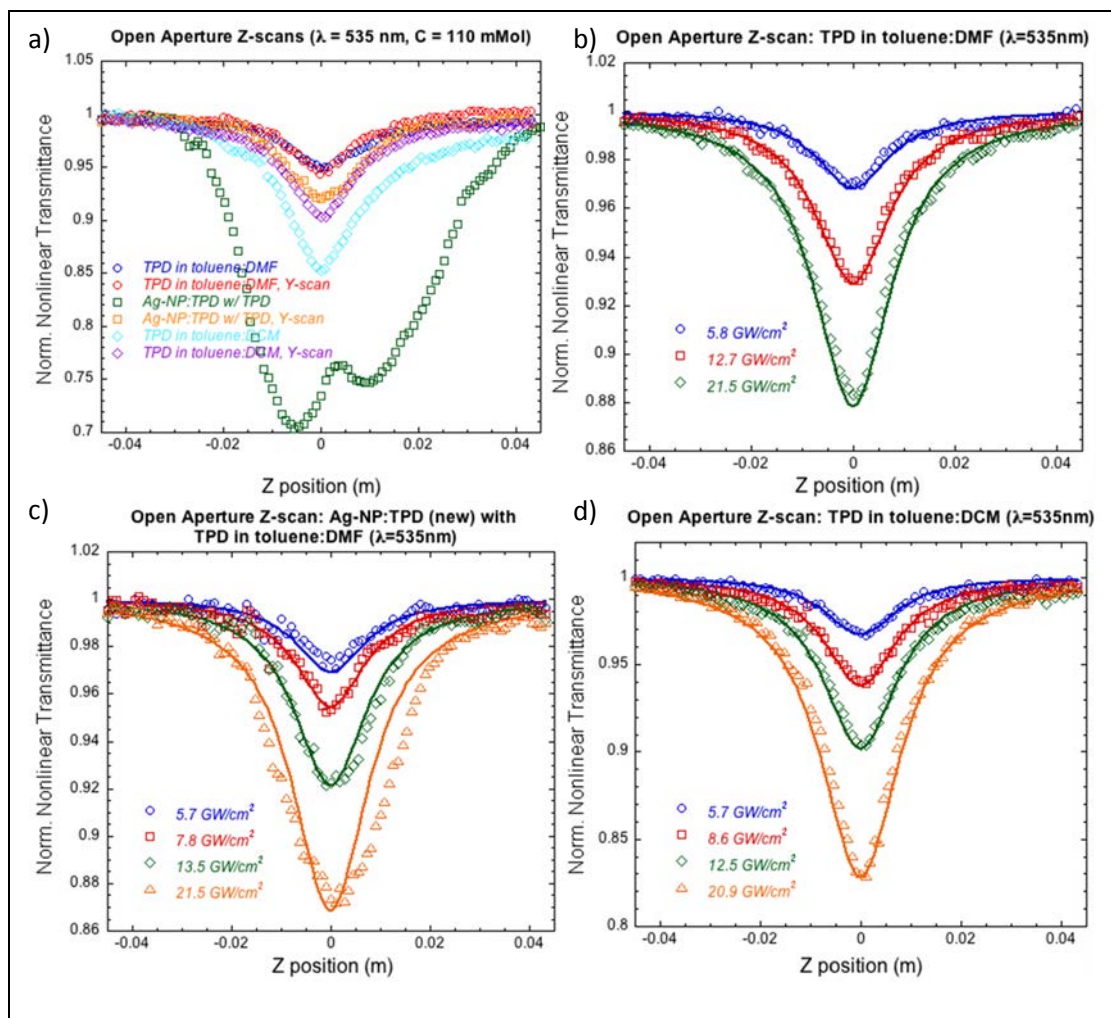
Figure 8. a) Comparison of z-scans without and with vertical scanning (Y-scan) of 0.11M solution of TPD in 1:1 toluene / DMF mixture – blue with and red without Y-scanning, TPD with AgNP – green with and orange without Y-scanning, TPD in 0.11M 1:1 toluene / DMF mixture – turquoise with and violet without Y-scanning. b) z-scan of TPD in toluene / DMF mixture, c) z-scan of AgNP with TPD in toluene / DMF mixture, d) z-scan of TPD in toluene / DCM mixture.

In all cases the two-photon cross-sections increases with increasing irradiance, which suggests excited state absorption (ESA) following the two-photon absorption (2PA). (ESA) is much more strongly dependent on irradiance for the TPD solution in toluene / DCM (green) than for TPD in toluene / DMF (blue), however at low energies they seem to be of similar value at irradiance 0 when extrapolating the plotted trend lines. The stronger dependence of the 2PA cross-section on irradiance indicates larger contribution of the ESA and the pure 2PA contribution can be obtained by extrapolation of the trend lines to irradiance 0. The two-photon cross-section behavior of TPD solution in presence of AgNP (green) has similar slop to the TPD in toluene /

DMF mixture and it is substantially offset, which results in higher value of 2PA cross-section at irradiance 0 when extrapolated.
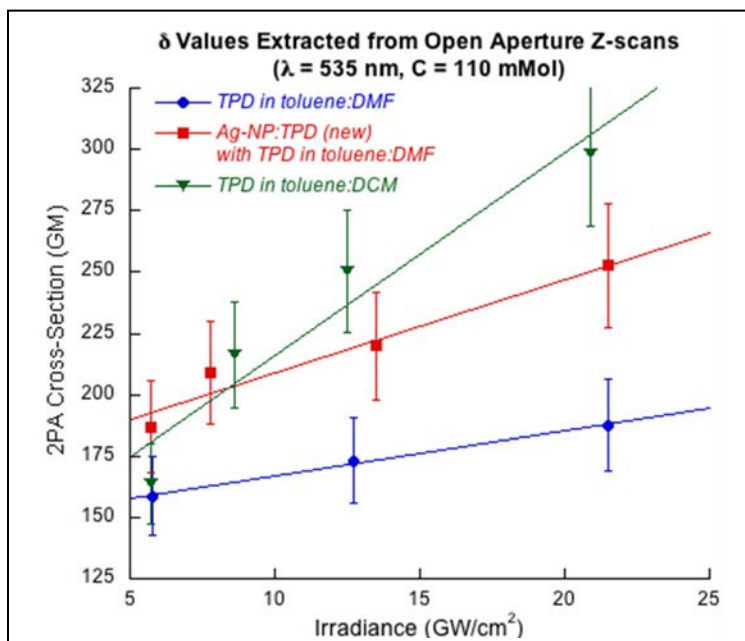
Figure 9. Two-photon cross-sections of TPD vs. irradiance for three different systems: 0.11M TPD solution in 1:1 toluene / DMF mixture – (blue), AgNP in 0.11M TPD solution in 1:1 toluene / DMF mixture – (red) and 0.11M TPD solution in 1:1 toluene / DCM mixture.

behavior of TPD solution in presence of AgNP (green) has similar slop to the TPD in toluene / DMF mixture and it is substantially offset, which results in higher value of 2PA cross-section at irradiance 0 when extrapolated.

Investigation of the plasmonic enhancement of silver aggregate/chromophore composites and the photophysics of gold nanoparticles with attached chromophores

We are investigating the plasmonic enhancement of nonlinear absorption properties of chromophores in proximity to metal nanoparticles or nanoparticle aggregates. Large enhancements in two-photon excited fluorescence have been reported previously for conjugated polymer films coated onto or thiolated chromophores adsorbed onto sedimented Ag nanoparticle clusters. Our team is working on several avenues to probe whether enhanced nonlinear absorption by plasmonic effects can be observed in pulse energy dependent transmission experiments. Such effects would be of high interest for use in ultrafast optical switching and in optical limiting. Convincing evidence of plasmonic enhancement of nonlinear absorption as opposed to irreversible laser induced processes such as photomodification of metal nanoparticles or aggregates is lacking. Thin films of fractal aggregates do not appear to be suitable systems for achieving clearly measureable nonlinear absorption enhancement, because of the limited interaction length and range of the enhanced field distribution around the particles and because of extreme localized heating in such films under excitation with energetic nanosecond laser pulses. It is our hypothesis that small-sized, organic soluble metal nanoparticle aggregates

25

dispersed at moderate concentration (~10% by volume and with an interaction length that provides a reasonable transmission say ~ 70%) dispersed in a neat chromophoric liquid or solid phase or polymer solid solution could allow for both significant enhancement of nonlinear absorption of laser pulses and dissipation of absorbed energy without major irreversible changes. To this end, we have been working to develop methods for the preparation or organic soluble and reasonably robust aggregates of metal nanoparticles.

As discussed earlier, we described an approach for preparation of narrow size distribution Ag nanoparticles and several routes to induce aggregation of the particles, while also imparting solubility in organic solvents. We also detailed nanosecond pulse studies that gave evidence of enhanced nonlinear absorption, but also resulted in modification of the nanoparticle clusters during the experiment.

In this report, we describe our efforts over the past year during which we have been: 1) developing solid phase chromophore-metal nanoparticle composites and 2) investigating fundamental photophysics of metal nanoparticle-chromophore interactions as well as interactions between chromophores adsorbed on metal nanoparticles.

6. **Chromophore-Ag nanoparticle cluster composites** We have investigated the use of two-photon absorbing chromophore materials, that are able to be prepared as glassy films by melt processing, as hosts for organic soluble aggregates of Ag nanoparticles. We choose a chromophore (SJZ-III-19, synthesized by the Marder group, Figure 10) with a D-π-D (D = electron donor) structural design with alkoxy solubilizing groups, whose structure is shown in Fig. 10. This material can be melt processed at 80 C and quenched to form an optically transparent glass. Oleylamine coated silver nanoparticle of 8 to 10 nm diameters were treated with naphthylthiol to induce aggregation. The resulting aggregates are rather bulky and ellipsoidal in shape and show relative broad Plasmon resonance in the visible and near infrared out to > 1100 nm, as shown in Fig. 11. A solid mixture of sjz-III-19 and AgNP clusters were prepared by dissolving sjz-III-19 and AgNP aggregates in toluene, followed by removal of the toluene by flowing N_2 gas over the solution. The resulting nanocomposite solid was then melted at 80 °C between glass slides separated by a 25 mm spacer and then rapidly cooled to form a glass.
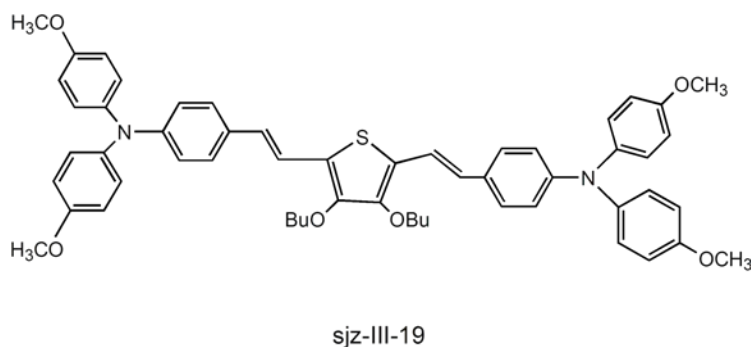
sjz-III-19

Figure 10. Structure of glass forming D-π-D compound; SJZ-III-19.
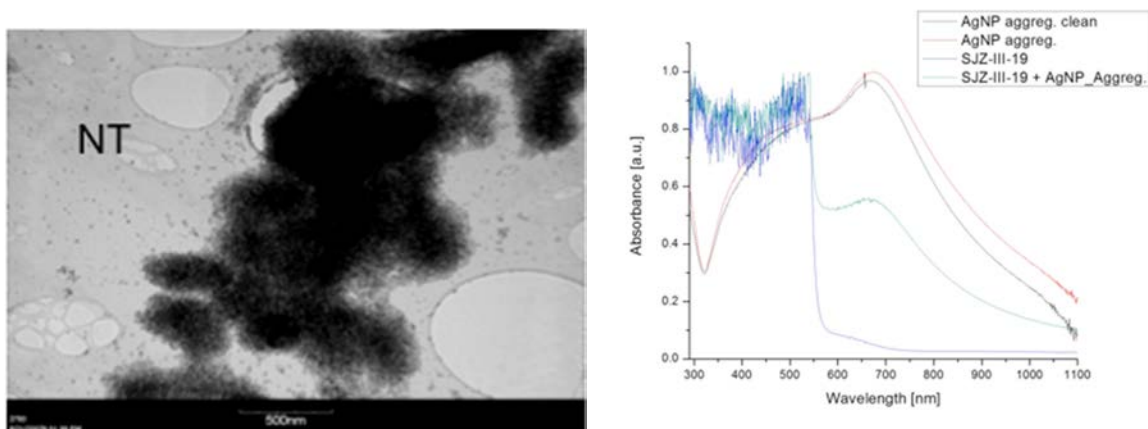
Figure 11. Left: TEM image of naphthylthiol coated Ag nanoparticle clusters, Right: Absorption spectra of Ag nanoparticle clusters, SJZ-III-19, and the SJZ-III-19/ Ag nanoparticle cluster glassy nanocomposite.

The neat SJZ-III-19 glass has very weak linear absorption in the range of 750-800 nm where the two-photon absorption band occurs. The nanoparticle clusters show strong Plasmon resonance in the same range which should be conducive to field enhancement of the two-photon absorption. Future studies will include optimization of the nanoparticle cluster loading to obtain a linear transmission of about 70% at 800 nm and energy dependent transmission measurements with femtosecond and nanosecond pulses.

7. Photophysics of gold nanoparticles coated with TPD chromophores

The photophysical properties of chromophore coated metal nanoparticles are of great importance with regard to the potential to realize plasmonic enhancement of nonlinear optical processes. Metal nanostructures can strongly influence the dynamics of both radiative and non-radiative processes leading to depopulation of excited states of dyes placed in close proximity to the metal. Energy and electron transfer from the photoexcited organic dye to the metal NP, as well as intermolecular interactions such as excimer formation, have been proposed as possible non-radiative channels of deactivation of excited states of dyes attached to these nanostructures. We have performed a fs transient absorption (TA) study addressing the influence of the linker length between a gold NP and a fluorescent organic dye on the excited-state deactivation dynamics of a TPD chromophore. Our results show that the excited state of the TPD dye is efficiently quenched by the Au NP and that a process involving chromophore-chromophore interaction can compete with the fast nanoparticle induced quenching and lead to the formation of a state with a 10-20 ps lifetime (perhaps an excimer) is turned on at the shortest linker length examined.
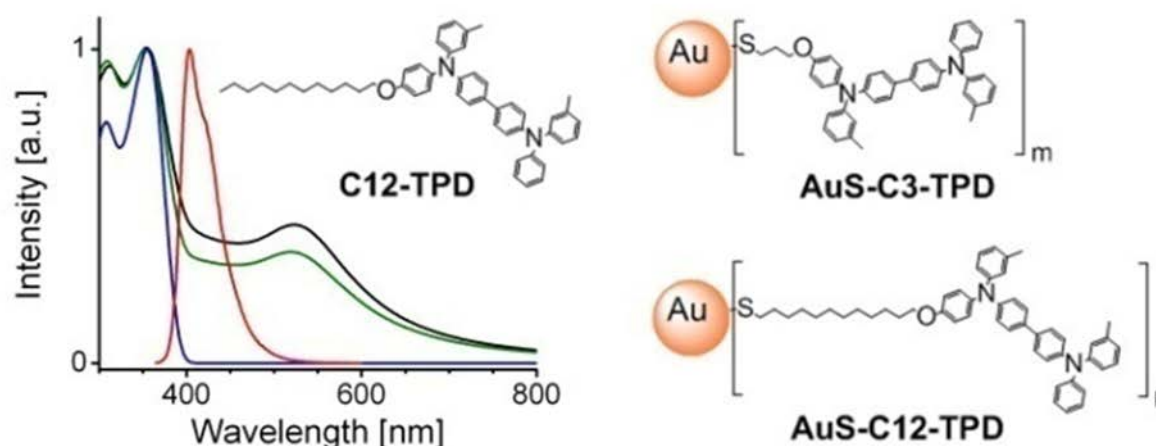
Figure 12. Absorption spectra of toluene solutions of AuS-C3-TPD (black line), AuS-C12-TPD (green line), and C12-TPD (blue line) as well as a fluorescence spectrum of a toluene solution of C12-TPD (red line). Structures of the systems studied herein.

Figure 12 shows a schematic representation of the studied systems and their absorption spectra, as well as the emission spectrum of a model compound, C12-TPD. The absorption spectra of the NP systems reveal the presence of the surface-plasmon resonance absorption band (~520 nm) typically observed for Au NPs with diameters larger than 2 nm.[11] Here, the diameters were estimated to be 3.5 ± 1.2 nm and 3.3 ± 1.1 nm for AuS-C3-TPD and AuS-C12-TPD, respectively. Absorption spectra of both NP systems reveal an absorption band around 350 nm, very similar to that measured for a toluene solution of C12-TPD, confirming the presence of the TPD moiety in the NP systems.

A sample of AuS-C12-TPD in toluene exhibited an ultrafast decay of the transient absorption (TA) signal (Figure 13). Fitting of the decay gave a time constant of 2.4 ps and a spectral distribution identical to an early time (ca. 1 ps delay) transient spectrum of photoexcited C12-TPD in toluene solution. For comparison, the excited-state lifetime of C12-TPD in toluene was measured to be ca. 700 ps. Thus, the lifetime observed for the TPD excited state in AuS-C12-TPD is more than two orders of magnitude shorter than for the same chromophore in solution, which is likely due to an efficient energy transfer from the photoexcited dye to the AuNP. In contrast to AuS-C12-TPD, AuS-C3-TPD showed rather different excited-state decay kinetics. Rather surprisingly, despite the dye being about 3 times closer to the nanoparticle surface in AuS-C3-TPD, the overall average TA signal lifetime (τav = 3.7 ps) was larger than that in AuS-C12-TPD (τav = 2.9 ps). The shapes of the kinetic profiles measured at 1000 and 1600 nm for AuS-C3-TPD in toluene are clearly different, implying the presence of at least two different species generated by photoexcitation.
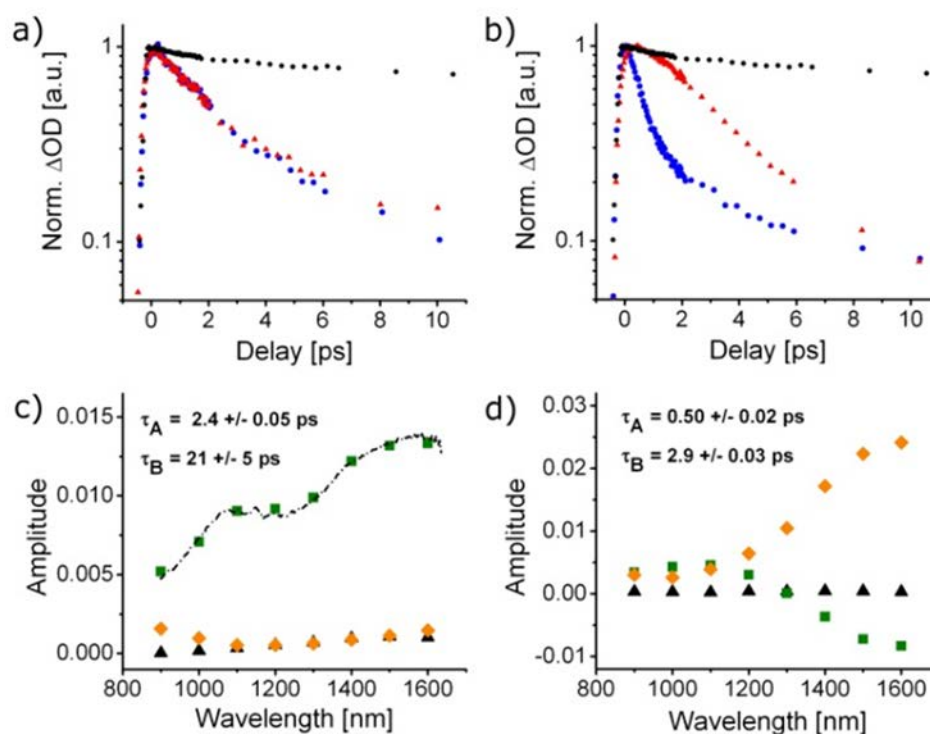
Figure 13. Normalized TA kinetic traces measured at (blue points) 1000 nm and (red points) 1600 nm for (a) AuS-C12-TPD and (b) AuS-C3-TPD in toluene; the black circles in both graphs represent the 1600 nm decay measured for a 0.1 M toluene solution of C12-TPD. Lifetimes and spectral distribution of amplitudes (green points for τA, orange points for τB, red points for an offset) from global fitting of the data with a sum of two exponential decays for (c) AuS-C12-TPD and (d) AuS-C3-TPD; the dashed line in c) shows the profile measured at a delay of ca. 1 ps for a 0.1 M C12-TPD toluene solution.

Measurements were also made on AuNPs coated with mixed monolayers consisting of dodecanethiol in combination with either TPD-C12-thiol or TPD-C3-thiol. A comparison of kinetic traces measured for AuS-C3-TPD with those measured for the corresponding mixed monolayer system (ca. 60% dodecanethiol and 40% of TPD-C3-thiol) shows that diluting TPD-C3-thiol with dodecanethiol on the surface of Au NPs leads to a change in the kinetics of the photoexcited sample, while no difference was observed between the decay kinetics of AuS-C12-TPD and the corresponding mixed monolayer system. These data suggest that the process leading to the alkyl-spacer-mediated differences in the photophysics involves interaction between surface-bound dyes (likely leading to an excimer or charge separated state) rather than interaction between the Au NP and the dye.

Future studies will be performed using Ag nanoparticle cores as well as different types of chromophores to understand better the role of chromophore- nanoparticle vs. chromophore-chromophore interactions on the surface of metal nanoparticles and to seek systems wherein the excited state or photogenerated species exhibit long lifetimes and strong excited state absorption.

8. Effects of AgNP on the relaxation of photo-excited TPD

A main goal of this work was to develop an understanding of the relaxation pathways involved in the deactivation of photoexcited bis(diarylamino) biphenyl (TPD) chromophores in close proximity to silver nanoparticles (AgNP). The TPD chromophores were attached to the silver nanoparticle core via an alkylthiol group. The TPD-AgNP systems were synthesized and characterized using Transmission Electron Microscopy (TEM), UV-visible absorption, infrared spectroscopy, and Nuclear Magnetic Resonance (NMR) spectroscopy, Inductively Coupled Plasma – Emission Spectroscopy (ICP-ES) and Thermogravimetric Analysis (TGA). Time-resolved photophysical processes in these systems were studied using femtosecond transient absorption spectroscopy.

Initial studies of the interaction of the TPD and AgNP addressed the linker length dependence of the dye excited state decay kinetics, wherein alkyl linker chains of 3, 4, 8 and 12 carbon atoms were used. These results showed that an ultrafast deactivation of the excited state of the TPD chromophore, which is three orders of magnitude faster than that of the free chromophore in solution, occurred in all of the systems (Figure 2a). However, an unexpected new transient species was observed for the systems with three and four carbon linker chains (Figure 2b). Further studies showed this species to be spectroscopically very similar to the TPD radical cation (Figure 3), suggesting a charge separation pathway in the excited state relaxation. Possible pathways for formation of the cation-like state included 1) direct two-photon photoionization of TPD, 2) photoinduced electron transfer from the excited TPD to the metal nanoparticle, or 3) a bimolecular mechanism that involves a pair of excited TPD molecules undergoing exciton-exciton annihilation and producing the cation like species from an intermolecular charge separation from the higher excited state formed via annihilation. These possibilities were examined through comparisons to the photophysics of alkyl substituted TPD in solution and in solid films, investigation of the pulse energy and TPD surface coverage dependence of the yield of the cation-like TPD species, transient absorption anisotropy decay dynamics, and kinetic modeling studies. Taken together, these investigations provide support for exciton-exciton annihilation being responsible for the formation of cation-like species. The packing of the TPD chromophores is concluded to be of critical importance in the generation of the cation like species but it is also possible that proximity to the silver nanoparticle plays a role in facilitating charge separation as well.
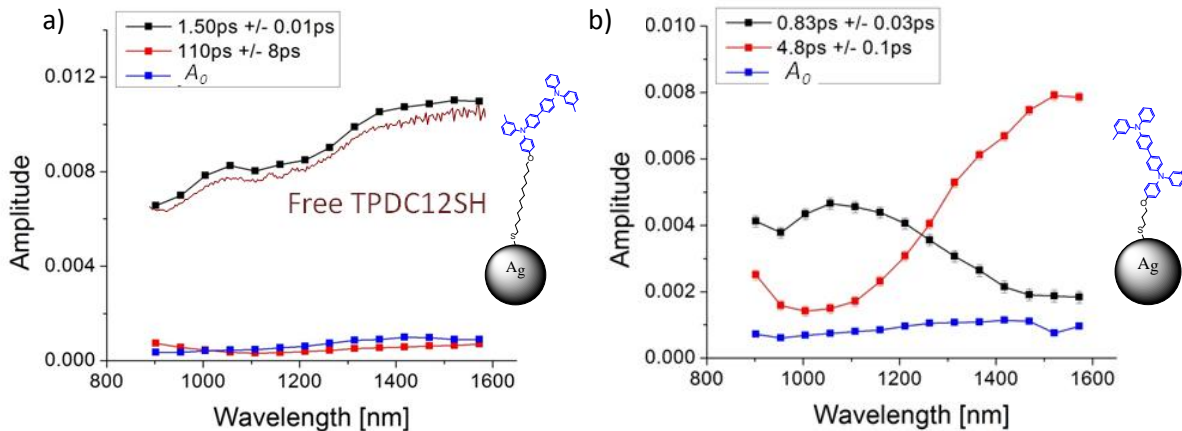
Figure 14. Spectral distributions of pre-exponential amplitudes obtained from global fitting using double exponential function for TPD-AgNP spaced by a) 12 carbon linker and b) 3 carbon linker. Plot a) also contains early stage transient absorption spectrum of a free TPD ligand. The lifetimes corresponding to the plotted amplitudes are shown in the legends. The lifetime corresponding to the free TPD ligand is ~1.6 ns.
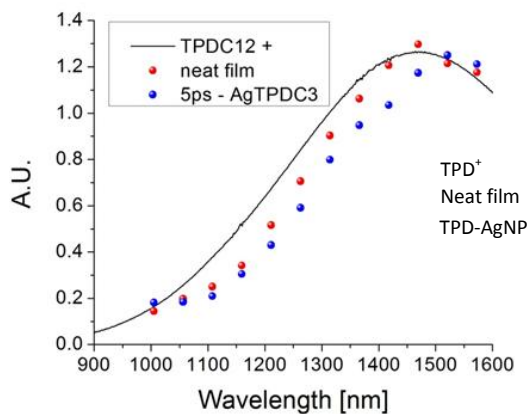

Figure 15. NIR absorption spectrum of radical cation of TPD in DCM overlaid with spectral profiles of the offset ($A_0(\lambda)$) component obtained from global fitting analysis of neat film of TPD moiety and spectral profiles of pre-exponential amplitudes associated with time constant of 5 ps of the sample TPD-AgNP separated by 3 carbon atom linker. Cationic band is not observed in dilute solutions of TPD or polystyrene films doped with TPD, which indicates TPD-TPD interactions leading to the cation formation.

9. Nanosecond Optical Limiting in TPD/AgNP aggregates

The earlier optical limiting experiments with ns pulses were repeated with freshly prepared Ag nanoparticle aggregates using the same geometry as described before. The influence of silver nanoparticle aggregates on optical limiting of nonlinear medium has been studied using nanosecond laser at 532nm in f/5 geometry with the beam focused inside 1 cm cuvette. The nonlinear medium was 0.12M solution of TPD in toluene. Ag nanoparticle aggregates has been prepared using BDT as the aggregating agent and dispersed in toluene and the concentration has been chosen to obtain 60-70% transmittance. (Limiting experimental conditions: Laser wavelength-532 nm, ~5 ns, **10 Hz**, 1 cm path length, f/5 optics, with the laser beam focused near back surface of the cell with a top hat spatial profile).
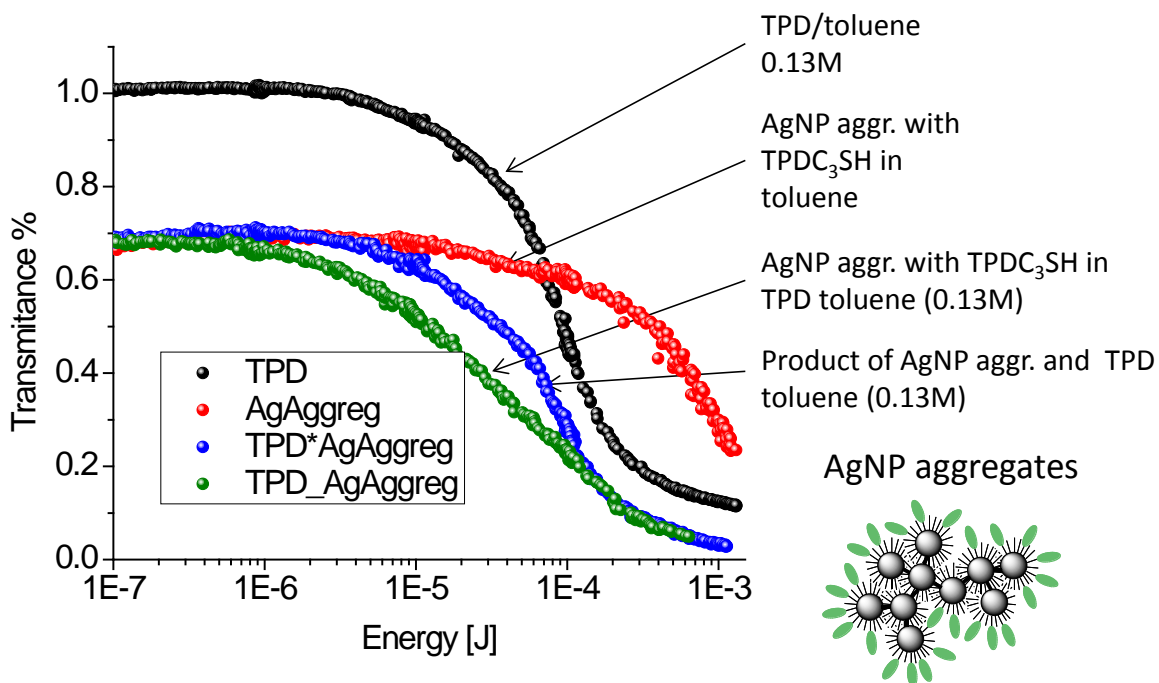
Figure 16. Optical limiting in mixture of a TPA dye (TPD, 0.13 M) and Ag nanoparticle aggregates at 532 nm.

Figure 16 shows the optical limiting responses from a neat TPA dye (TPD in Toluene), neat Ag nanoparticles with TPDC3SH in toluene as well as that of a mixture of TPD/Ag nanoparticle aggregates in Toluene. The figure also contains (blue) a limiting trace obtained from a product of neat TPD dye limiting and neat Ag nanoparticle aggregates. Although the overall suppression of the pulses not very different between the OL responses, the threshold energy for limiting is significantly reduced in the case of TPD/Ag nanoparticle aggregates compared to the neat TPD and neat Ag nanoparticle aggregates. This suggests that the presence of plasmonic absorption (arising from presence of Ag nanoparticle aggregates) in the TPD/Ag aggregates in the vicinity of the TPA absorbing TPD chromophores reduces the threshold for limiting owing to the

resonance between the two-photon absorption maximum of TPD and the aggregate absorption band around 532 nm. However, the absence of any significant increase in the suppression of the over all pulses in the case of TPD/Ag nanoparticle aggregates compared to the neat TPD and neat Ag nanoparticle aggregates is essentially due to the limited concentration of the TPD itself. In order to increase the concentration of the TPA dye, we have attempted to use more soluble TPA chromophores having similar TPA absorption cross-sections.

First, we tried to use the mono-thiophene based BSB-like TPA chromophore to attain higher concentration the owing to the presence of the alkoxyl groups on the thiophene moiety. This chromophore although has a moderate TPA cross-section, does not have higher solubility than 0.1 M.
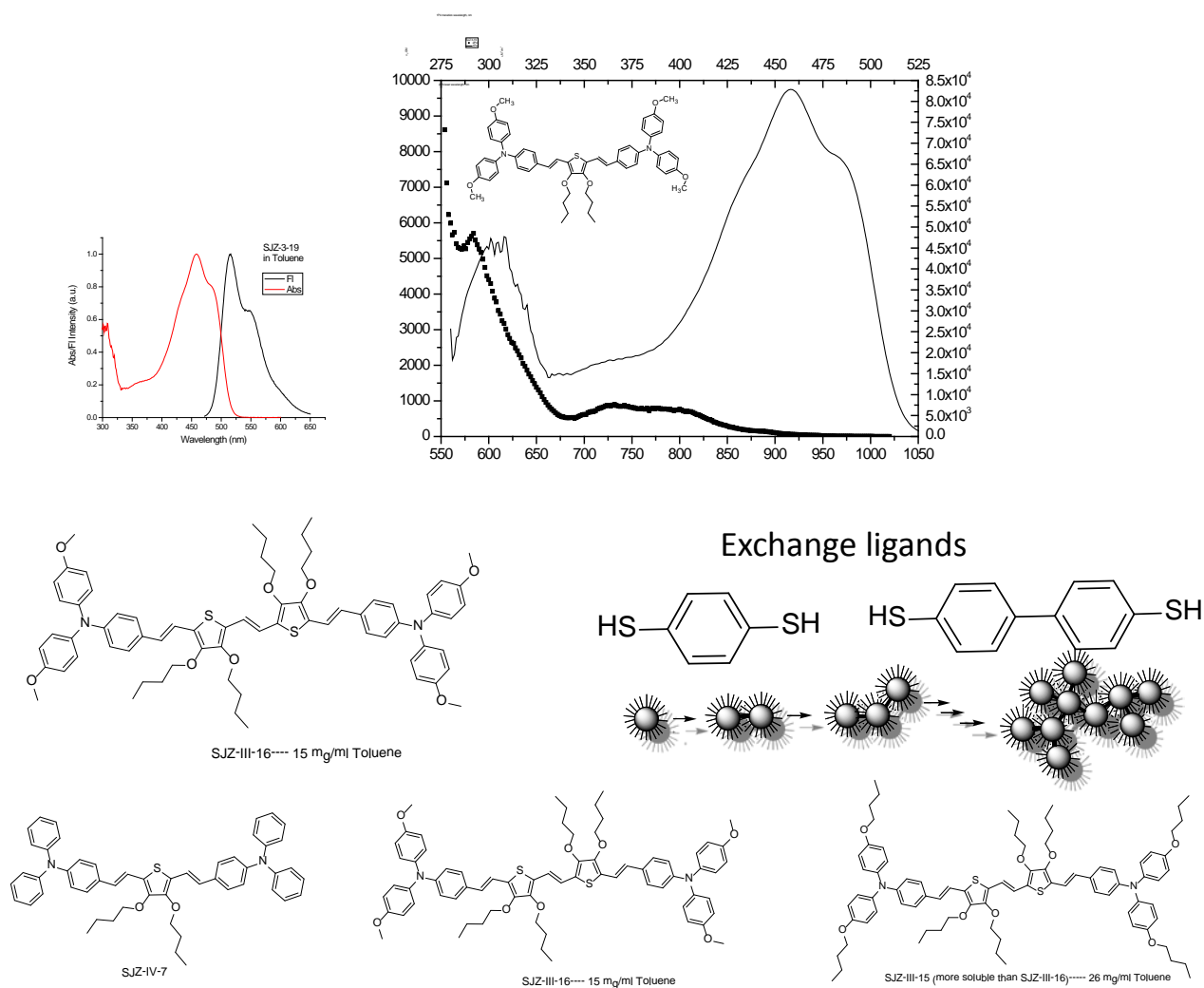
Figure 17: Linear absorption and Two-photon absorption spectra of a monothiophene TPA chromophore (SJZ3-19) in Toluene.

Earlier screening of BSB dyes in our group has shown the following chromophore (labeled as liquid TPA chromophore and will be referred to as HxThio in this report) to be a useful material for near-IR optical limiting. During our studies we have also found that this dye is extremely soluble in Toluene as well as a few other solvents. Owing to the high solubility (1.5 M) of this chromophore we have remade this chromophore to investigate the use of this chromophore in the plasmon absorption enhanced TPA optical limiting. The structure, absorption, fluorescence and limiting behavior are shown in the following figure "17 addition".

Higher concentration of TPA chromophore

Liquid TPA Chromophore
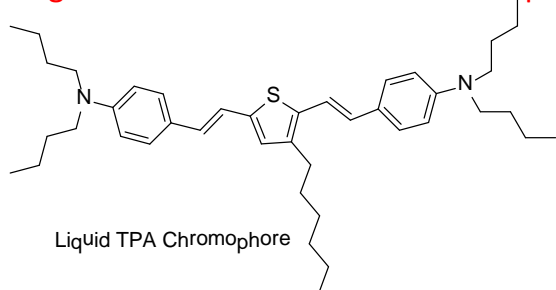
λ nm, (TPA)	δ (GM)
690	1,500
730	1,000

Absorption and fluorescence spectra of ThipheneBSB in Toluene
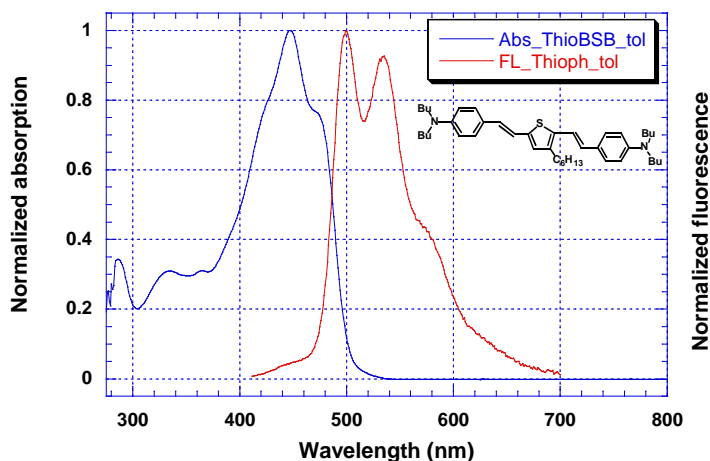
Normalized OL - ThiophBSB / Toluene @ 690 and 730nm 0.15 M
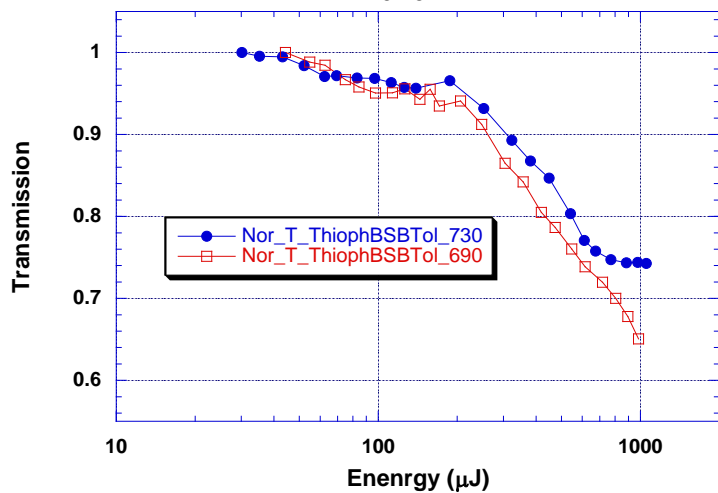
Fig. 17 addition

HxTHio chromophore was synthesized in our group by one of our graduate student, John Tilloston. The synthetic scheme employed is shown below starting with 2, 5-dibromo-3-hexylthiophene in several steps. The chromophore was purified by repeated recrystallization from solution. The linear absorption and fluorescence spectra of HxThio in Toluene is shown the following Figure 18.
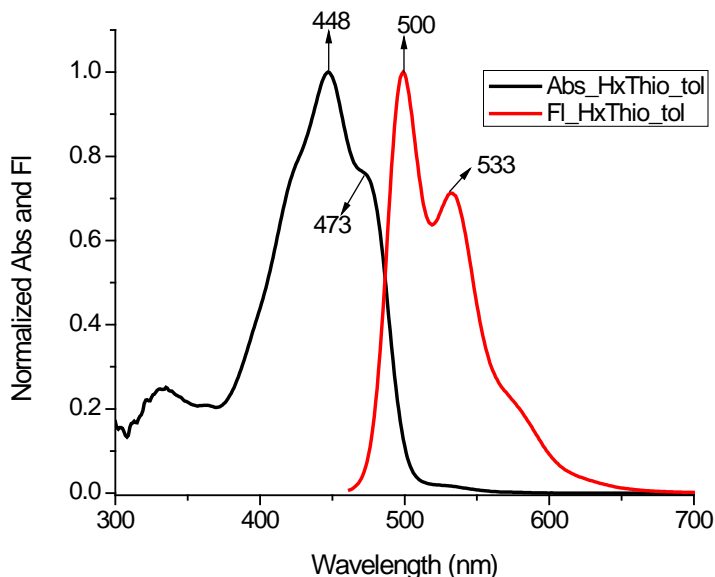
Figure 18: Linear absorption and fluorescence spectra of HxThio in Toluene.

The two photon absorption spectra of the chromophore were measured using the two-photon induced fluorescence technique (Rapid, broadband two-photon-excited fluorescence spectroscopy and its application to red-emitting secondary reference compounds Nikolay S. Makarov, Jochen Campo, Joel M. Hales, Joseph W. Perry, Optical Materials Express, 2011, 1, 551). The measured two photon absorption spectrum along with it's two-photon cross section are shown Figure 19. The maximum cross-section of the TPA spectrum is 570 GM at 740 nm along with two more peaks at 810 nm (70 GM), 620 nm (~600 GM with one-photon resonance contribution). The TPA wavelength maximum is necessary to choose the appropriate nanoparticle aggregate having absorption around the same wavelength range as the two-photon maximum.
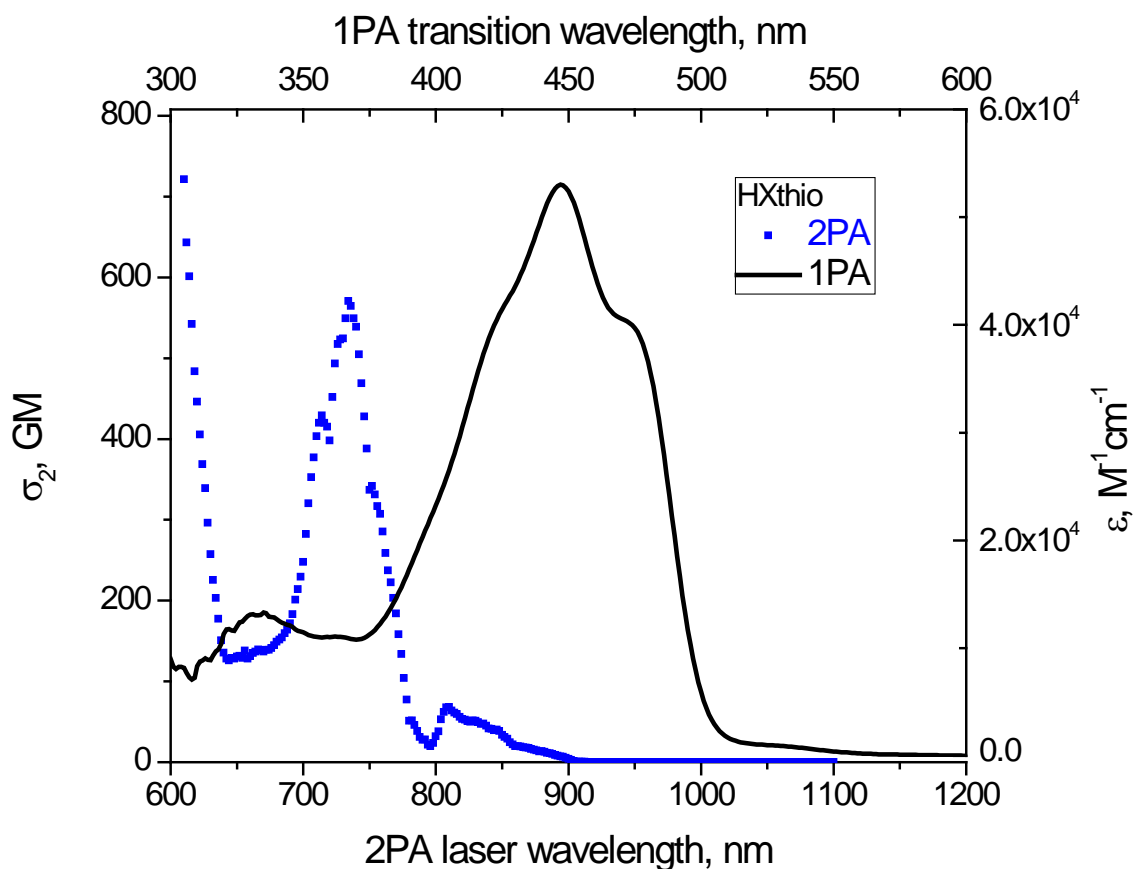
Figure 19: Linear and two-photon absorption spectra of HxThio in Toluene.

We have also measured the femtosecond pump-probe measurements to obtain the excited state absorption spectrum of HxThio in toluene. The excited state absorption shows maxima at 620, 700 and 920 nm (Figure 20). The excited state absorption at 700 and 920 nm are assigned to an excited singlet state with a similar decay time and the absorption at 620 nm is attributed to the triplet state with a decay time constant of about 1 ns. As a result, it is possible to carry out optical limiting experiments incorporating AgNP-aggregates with HxThio in Toluene @ 740 (singlet) and 620 nm (triplet).
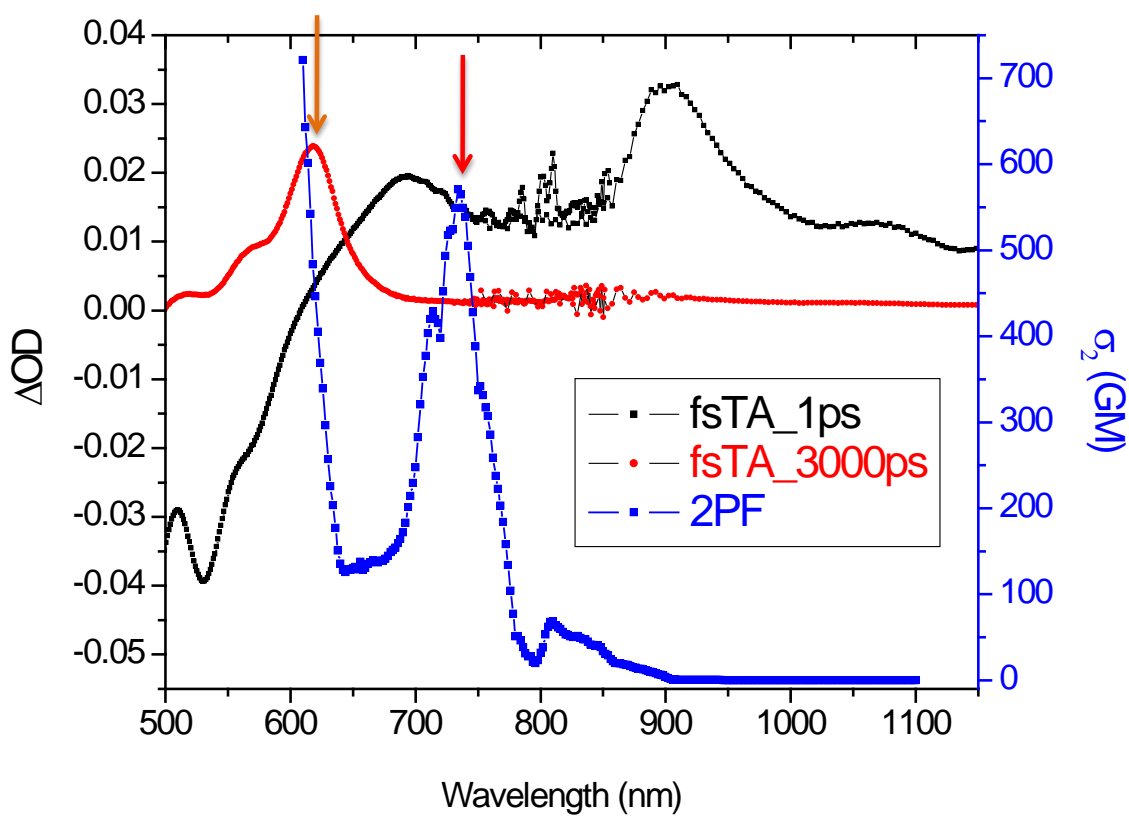
Figure 20: Two-Photon Absorption and fs-Transient Absorption Spectra of HxThio in Toluene.

Synthesis of Silver nanoparticle aggregates: The initial synthesis of Ag nanoparticle was accomplished by capping the as-synthesized particles with oleylamine to prevent aggregation and growth of larger Ag particles. The reaction was completed in 6.30 hrs vs 24 hrs used earlier. It seems like the purity of OLA may hold the key deciding the reaction time. The OLA was purified by vac. distillation and stored under inert atmosphere prior to the reaction. The nanoparticles were characterized initially by absorption, dynamic light scattering (DLS) and TEM measurements. Before getting to the results on the optical limiting experiments, we present the preparation of the nanoparticle aggregates in the following.

Silver nanoparticles capped with oleylamine were prepared by refluxing Silver nitrate and oleylamine in o-xylene at 136 °C. The progress of the synthesis was monitored by absorption spectra of the reaction mixture Figure 21. The particles were centrifuged and redissolved in Toluene. Ag nanoparticle aggregates were prepared by using various aromatic dithiols as cross-linkers. The nanoparticle aggregates were produced by mixing the Ag nanoparticles with various volume ratios of 1,4-Benzenedithiol (BDT), 4, 4'-Biphenyldithiol (BPDT), Naphthalene-9-thiol (NaphDT). Depending upon the required absorption range (to match with the TPA absorption

maximum of the chromophore) for the optical limiting experiments, different volume % ratios of the Ag nanoparticle and thiol were mixed in Toluene.

CH$_3$COOAg + OLA

oleylamine (OLA)

o-Xylene

reflux at 136 C

AgOLA NP

NH$_2$
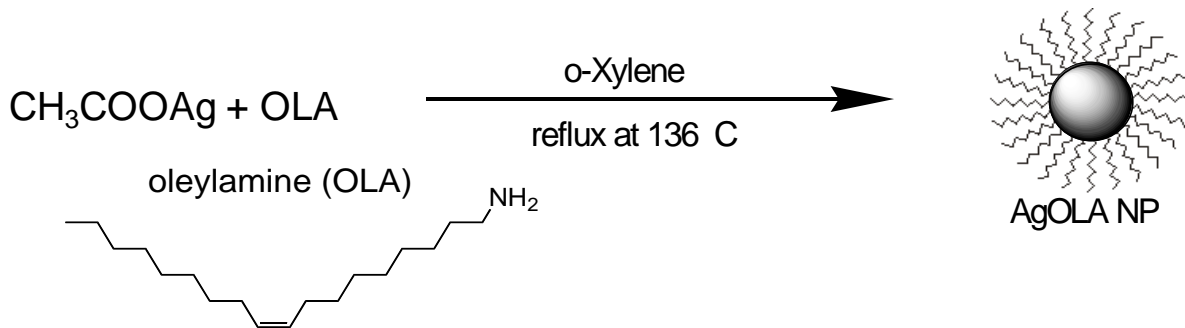
Synthesis of OLA capped Ag nanoparticles
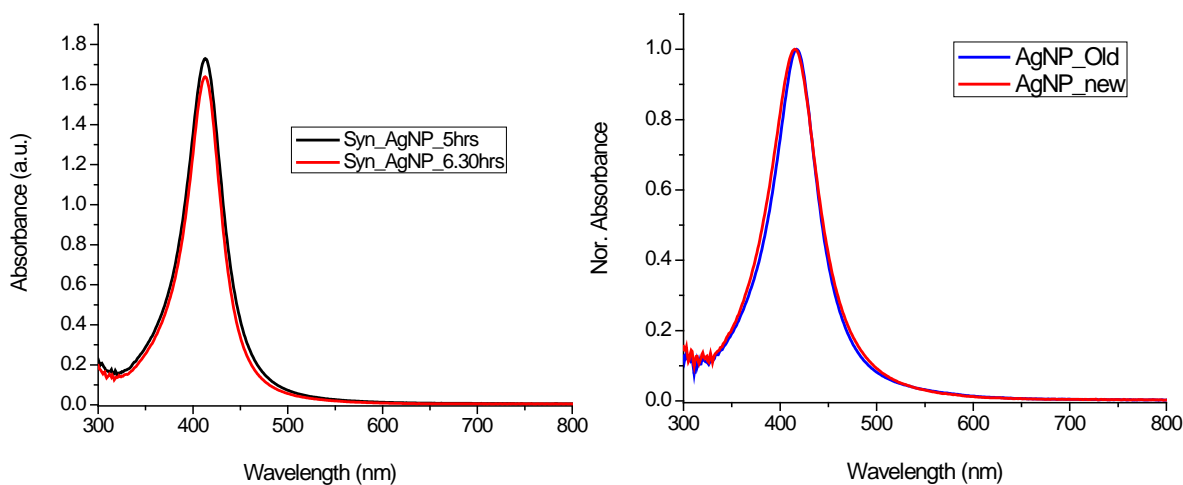
Figure 21: Synthesis of oleylamine-capped AgNP followed by absorption spectra (left after 5 and 6.30 hrs after the starting of the reaction. The right spectra show the reproducibility of the AgNP synthesis.

The following bulleted text refers to Fig. 22.

- Femtosecond Z-scan traces were obtained using an amplified femtosecond laser and OPO. The tunable laser system was used to measure Z-scan traces at 730 nm and 620 nm. The Z-scan data are shown in Figure 22. Z-scan measurements   on 25 um samples prepared from 1 M HxThio in Toluene sandwiched between glass slides with a 25 um PTFE spacer. Figure 22 shows the Z-scan data for HxThio chromophore, along with that for neat Ag nanoparticle aggregates and the mixture of HxThio+Ag nanoparticle aggregates at different laser power at 730 nm. Neat HxThio chromophore samples show a linear pump power dependence while the nanoparticle aggregate and the HxThio+aggregate z-scan traces exhibit a complex behavior possibly due to the breaking of the aggregates at higher laser power. In summary,
- HxThio chromophore only: Transmittance decrease with increasing power

- Ag nanoparticle Aggregate only: No consistency
- HxThio chromophore + Ag nanoparticle Aggregate: At higher power Transmittance increases.
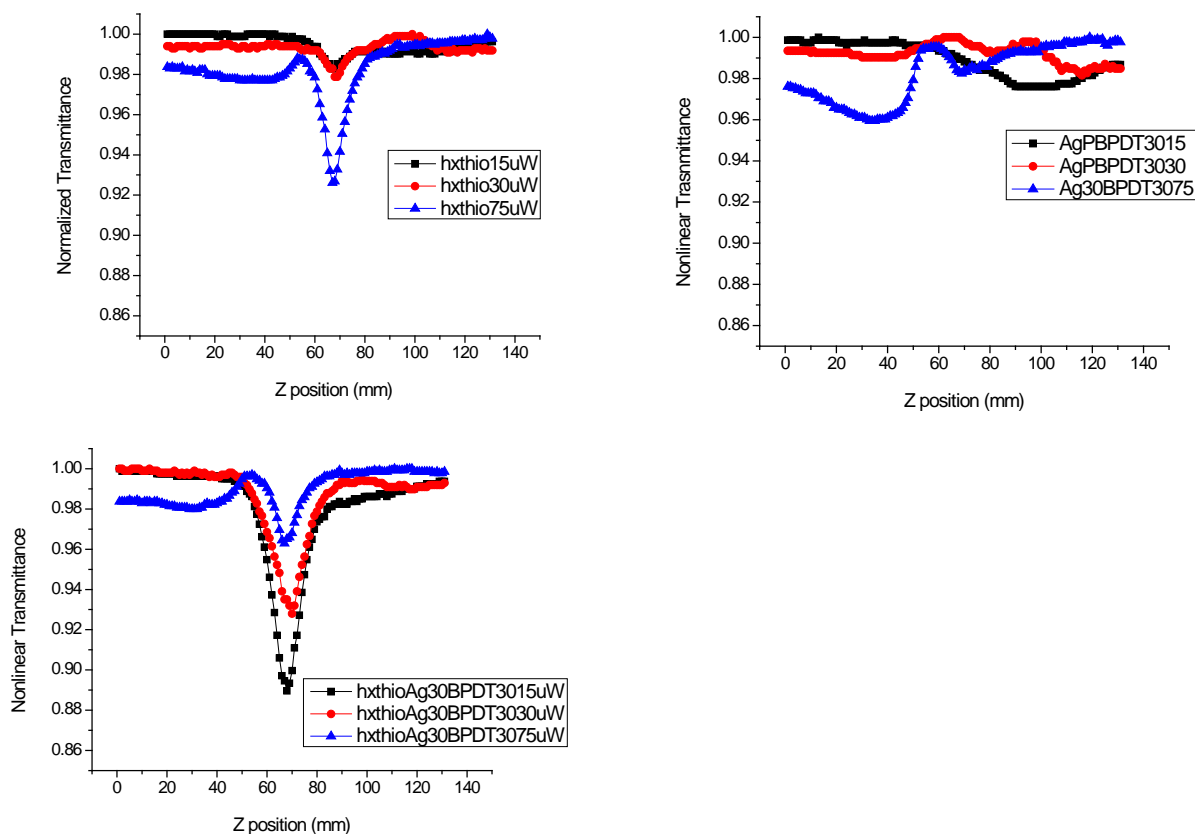
Figure 22: Pump power dependence of z-scan traces at 730 nm for neat HxThio, neat Ag aggregates and HxTHio+Ag aggregates.

The z-scan traces of the HxTHio+Ag aggregates at different power are shown in Figure 23 below. Except at 75 µW (the highest power used in the z-scan measurement), the traces show large increase in transmittance corresponding to an increase in the two-photon cross section of the chromophore-aggregate mixture. β values obtained by curve fitting of the z-scan traces vary from 0.5 to 28 for the chromophore-aggregate mixture at a laser excitation power of 15 µW at different spots. It is unclear at this time why the β values varied from spot to spot. We will try to measure the z-scan traces (using femtosecond pulses) and optical limiting (nanosecond pulses) in solution using a 1 cm cuvette which seem to be necessary to have sufficient absorption at the wavelength of interest from the Ag aggregates.
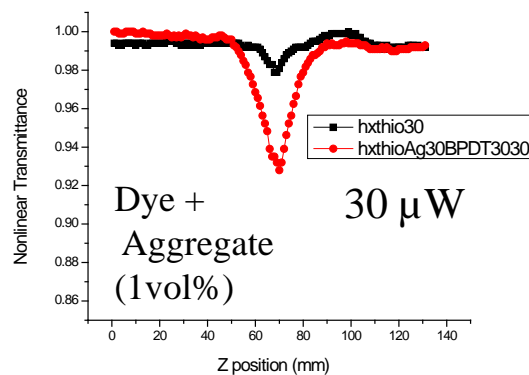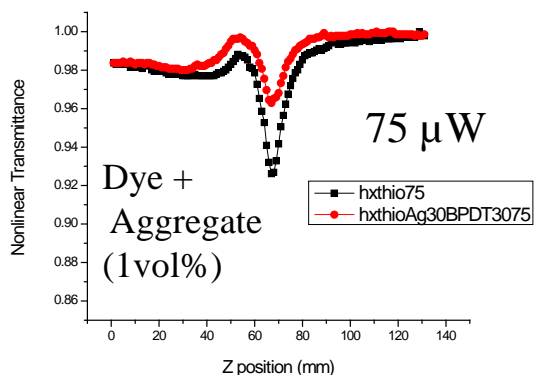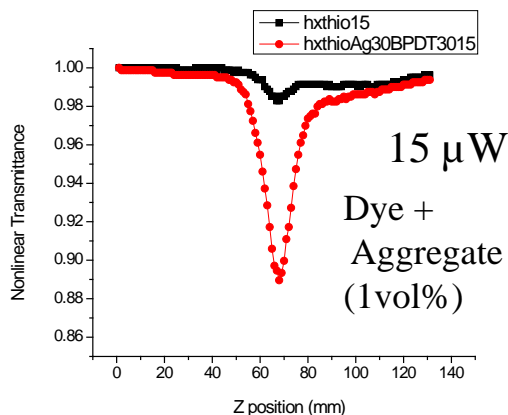
Figure 23: The z-scan traces of the HxTHio+Ag aggregates at different power.

In yet another approach toward demonstration of plasmon enhanced optical limiting, we have attempted to make use of the core-shell nanoparticle aggregates along with water soluble TPA chromophores. The core-shell nanoparticles consist of a Ag core and Silica shell. The silica shell is formed by the hydrolysis of tetraethoxysilane (TEOS) along with Ag core. The amount of TEOS used in the process determines the shell thickness (REFERENCE). The absorption spectra of the core-shell particles formed following hydrolysis of different amounts of TEOS. The measured spectra show broad spectral features in the near IR region (**Figure 24**). SEM and TEM images of the core-shell particles reveal the presence of silica shell enclosing oligomeric aggregates of Ag particles as shown below.
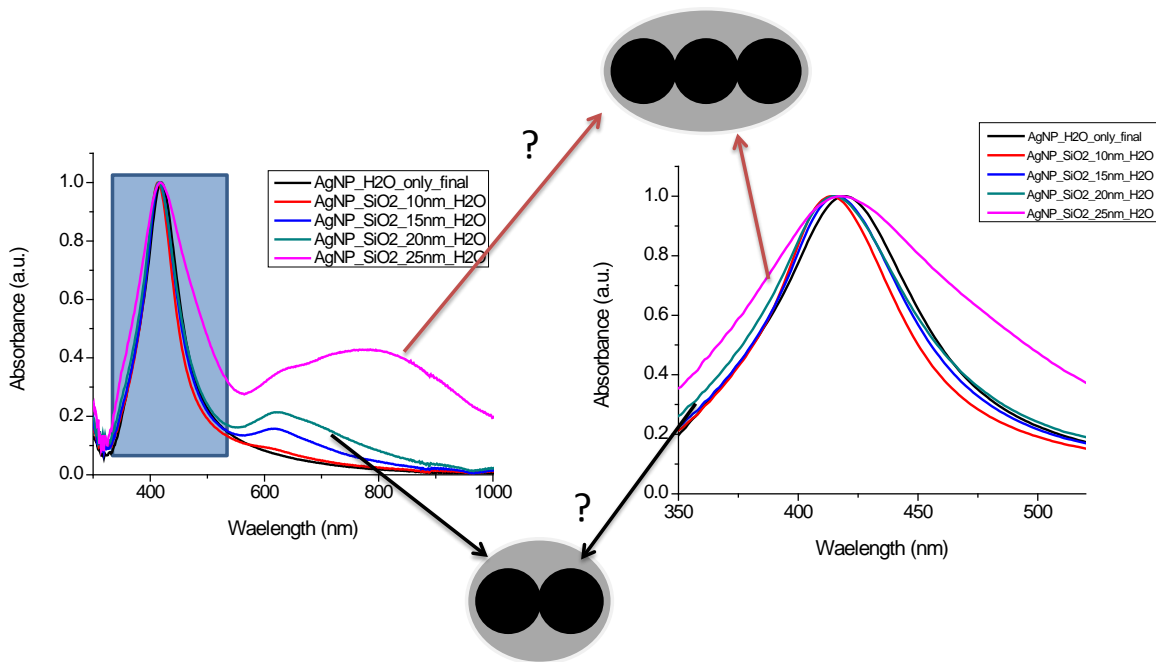
Figure 24: Absorption spectra of core-shell particles in water synthesized by mixing Ag core particles with different amounts of TEOS.

Absorption spectrum of the water soluble TPA dye (SO_3STNH_2) in water along with its chemical structure is shown below (Figure 25). Optical limiting responses of the dye in water, N-methylformamide and N, N- dimethyl formamide at 532 nm.

Absorption maximum @ 345 nm
Fl maximum @ 450 nm in Water

SO3STNH2 in water exhibits nanosecond
OL in the region of 532-600 nm
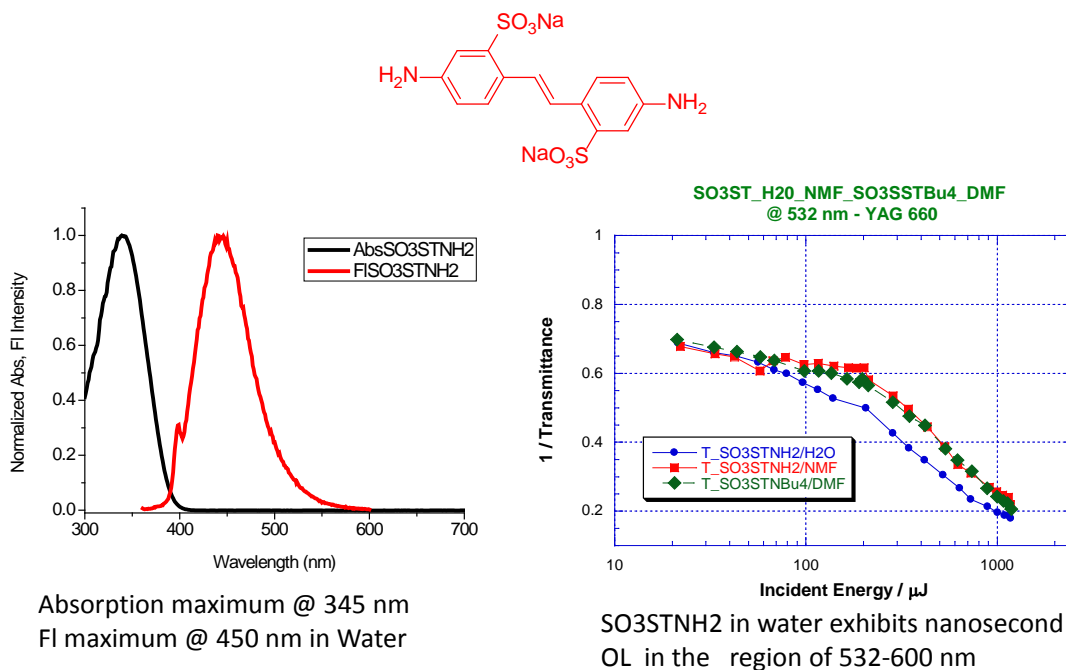
Figure 25: Absorption spectrum of the water soluble TPA dye (SO_3STNH_2) in water.

The transient absorption and TPA spectra of the SO_3STNH_2 in water are shown in Figures 26 and 27 respectively.
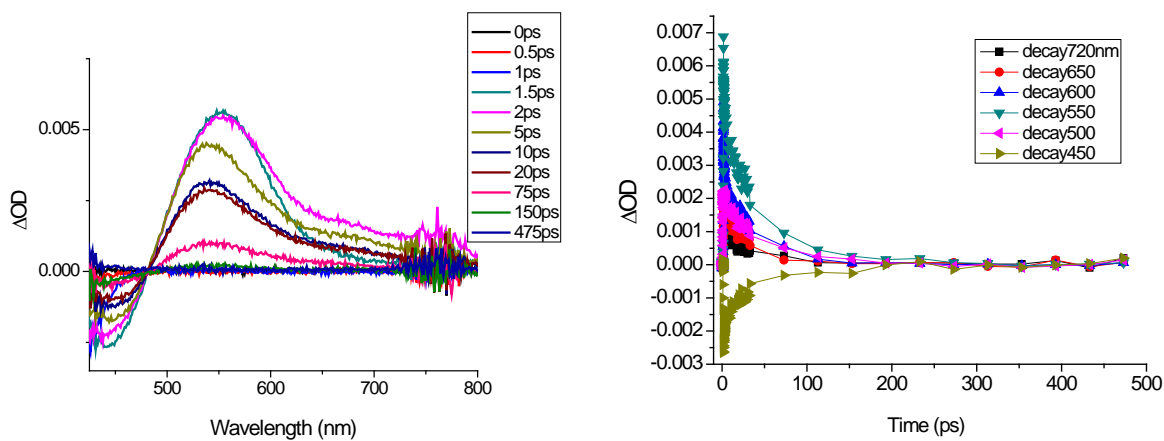
Dynamics @ 550 nm
Faster component: 0.7 ps
Slower component: 46 ps

Figure 26: Femtosecond transient absorption spectra of SO_3STNH_2 in water.
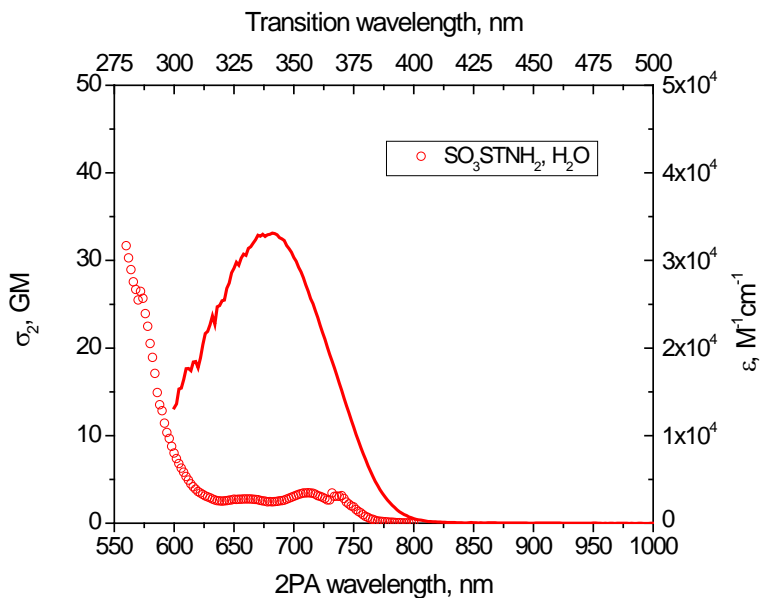
TPA maximum around 550 nm (~32 GM) and other TPA peaks at 660, 715 and 740 nm
Have cross-sections that are lower than 10 GM

Figure 27: Two-photon absorption spectra of SO_3STNH_2 in water.

The TPA data and transient spectral data are summarized as: Two photon cross-section : ~30 GM @ 550 nm, excited state absorption at 550 nm has an excited state life-time of ~30 ps.

For the optical limiting experiments, 300 μL of AgNP-Silica (~10 nm) core-shell particles were added to 2.5 ml of 0.1 M solution of SO_3STNH_2. 2.5 ml of 0.1 M solution of dye in water and 300 μL of AgNP-Silica (~10 nm) core-shell particles were used as references to determine the potential effect of the core-shell particles on the limiting behavior of the TPA dye. Absorption spectra of the three solutions mentioned above are shown in Figure 28. The results of the limiting measurements are shown in Figure 29. All the three solutions exhibit strong limiting behavior. However, we do not see any plasmon induced enhancement as the core-shell particles scatter stronger than the dye and dye+core-shell particles. Although the solutions were stirred during the measurements, the core-shell particles show a tendency to settle down increasing the scattering of the light.
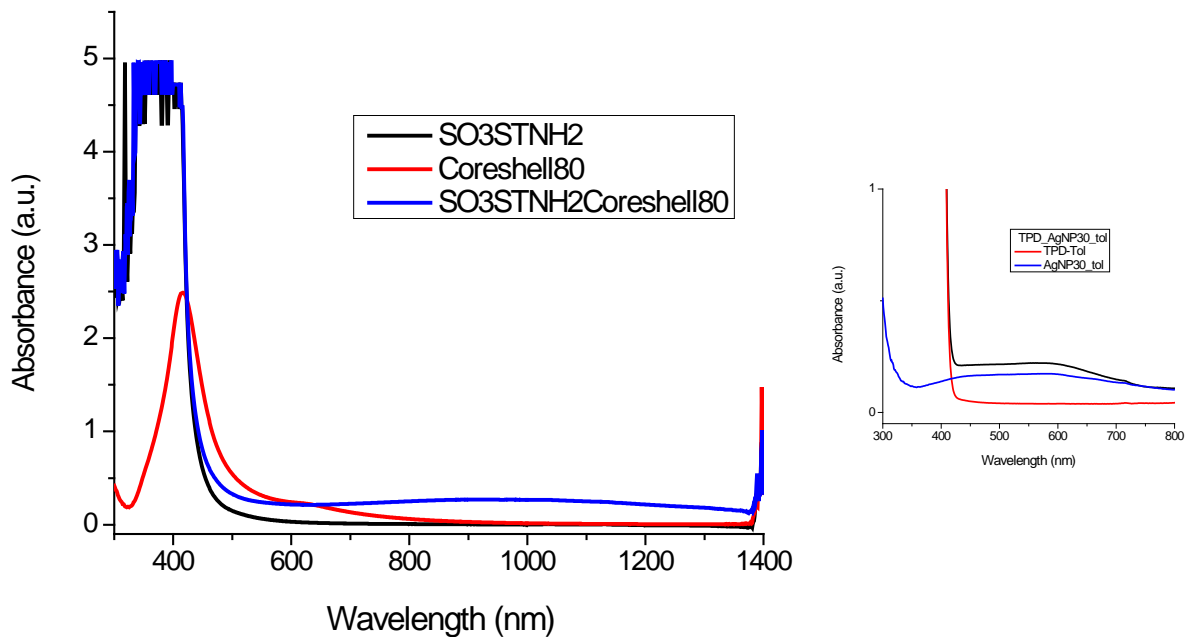
Absorption spectra of the TPA dye+Core-shell mixture has interesting features in the NIR region

Figure 28: Absorption spectra of 300 μL of AgNP-Silica (~10 nm) core-shell particles in 2.5 ml of 0.1 M solution of SO_3STNH_2, 2.5 ml of 0.1 M solution of dye, and 300 μL of AgNP-Silica (~10 nm) core-shell particles in water.
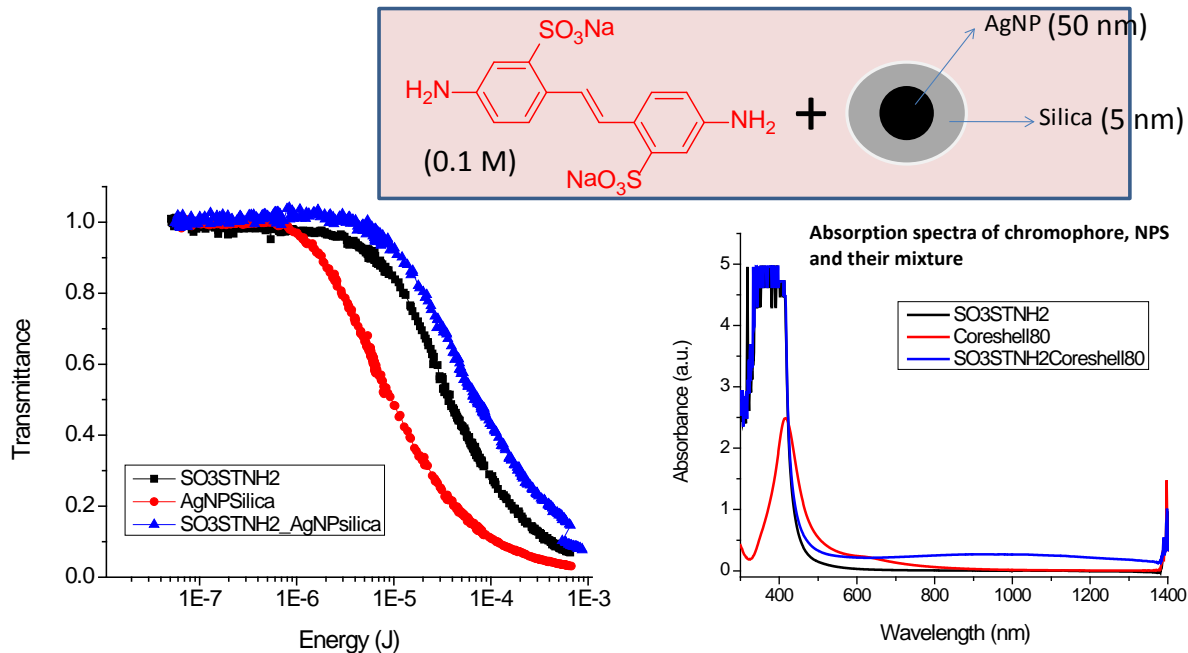
Figure 29: Optical limiting traces of SO$_3$STNH$_2$, AgNP-Silica (~10 nm) core-shell particles and SO$_3$STNH$_2$ and 300ul of AgNP-Silica (~10 nm) core-shell particles in water.

Enhanced Optical Limiting in Dendronized RuPc and Ru Nc

Ruthenium phthalocyanines and naphthalocyanines with two axially-coordinated G3 dendrimers (RuPcG3 and RuNcG3) were prepared at various concentrations in PMMA films to demonstrate the effectiveness of the coordinating ligand in preventing the adverse effects of aggregation on the optical limiting (OL) of nanosecond, 475 nm laser pulses, such as reduced yields of the excited triplets used for reverse saturable absorption, due to energy transfer quenching of the excited singlet precursors, and a decrease in the transmittance of ambient light at the OL wavelength. In the more strongly aggregating, pyridine-coordinated model compounds, RuPcPy and RuNcPy, there was no observable decrease in the excited triplet yield, even at high concentrations, presumably because the large spin-orbit coupling induced by the Ru core resulted in a singlet-triplet intersystem crossing rate that was significantly faster than the energy transfer rate. However, highly concentrated RuPcPy and RuNcPy films exhibited increased ground state absorption in the visible region. This was absent from the absorption spectra of PMMA films containing large amounts of RuPcG3 and RuNcG3, which made it possible to prepare very transmissive, thin films of these materials at high concentrations.

(a)   **(b)**
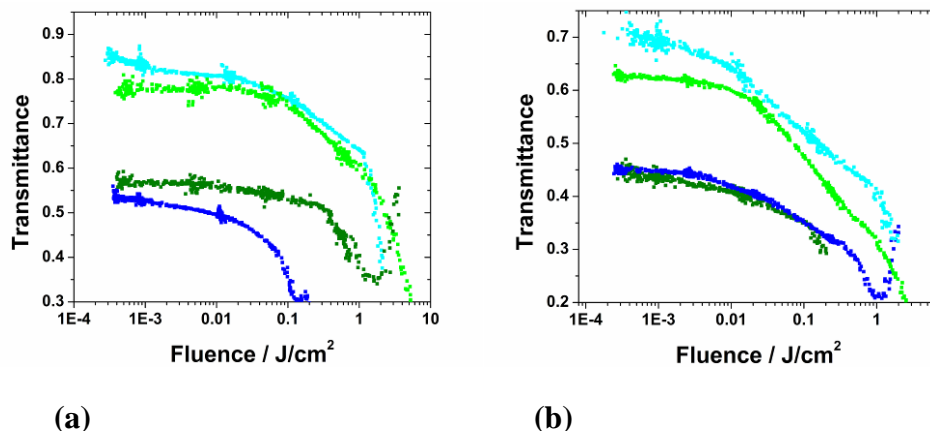
Figure 30. (a) OL of RuPc films. 8.4 µM RuPcG3 in PMMA dropcast (●), neat RuPcG3 dropcast (●), 8.4 µM RuPcPy in PMMA dropcast (●), and 273 µM RuPcPy in PMMA spincast (●). (b) OL of RuNc films. 7.2 µM RuNcG3 in PMMA dropcast (●), 155 µM RuNcG3 in PMMA spincast (●), 7.2 µM RuNcPy in PMMA dropcast (●), 154 µM RuNcPy in PMMA spincast (●). Low concentrations films were ~100 µm thick for RuPc and 70 µm thick for RuNc, high concentration films were ~4 µm thick for RuPcPy and RuNcG3, 100 nm thick for neat RuPcG3, and ~2 µm thick for RuNcPy. Excitation was with 475 nm, 6 ns pulses focused in an f/5 geometry to a 20 µm spot.

Summary:

➢ Several routes to induce aggregation of the particles, while also imparting solubility in organic solvents (this is important as TPA chromophores with large cross-sections are only soluble in organic solvents) have been demonstrated.
➢ Demonstrated tuning (500 – 900 nm) of absorption spectra of Ag and Ag-core silica-shell nanoparticle aggregates with various dithiols to match with the two-photon absorption maxima of chromophores.
➢ Highly soluble TPA chromophore (concentrations in the order of 1.5 M) synthesized which would make it possible to increase the number of dye molecules in close proximity to the nanoparticles (increase in the interaction area of dye with the nanoparticle).
➢ Investigated the optical limiting behavior of water soluble TPA chromophores with Ag-core Silica-shell aggregates in water.
➢ Significant decrease in the optical limiting threshold of TPD chromophore/Ag nanoparticle aggregate mixture compared to TPD chromophore or Ag aggregates.
➢ Dendronized phthalocyanines reduce aggregation significantly allowing optical limiting measurements at higher phthalocyanine and naphthalocaynine concentrations in thin films.

CREOL, Univ. of Central Florida: Eric Van Stryland and David Hagan research groups

Enhanced two-photon absorption in an organic dye in a colloidal suspension with metal nanoparticles

A very enticing orders of magnitude enhancement of two-photon absorption reported by a CREOL researcher was verified during the course of this research. We set up a similar experimental procedure to that reported by Cohanoschi *et al*. (J Phys. Chem. B 2005, 109, 14506-14512). The gold nanoparticles used for this experiment were provided by Dr. Hernandez (Chem. Dept and CREOL). The absorption spectrum of such particles presents a typical Surface Plasmon Resonance (SPR) band located at 530 nm.
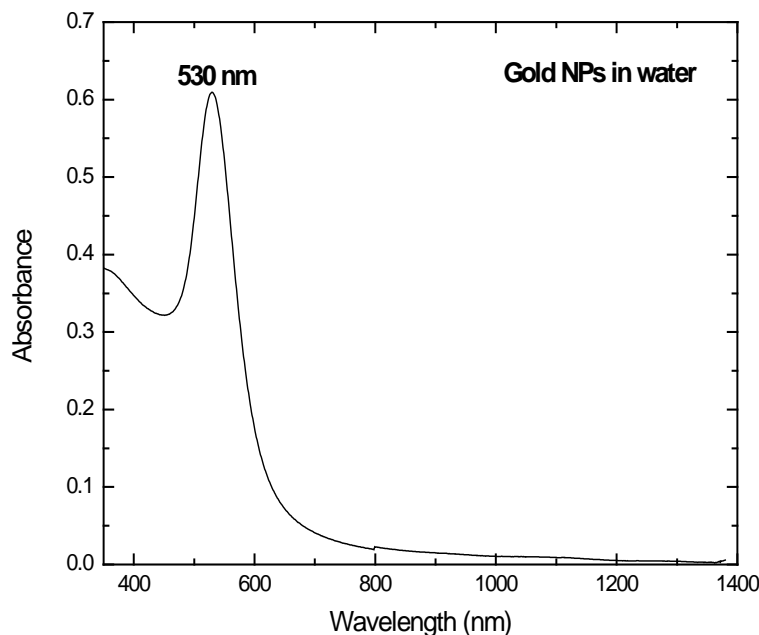
Figure 1. Linear transmission of colloidal suspension of Gold Nanaoparticles showing the SPR band near 530nm.

Figure 2 shows spectra of several prepared colloidal solutions of Au nanoparticles with the addition of NaCl to initiate the formation of metal particle aggregates. It has been observed that this is a necessary condition for observing enhanced nonlinearities in transmission experiments. A broad absorption band centered near 1 micron grows as the aggregates grow and the 530nm SPR band is reduced.
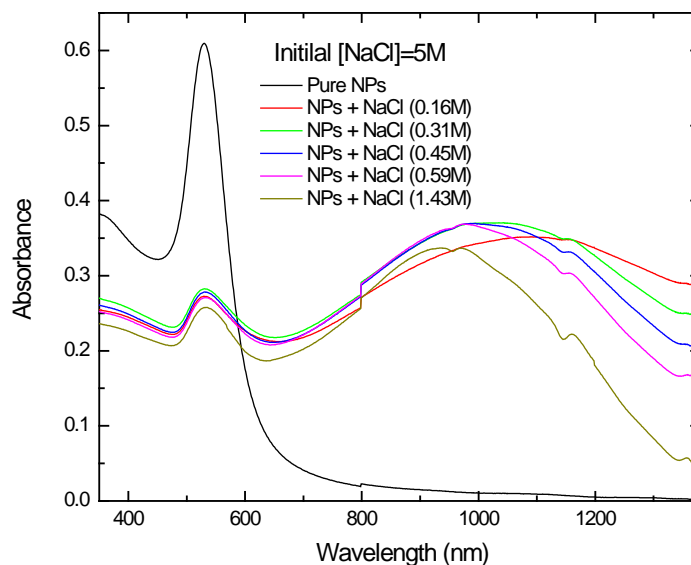
Figure 2. Linear spectra of pure Au nanoparticles in colloidal solution along with several solutions with NaCl added at different concentrations to initiate aggregation.

It is also observed that the plasmon band around 530 nm is not shifted or broadened in the presence of the dye molecules as reported by Cohanoschi et al. See Fig. 3 from that paper. This suggests that there is no change in the dielectric constant surrounding the particles, i.e. the interaction between the particles and the dye molecules seems to be negligible. As observed in the absorption spectra below, the formation of "hot spots" (particle aggregates) is also achieved under these experimental conditions.
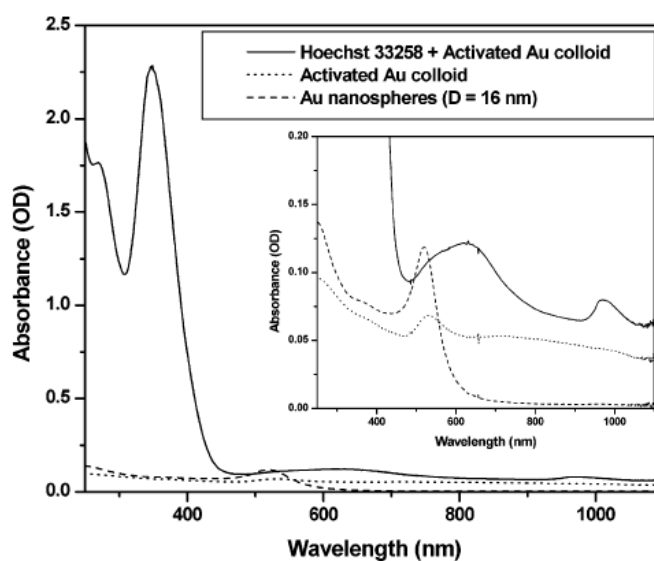
Figure 3. From Ref. (J Phys. Chem. B 2005, 109, 14506-14512) showing the linear absorbance for the various solutions as indicated. The solid line in the inset shows the absorbance for a

solution that yields large enhancement of nonlinear absorption. The inset shows a magnified portion of the important spectral region.

At higher concentrations (e.g. 1.43 M), the aggregates seem to have a narrower size distribution. Additionally, the concentration of aggregates is also increased compared to the concentration of non-aggregated particles.

A solution containing the gold nanoparticles aggregated by the action of the electrolyte was chosen to prepare the final solution to be used in the 2PA measurements in the presence of the dye. The quantities that were used are listed in the following table; however, several tries were needed to see the enhancement:

Trial	Dye conc. (0.01M)	NaCl added	Final dye concentration	Final NaCl concentration
M	0.1 mL	0.6 mL (Sln. L)	1.43 mM	1.23 M

This set of concentrations with the linear spectra shown in Fig. 4 worked transiently, i.e. as the particles aggregated we saw (after about 30 minutes) enhanced nonlinear absorption as shown in Fig. 5.
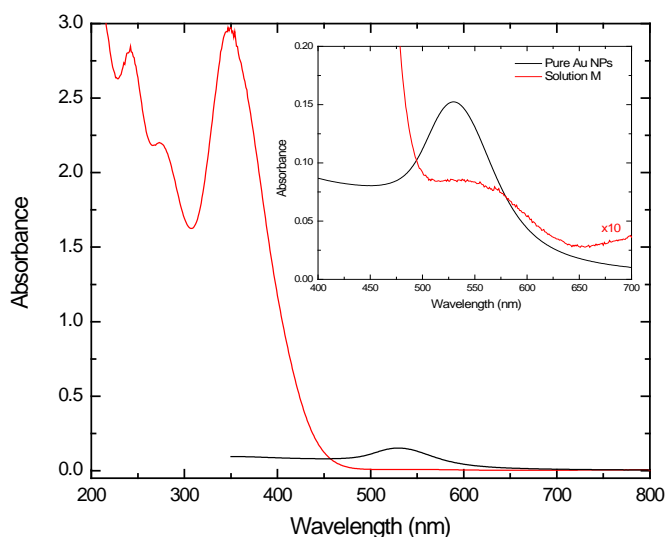
Figure 4. Linear spectra of the solution used for the Z-scan experiments of Fig. 5. The red curve shows the spectrum prior to introduction of the Au. The inset shows the Au only and the final colloidal solution of Au plus Dye (red) after ~ ½ hour prior to precipitation.

48
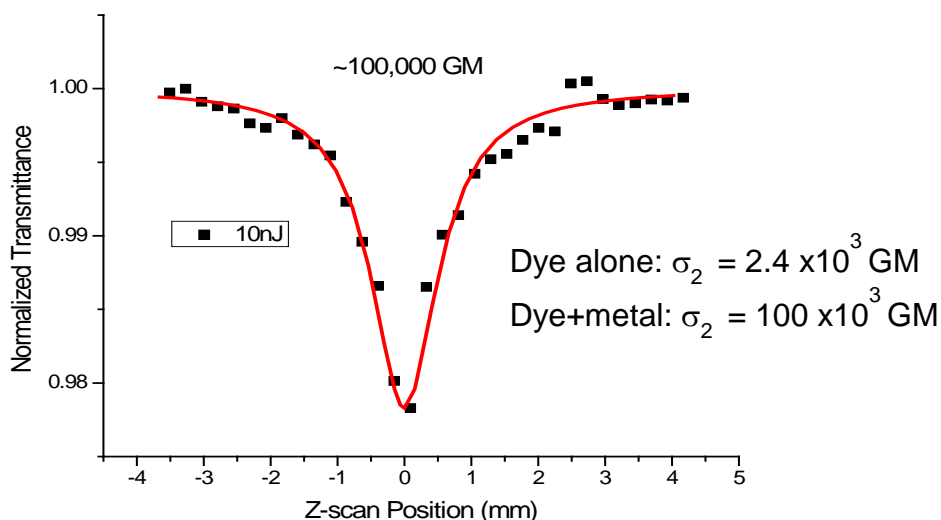
Figure 5. Z-scan data for the colloidal solution with Dye at a concentration of 1.4×10^{-3} M. At this concentration no signal can be observed without the metal nanoparticles. The wavelength used was 532 nm and ~12 ps (HW1/eM) pulses in a 1 mm cell. The peak irradiance at focus was 290MW/cm^2 fit with a 2PA coefficient of 0.237 cm/GW.

Figure 5 shows an enhancement from a 2PA cross section for the dye by itself of $\sigma = 2400$ GM to an enhanced cross section in the presence of metal nanoparticle aggregates of 100,000 (a factor of >40). The enhancement observed in the 2PA by our chemistry colleague at CREOL Florencio Hernandez who helped us with these experiments was 480, i.e. more than another order of magnitude. We think that with the proper chemistry, we could reach larger enhancements. And this is without large increases in the linear absorption.

After sample preparation it takes about 20 minutes for aggregates to form. Even then it is very difficult to find the right area with aggregates. After about one hour the gold nanoparticles begin to precipitate and the effect ends. In attempts to make the sample more stable we tried to use more viscous solvents. So far Glycerol and Polytetrahydrofuran didn't give the desired result.

Enhancement of two -photon absorption in CS_2:

In addition, we incorporated silver nanoparticles into carbon disulfide, CS_2, which exhibits 2PA near the Au nanoparticle plasmon resonance. The 2PA coefficient we measured in CS_2 is 2.55

cm/GW. The Au nanoparticles exhibit a nonlinearity of their own which is essentially a saturation of the linear absorption which is reasonably described by 2-level saturation model. With the metal nanoparticles suspended in the CS_2 the saturation is observed as a background with the 2PA signal near Z=0 in the Z-scan shown below. The measured 2PA coefficient is now 12 cm/GW giving an enhancement of 4.7 compared with the neat liquid.
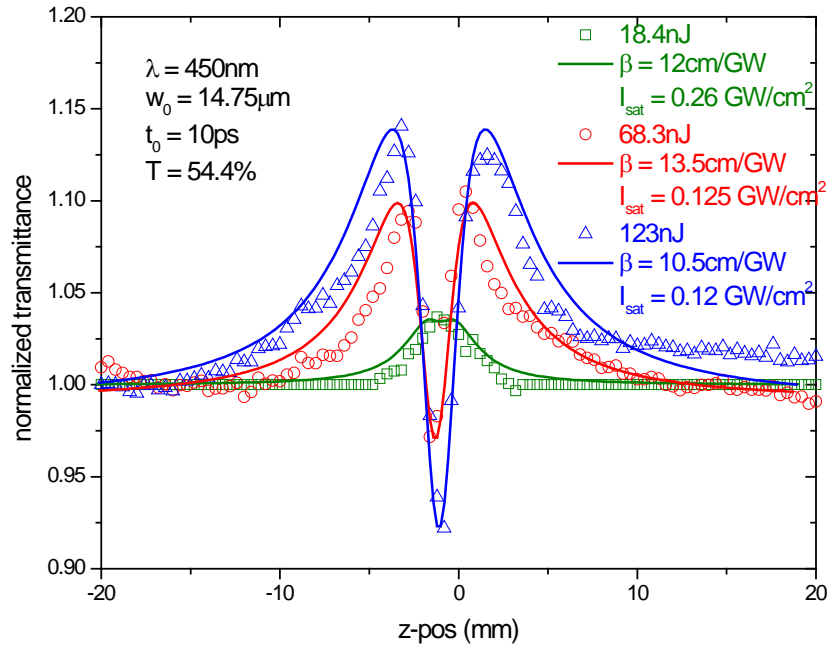
Figure 6. Z-scan data for a colloidal solution of liquid CS_2 and Au nanoparticles. The wavelength used was 450 nm with a pulsewidth of ~10 ps (HW1/eM) where the linear transmittance of the solution was 54.4%. Three input energies are shown.

University of Arizona: Nasser Peyghambarian and Robert Norwood groups

Summary of Accomplishments:

- Developed azobenzene based samples with optimum optical transmission
- Determined the response time of the dynamic refractive index change of azobenzene doped polymers;
- Designed nonlinear mirrors based upon the combination of two photonic band gaps, yielding the potential for limiting over a 100nm bandwidth;
- Developed samples for optical limiting based upon a nonlinear refraction in a photonic band gap system;
- Identified and measured the two photon absorption cross section of the polymer to be used as the matrix for composite films;
- Designed and fabricated Fabry-Perot mirrors with moderate finesse capable of providing enhancements of 3-4 while preserving broadband operation
- Lead(II) tetrakis(4-cumylphenoxy) phthalocyanine (PbTCPc) was doped into plasticized PMMA at up to six weight percent and exhibited robust nonlinear absorption and a high damage threshold;
- When fabricated within a Fabry-Perot etalon, PbTCPc films exhibited limiting thresholds reduced by a factor of 3 (37 mJ/cm^2 compared to 110 mJ/cm^2);
- Direct comparisons between high glass transition temperature dye doped optical polymers and their plasticized counterparts evidence the benefits of plasticization with respect to optical damage threshold, leading to significant (3-5x) improvements;
- Developed nanoimprinting technique suitable for a broad class of melt-processable polymers that allows for the patterning of nonlinear optical polymer with practically arbitrary dimensions and subsequent coating with metals suitable for plasmonic field enhancement;
- Demonstration of several azobenzene doped polymers with promising optical limiting performance for nanosecond pulses;
- Demonstrated broadband device designs suitable for both nonlinear absorptive and nonlinear refractive materials;
- Demonstrated enhanced nonlinear transmission in porphyrin complexes containing rhenium selenide clusters, with the enhancement due to the cluster hypothesized to derive from the heavy metal atom effect (enhanced intersystem crossing) and decreased aggregation;
- Extensively characterized a cobalt oxide/polymer composite system, observing nonlinear reflection for multilayer stacks, extremely high damage threshold and saturable absorption at high fluences (0.1 – 1.0J/cm^2);
- Fabricated a series of samples consisting of BDPAS on various plasmonic structures supplied by V. Drachev (Purdue) for characterization by both Purdue and CREOL, with the purpose being to look for enhancement in the two photon absorption coefficient due to plasmonic resonance;
- Designed and fabricated multiple window Fibonacci mirrors that can be used for a nonlinear Fabry-Perot device with multiple operating regions;

- Fabricated metal coated nanoimprinted polymer structures with tunable plasmonic features as observed by UV-VIS spectrophotometry.
- Linear and nonlinear optical characterization of the unique Co_3O_4/PVA polymer nanocomposite evidencing nonlinear refraction, RSA and saturable absorption in various fluence regimes; a NLA coefficient $\beta = 6.2 \times 10^{-5}$ cm/W and a nonlinear refractive index $n_2 = -1.08 \times 10^{-9}$ cm^2/W were obtained for this material;
- Development of new multiple window mirror design based on the Thue-Morse sequence which allows for thinner and simpler multilayer structures than the previously demonstrated Fibonacci mirrors;
- Fabricated self-assembled gold nanoparticle arrays on glass substrates that are suitable for overcoating with nonlinear optical polymers and other organic materials.

Technical Report

Azobenzene based samples

Azobenzene moieties can play a major role in low-power optical limiting in their capacity as photosensitive chromophores. The principle of photoisomerism in azobenzene is based on the changes in the molecular shapes of trans and cis isomers. The trans form is rod shaped and the cis form is bent. In the solid-state, this photoisomerism can also be accompanied by orientation of the chromophores in the direction perpendicular to the polarization of the incident radiation, leading to large photo-induced birefringence. Figure 1 illustrates a high performance azobenzene copolymer that we have evaluated, PCDY50. The copolymer has two different azobenzene sidechains which exhibit cooperative photoisomerism to enhance both the speed and size of the induced refractive index change.
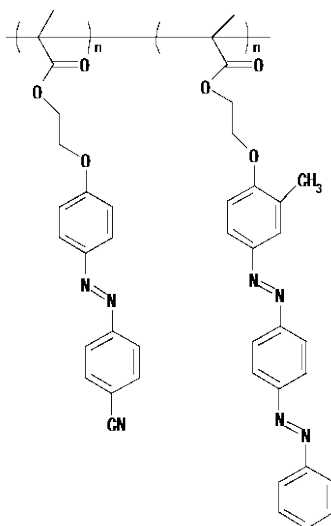
Figure 1. PCDY50 azobenzene copolymer

When an amorphous polymer incorporating azobenzene is irradiated with linearly polarized light, the trans form is converted to cis form. The cis form often relaxes to the trans form very quickly. During this process, the molecular direction of the relaxed trans form need

52

not be in the original direction. The molecular axis of some of the relaxed trans molecules becomes perpendicular to the electric field of the incident beam and these molecules do not subsequently interact with the incident light. This is because their dominant transition dipole moments are now perpendicular to the direction of the incoming light. Over time, more and more molecules adopt this perpendicular orientation and become excluded from the rapid photoisomerization cycles, thus increasing the birefringence.

Since photoisomerism results in a change in the refractive index and the build up of birefringence in the material, these changes can be exploited to achieve optical limiting in a number of device geometries. Since molecular motion is required to achieve this optically induced refractive index change, it is crucially important to understand the dynamics of the photoisomerization/orientation process in azobenzenes, since this will determine the pulse length regimes in which these materials can be used.

Sample Development and Optimization of % Transmittance (%T)

Several model systems were developed to test the dynamics of photoisomerism in azobenzene-doped polymers. Poly (methyl methacrylate) (PMMA) was used as the polymer matrix, owing to its high optical quality and compatibility with a broad range or nonlinear optical chromophores. We have selected the following sample from several samples developed to study the dynamics of photoisomerism: JTLM1: PMMA -95 wt%; Disperse Red 1 (DR1) – 5 wt%. Figure 2 shows the low intensity UV-VIS transmission spectrum of the JTLM1 polymer sample, where we see that the minimum transmission occurs at close to 500nm with good transparency from 550nm to 700nm.   Films prepared by spin coating were used to optimize the transmission.   JTLM1 with about 40%T at 532nm was selected for the preliminary studies
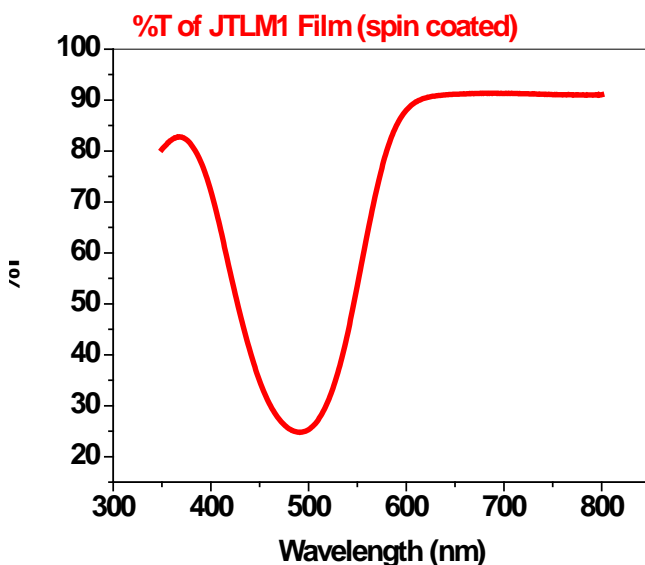
Figure 2. Transmission of JTLM1 sample.

Measurement of Nonlinear Transmittance Using Pulsed Laser

Figure 3 demonstrates the behavior of the film as the input pulsed laser intensity is varied from 0 to 1 MW/cm^2. It is observed that as the laser power is increased, the transmittance increases initially and then slightly decreases. The increase in intensity can be attributed to dichroism that occurs upon photoisomerism/orientation of the Disperse Red 1 chromophore. Up to these levels of intensity the transmission change has been observed to be reversible.
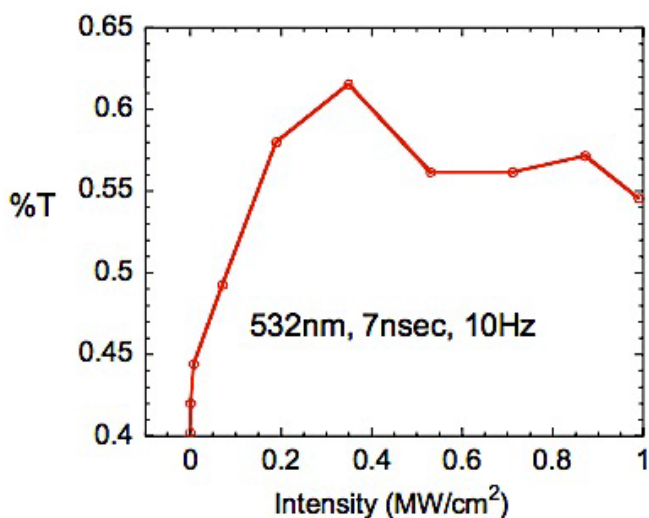
Figure 3. Transmission of JTLM1 film vs. the intensity of the pulsed laser at 532nm.

Response Time Measurements for Longer Pulses

It is known that azobenzene systems can exhibit a number of different mechanisms (photoisomerism, photo-induced orientation, dichroism) that can contribute to optical limiting. In order to elucidate the size and speed of the different mechanisms, especially with an eye towards modifying material composition to improve performance, we have also setup a response time measurement system using a cw 532nm laser and a faster chopper/modulator.
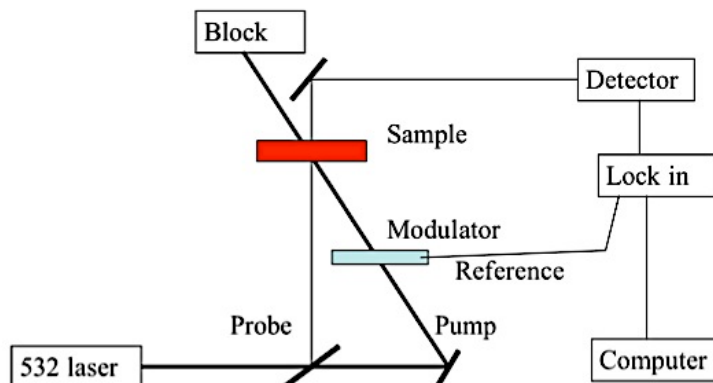
Figure 4. Setup for measuring quasi-cw response in azobenzene copolymer samples

In this case the pump beam generates changes in the optical properties of the sample and a much weaker probe beam will experience an increase or decrease in its transmittance, which is observed by using phase sensitive techniques. The in-phase signal has same phase as that of the pump laser beam and out-of-phase signal has a 90° phase shift relative to that of the pump beam. When the sample responds to the pump laser instantly, there is no phase difference between $\Delta T/T$ and the pump beam, whence the out-of-phase signal equals zero. But when the modulation frequency of the pump beam increases, the sample may not be able to respond to the pump laser instantly, whence a $|\Delta T/T|$ out-of-phase signal emerges and increases while the magnitude of in-phase signal reduces. At sufficiently high frequencies both the in-phase and out-of-phase components are unable to keep up with the pump beam and are reduced to small values. Since the pump beam is expected to induce birefringence, it is also possible to observe the dynamics by placing the sample between crossed polarizers.

The response time is estimated from Figure 5 as approximately 1 msec, when the magnitude of the change of in-phase and out-of-phase signals are equal. A 10% enhancement of transmittance is shown in the material under low laser intensity, which is also consistent with pulse laser measurements.
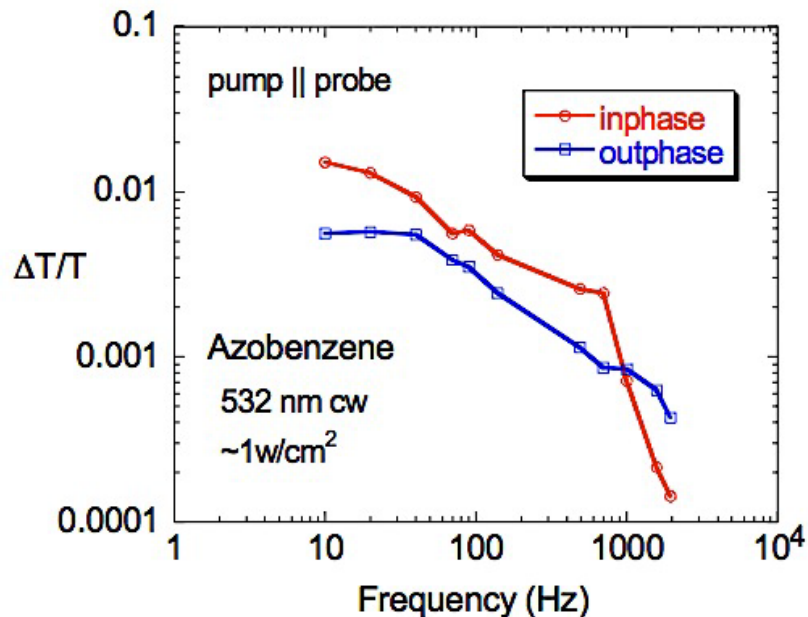
Figure 5. Estimation of the response time from $\Delta T/T$ vs. frequency plot.

For further information on the material response of the PCDY50 polymer we modified the setup of Figure 4 to be able to directly observe optical limiting based on nonlinear refraction. Since the index is expected to decrease with pump intensity (i.e. the effective n2 is negative), a sample placed after the focus will cause further beam divergence, resulting in reduced intensity getting through a fixed aperture as shown in the inset of Figure 6. Here we show optical limiting at a pump repetition rate of 500Hz, confirming the millisecond response time results shown above.

55
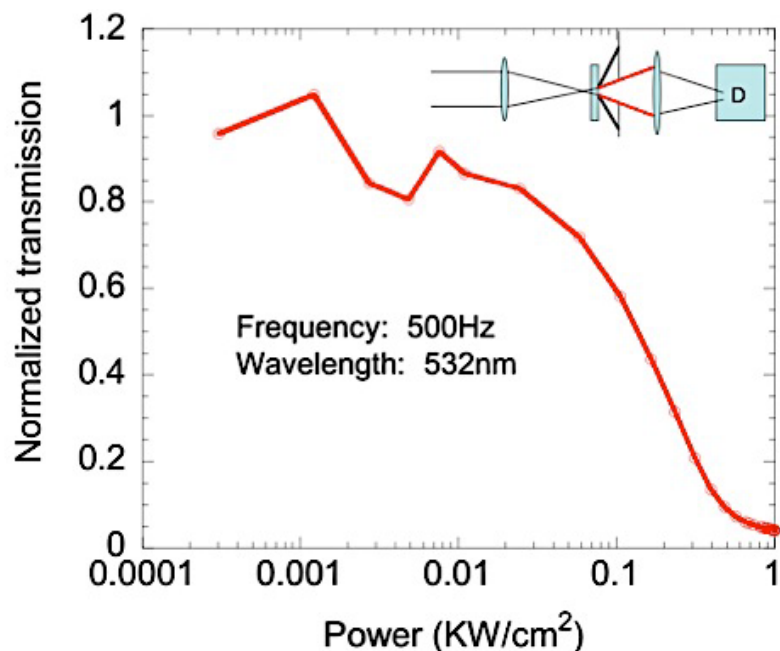
Figure 6. Optical limiting behavior for PCDY50 with the geometry shown in the inset

divergence, resulting in reduced intensity getting through a fixed aperture as shown in the inset of Figure 6. Here we show optical limiting at a pump repetition rate of 500Hz, confirming the millisecond response time results shown above. Our future work on the azobenzene polymer systems will focus on

- broadening the spectral response, through selective substitution of various azo-chromophores;
- reducing the response time through engineering of the glass transition temperature and chromophore mobility

Two Photon Polymer Based Samples

We have developed a two-photon polymer based composite for optical limiting by two-photon absorption (TPA). These polymer composites can be melt-processed and used as a host for excited state absorbing moieties like fullerenes and/ reverse saturable absorbers like phthalocyanines. The polymer used is an acrylic polymer with tetraphenydiaminobiphenyl (TPD) pendant groups (PATPD) (Figure 7). The TPD groups have excellent transparency throughout the visible above 420nm, and TPD has relatively strong TPA with a cross-section of about 400 GM at 450nm. We used 9-ethylcarbazole (ECZ) as a plasticizer to make polymer films from a melt-process. The use of this plasticizer provides for the fabrication of thick films

(up to several hundred microns) without cracking or other defects. We have also successfully used this material as the host for state-of-the-art photorefractive polymer systems.
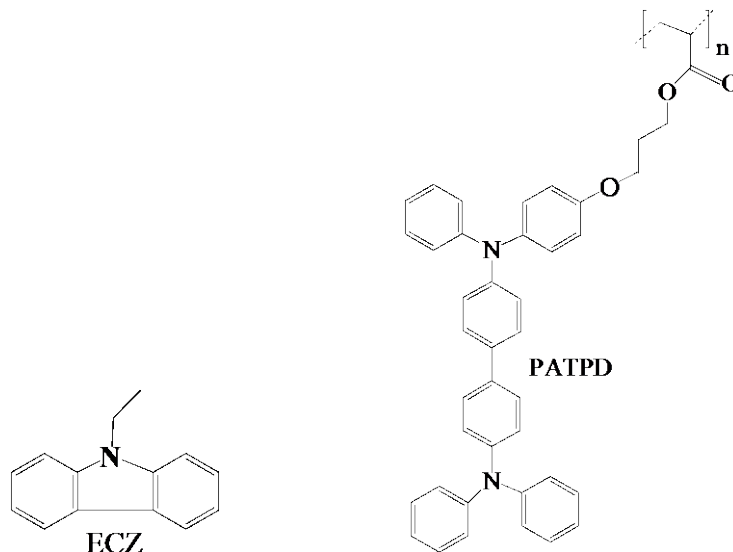
Figure 7. Chemical structures of components used in the host for the TPA composites

Transmittance of PATPD/ECZ films

The transmittance of PATPD/ECZ films prepared with different thicknesses are shown in Figure 8. The high transmittance in the visible wavelength range clearly demonstrates the advantage of using this polymer as an active TPA polymer matrix.
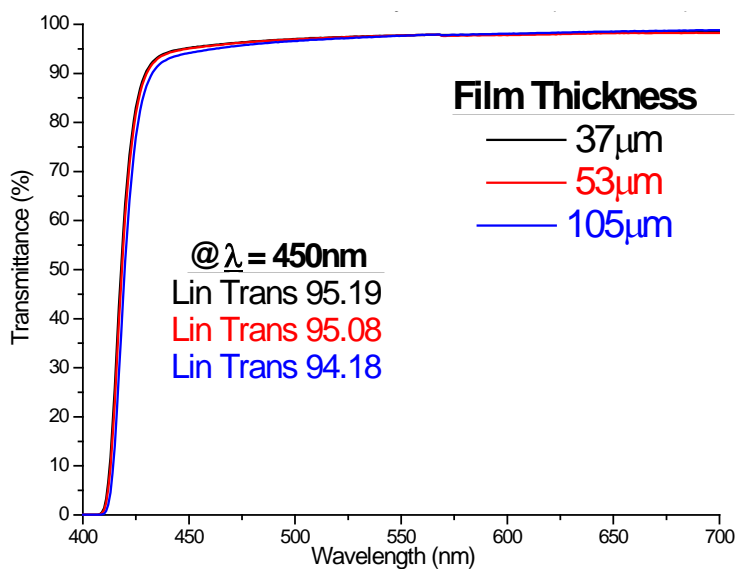
Figure 8. % Transmittance of PATPD/ECZ 70/30 films with different thickness.

Two Photon Absorption (TPA) Characteristics

Two-photon absorption cross-section values were determined using the open aperture Z-scan technique by CREOL. The two-photon cross-sections given in Figure 9 demonstrate the application of this polymer as a TPA host.
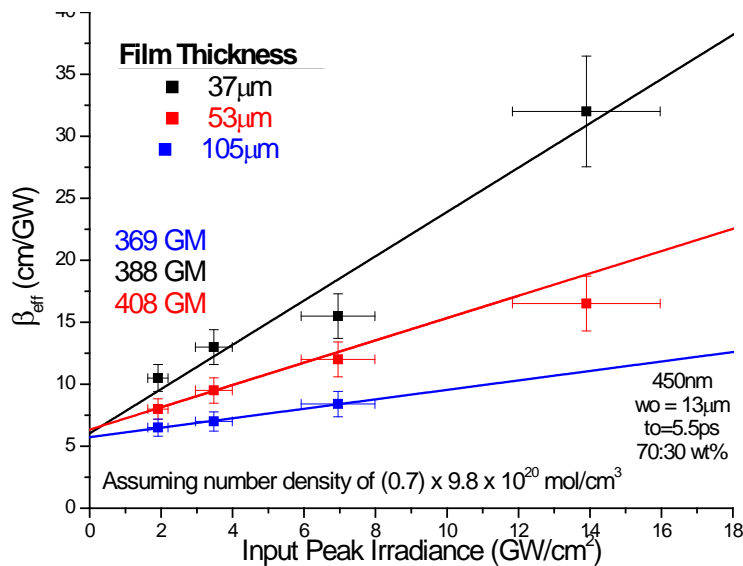
Figure 9. Determination of TPA values from Z-scan technique

Resonant Structure Design and Fabrication

Nonlinear reflector design

To exploit the large nonlinear refractive index change in azobenzene copolymers and other highly nonlinear materials, we have designed one and two photonic band gap (PBG) devices that function as nonlinear reflectors (Figure 10). The devices are designed so that for low input intensities the alternating quarter-wave layers have equal refractive indices (n = 1.60), in which case the only reflection is due to Fresnel reflections at the interface between the film and air and the interface between the film and the glass substrate. At high input intensities, the refractive index of the nonlinear material drops, at saturation, to 1.40, resulting in the emergence of a highly reflecting Bragg mirror. If a single PBG is used, the Bragg condition results in protection over an approximately 50nm bandwidth for 20 layer pairs. However, for the same 20 layer pairs, a two PBG device
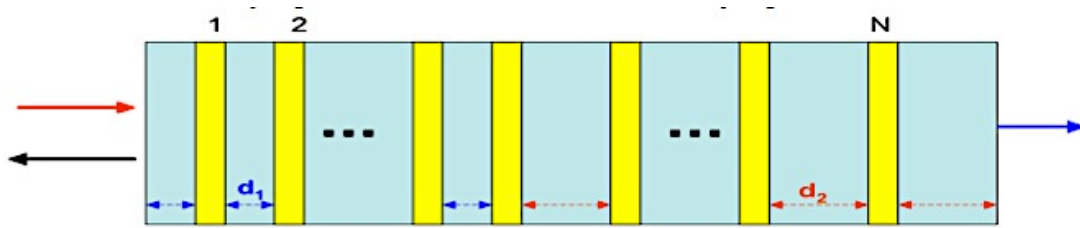
Figure 10. Nonlinear reflector design based on a classic Bragg mirror. When $d_1 = d_2$, one PBG exists, while for $d_1 \neq d_2$ there are two PBGs

can achieve protection over a 100nm bandwidth, assuming that the material responds over that bandwidth as well. Figure 11 compares the performance of one PBG and two PBG systems, clearly evidencing the broader operating window for the two PBG device. We have also found that the inclusion of real material dispersion in the model tends to improve the performance further.
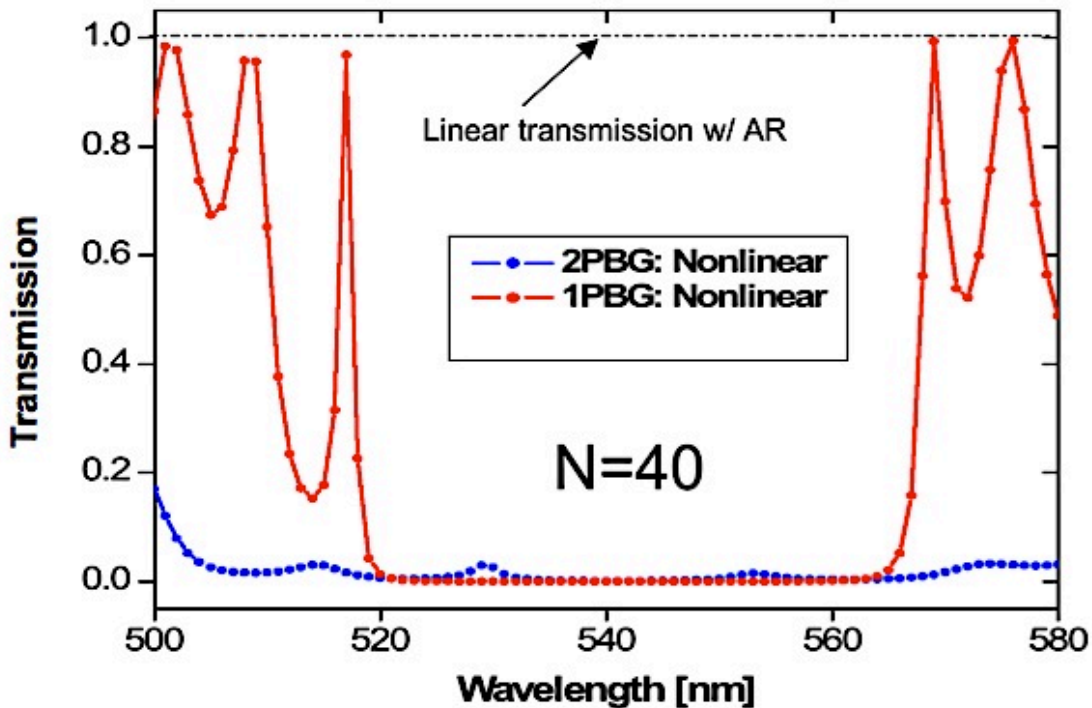
Figure 11. Comparison of predicted performance of 1PBG and 2PBG limiters

Nonlinear reflector fabrication

Based on the sample design shown in Figure 10, nineteen layers of alternative DR1/PMMA and polyvinyl alcohol (PVA) (ten DR1/PMMA and nine PVA layer) of high optical transparency has been successfully spin coated on a glass slide. Each layer of DR1/PMMA was designed to absorb about 3% of the incident light so that the final device would have than 30%-50% transparency, depending on the number of layers used. The refractive index of the DR1/PMMA at 532nm is 1.53, while that of the PVA is 1.49, a reasonably good match; for 10 layer pairs, the reflectivity from this slightly mismatched structure is calculated to be less than 2%. The thicknesses (d) of the quarter wave layers were chosen to be approximately 80 nm, and films were formed by spin coating. The polyvinyl alcohol was chosen both because it provides a reasonably good index match, and it is soluble in aqueous solvents as opposed to organic solvents. This means that alternating layers of DR1/PMMA and PVA can be deposited with partial dissolution of the previous layer. Figure 12 shows the transmission through the 19 layer mirror as a function of layer thickness, where we can see that the transmission in the DR1 absorption band steadily grows with increasing layer number, as expected.
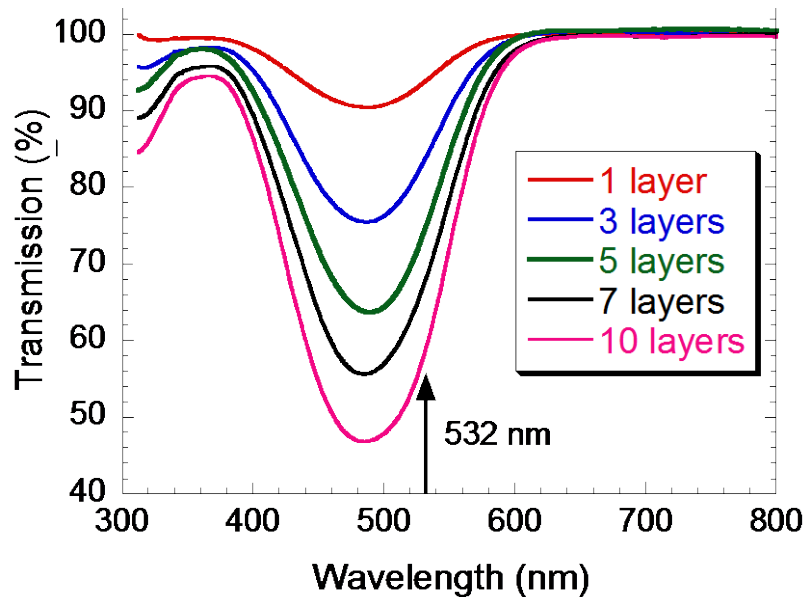
Figure 12. Transmission of DR1/PMMA based nonlinear reflector as a function of layer number, showing the gradual decrease in transmission in the DR1 absorption band as the device is built-up as well as the high transmission away from the absorption band

Fabry-Perot etalon design and fabrication

While the requirement for broadband operation precludes the use of high finesse, narrowband etalons, low finesse etalons can still provide field enhancements of a factor of 3-5 or so. In anticipation of the need to provide enhancement in every way possible, we designed and fabricated dielectric mirrors suitable for low-finesse Fabry-Perot etalons. Figure 13 compares the calculated performance with the measured reflectivity, indicating good fabrication tolerances.
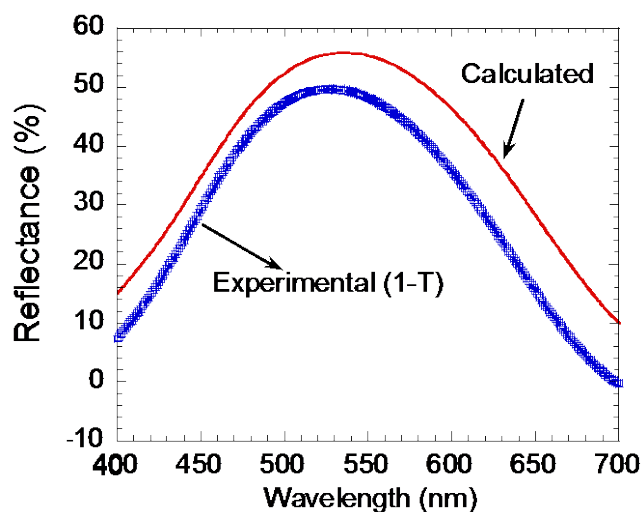
Figure 13. Comparison of calculated and experimental reflectance of mirror designed for low finesse Fabry-Perot etalons centered at 550nm

Nonlinear absorbing polymer composites

Nonlinear optical chromophores for optical limiting are ordinarily characterized in dilute solution and this is the best way to determine the intrinsic molecular response. However, in most practical limiting systems, thin films as opposed to solutions are required, and the response of molecules in the solid state can change significantly from that in solution, due to local field effects and chromophore-chromophore interaction, among other sources. Polymer thin films are often formed from solution by spin coating, however, melt-processing allows for the formation of thick films (50-100μm) and also helps to further disperse chromophores that have been introduced to the polymer matrix through initial solution processing. We have used melt-processing to make polymer films doped with up to 10wt% nonlinear optical chromophore, with thicknesses up to 105μm, and these films exhibit excellent optical clarity and uniformity. Figure 14 shows examples of nonlinear absorbers that have been incorporated into optical polymers such as polymethylmethacrylate, polystyrene, and poly (acrylic tetraphenyl diaminobiphenylamine) (PATPD). Fig 14(a) is lead(II) tetrakis(4-cumylphenoxy)

phthalocyanine (PbTCPc), which exhibits strong reverse saturable absorption in the 500-600nm region of the spectrum, while Fig. 14(b) shows a newly developed azobenzene dye (JF138) whose $\pi-\pi*$ transition is shifted from the 450-500nm region down to the 350-400nm region resulting in an extended region of transparency (throughout the visible) and nonlinear absorption that preliminary findings indicate originates in weak absorption from the n-$\pi*$ transition located from 400-550nm. Figures 15(a) and 15(b) give the absorption spectra for dye doped films that are 53µm thick with 1wt% PbTCPc in PATPD plasticized with ethyl carbazole (ECZ) and 10wt% azobenzene JF138 in PMMA plasticized with diisophthalate (DIP), respectively. We have shown separately that plasticized composites exhibit both higher damage thresholds and lower optical limiting thresholds, as has been corroborated by work in the **Perry** group.

The materials were further characterized with a standard optical limiting measurement system employing 532nm pulses, approximately 8 nsec in duration, at a 1Hz repetition rate. A polarizer arrangement was used to provide for continuously adjustable pulse energy, with a reference detector measuring the input energy and a sample detector measuring the output energy. Figure 16 (a) and (b) we show the optical limiting behavior at 532nm for the samples whose spectra are shown in Figure 15. Note that the nonlinear absorption was verified in the PbTCPc case by open aperture Z-scan measurements. The limiting thresholds are seen to be quite competitive, justifying our selection of these materials as candidates for further development within device formats as discussed below.
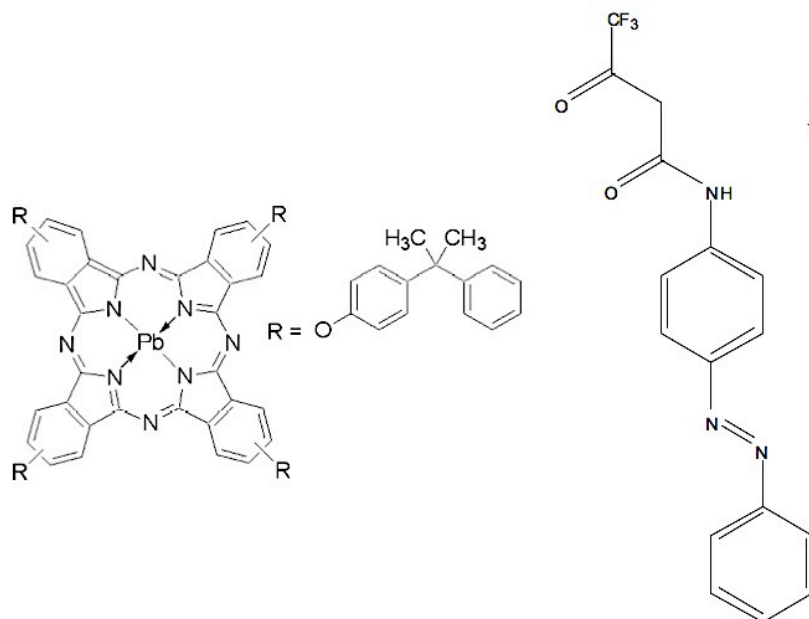

**Figure 14.** (a) PbTCPc; (b) Blue-shifted azobenzene
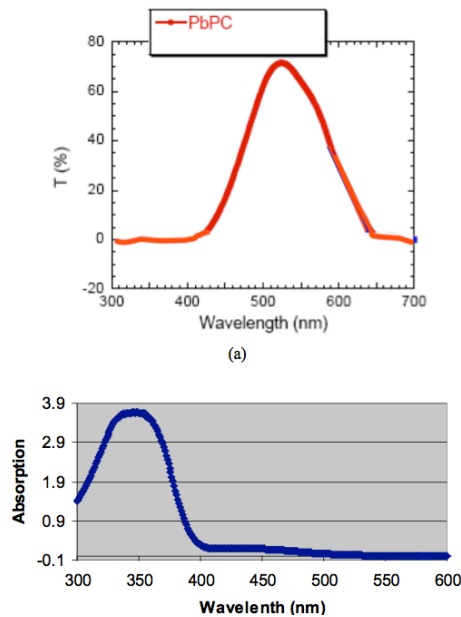
Figure 15. (a) Transmission spectrum for 53μm film PbTCPc 1wt% in PATPD; (b) Absorption spectrum for azobenzene JF138 at 10wt% in plasticized PMMA

Figure 16. (a) Optical limiting results for 53μm film PbTCPc 1wt% in PATPD; (b) Optical limiting results for azobenzene JF138 at 10wt% in plasticized PMMA
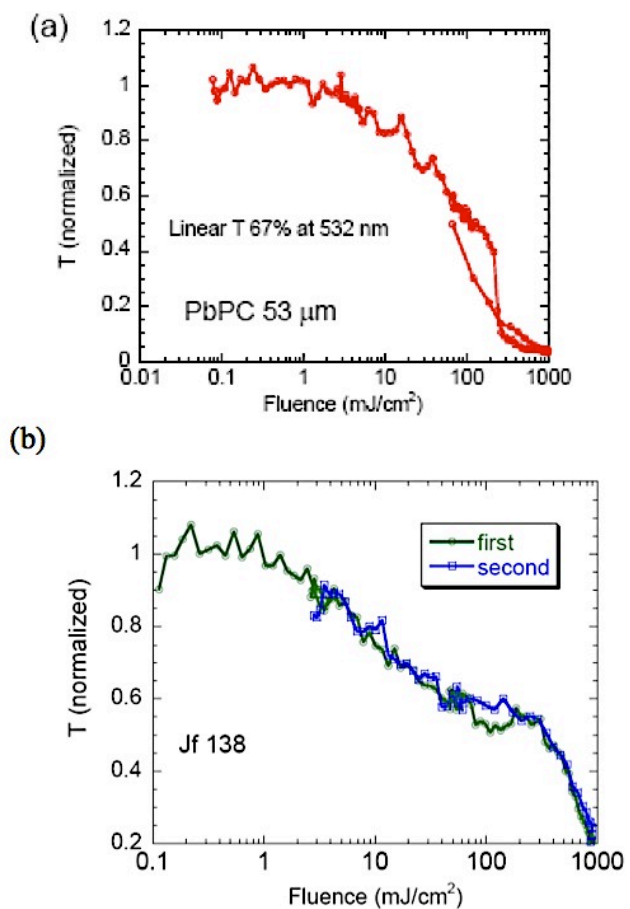
Cavity enhancement of the nonlinear response

The resonant modes of an optical cavity undergo multiple-reflection between the two mirrors of the cavity. The energy carried by these modes, and corresponding light intensities are strongly enhanced inside the cavity. If the cavity is filled with a nonlinear material, the nonlinear response will be enhanced due to the high intensity of light inside the cavity. To demonstrate this concept we constructed a nonlinear cavity from two dielectric mirrors and lead PbTCPc (Sigma-Aldrich) doped into PATPD with the plasticizer ECZ. The PATPD-ECZ mixture and PbTCPc were dissolved in a solvent (dichloromethane) with a weight ratio of 99:1 and mixed together by sonicating for 30 minutes. The solvent was then evaporated off using a rotary evaporator and the resulting material dried at 35°C under vacuum for several hours. The solid composite was melt-processed between two glass plates with glass spacer beads in between to adjust the thickness to 53μm. Phthalocyanines exhibit nonlinear transmission at 532nm (pulsed) via a nonlinear absorption (NLA) process. NLA is attributed to a mechanism in which the excited states are populated by multi-step absorption leading to reverse saturable absorption (RSA). RSA occurs as a result of a intersystem crossing from the lowest excited singlet (S_1) to the strongly absorbing lowest triplet state (T_1) and subsequent population increase during the laser pulse irradiation. The rationale behind selecting substituted lead phthalocyanine is that spin orbit coupling can enhance the population of the triplet states in lead phthalocyanine due to the heavy metal atom (lead) effect. The heavier the central metal atom, the more probable is the intersystem crossing which results in a larger population of the triplet state. This will enhance the absorption cross section of the triplet state resulting in enhanced RSA and hence improved nonlinear response. The Fabry Perot (FP) cavity was constructed with mirrors having a reflectivity of about 70% at 532nm, and filled with 53   □m of the PATPD
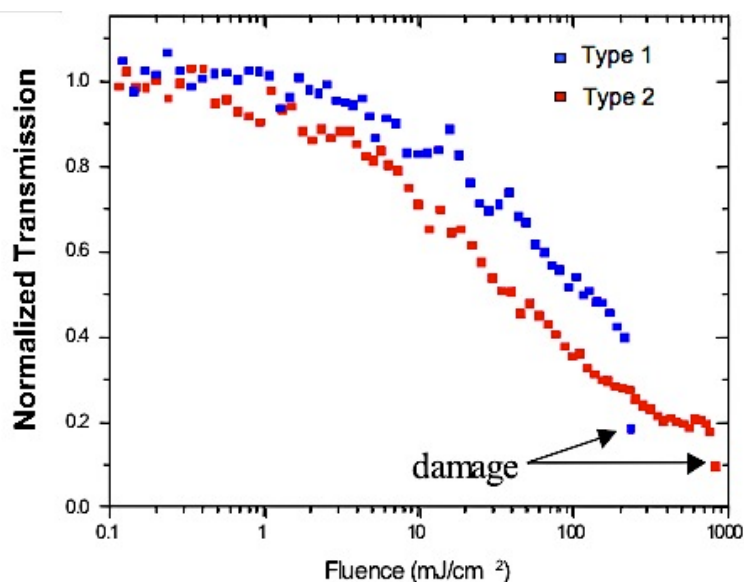

Figure 17. Cavity enhanced optical limiting response for PbTCPc/PATPD composite; Type 1 sample is a polymer film on glass, while Type 2 is a Fabry-Perot

The Fabry Perot (FP) cavity was constructed with mirrors having a reflectivity of about 70% at 532nm, and filled with 53 mmot. the Based upon the PbTCPc co absorption of the PbTCPc at 532nm and the mirror reflectivities, this should result in an enhancement of the intensity inside the cavity by approximately a factor of 3. The nonlinear response was evaluated using a frequency doubled Nd:YAG laser (532 nm), which provided 5-8ns pulse widths at a repetition rate of 1Hz. We used two polarizers in series to act as an attenuator to adjust the incident laser energy; then the input laser was split into two beams of which one was employed as a reference, and the other was focused onto the films with a 10 cm focal length lens. The incident and transmitted laser energy were collected with a lens and measured simultaneously with two identical photodiodes. Fig. 17 shows the nonlinear response characteristics of the two structures (Type 1 – film on glass, Type 2 – film in FP) under the same conditions.

As can be seen in Fig. 17, the experiment results clearly show a reduction in the nonlinear threshold fluence (defined as the fluence where the transmittance is 50% of linear value) by about a factor of 3, from ~110 mJ/cm^2 in the mirrorless sample to ~ 40 mJ/cm^2 in the single cavity sample. Moreover, the damage threshold in the cavity is nearly 4 times higher than that in the sample (~800mJ/cm^2 compared with 225mJ/cm^2).

Note that the dielectric mirror in our experiments has reflectivity R~70% at a laser wavelength of 532nm, and that at the level of linear absorption, the total transmission of the cavity in the whole visible region (defined as integration of the transmission in the considered region) is about 25% which is quite low, while the linear transmission in the NT region is only about 10%. Further optimization is required to increase the total linear transmission of the PATPD/PbTCPc FP cavity to a more acceptable level (> 30%) while still maintaining the benefits of lower limiting fluence and increased damage threshold. In principle, we can optimize the mirror to increase the total linear transmission in the visible region to higher than 60%.

Nonlinear mirror devices

In addition to Fabry-Perot devices for optical intensity enhancement, it is important to consider other classes of devices that could make use of refractive optical nonlinearities. Figure 18 shows a multilayer structure that incorporates two photonic band gap structures with different periodicities. In the "off" state all of the layers shown in the device have the same refractive index at low optical intensities, and therefore the device
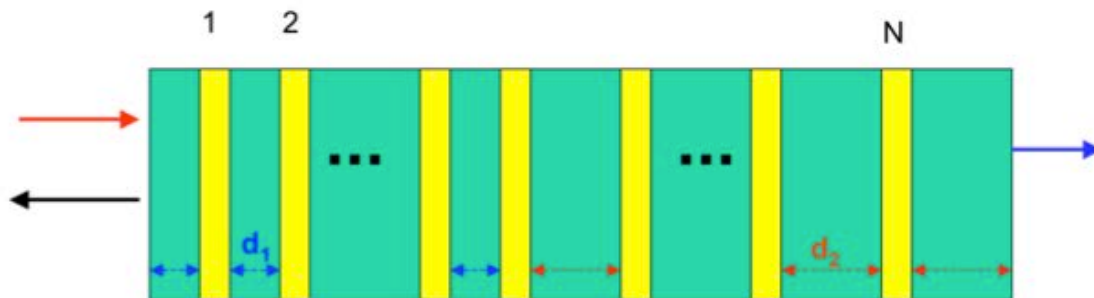

Figure 18. Nonlinear mirror structure with two photonic band gaps

appears to be transparent. As the intensity is increased, the nonlinear material (shown in yellow) experiences a change in index and a photonic band gap mirror begins to appear. If large refractive index changes (~0.1) can be achieved, then nonlinear transmission behavior such as that shown in Figure 19 is possible for 40 layer pairs with quarter wave thicknesses; with two photonic band gaps we see that the overall bandwidth can be 100nm or so. In order to make such a device a reality, it is necessary to have both materials with high optical nonlinearity, and matching layer materials that have the same refractive index as the nonlinear layer. We have developed organically modified sol-gel matching layers that span refractive indices from 1.45 to 1.65; these materials have the required optical properties, and they also have the important feature of being crosslinked materials, which makes it possible to solution deposit other materials on top of them without the initial layer being dissolved.
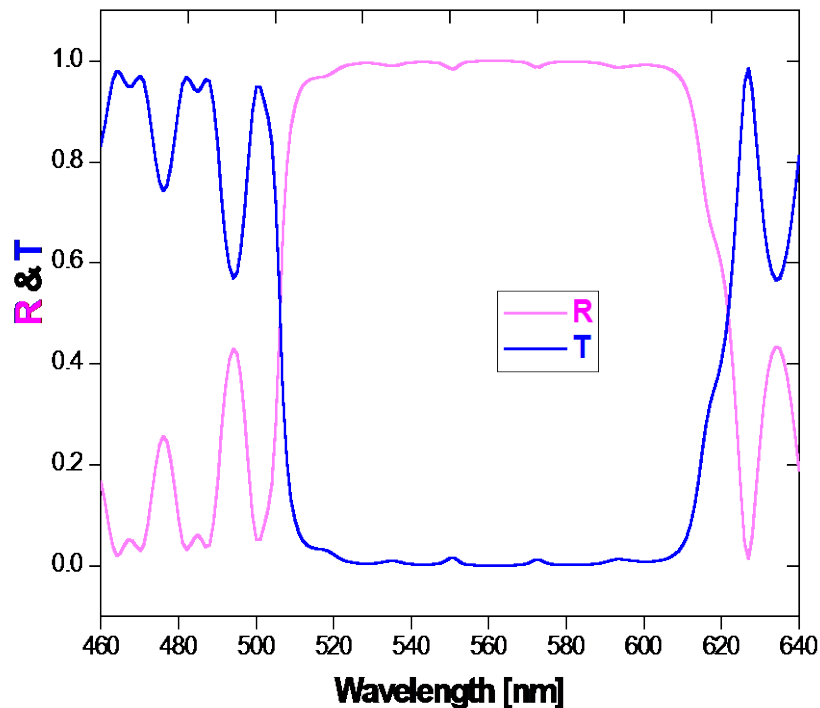
Figure 19. Spectral performance of nonlinear mirror with two photonic bandgaps

Support of plasmonic enhancement test structure fabrication

One of the key areas of research focus in the program was to demonstrate plasmonic enhancement of the nonlinear optical response of organic molecules, by taking advantage of advances that have occurred in nanofabrication of metal structures. We worked closed with both **Drachev** and **Shalaev** at Purdue, **Marder** at Georgia Tech, and the group at **CREOL** to make test structures to demonstrate this enhancement. The plasmonic structures were provided by Purdue. Three samples were made and coated as follows:

- **Marder** TPA chromophore SJZ-3-16, deposited as an organic glass by a melt process;
- The standard TPA chromophore *N,N'*-diphenyl-*N,N*-bis (3-methylphenyl) 1,1'-diphenyl-4,4' diamine (TPD), deposited by thermal evaporation (400nm);
- The TPA chromophore E-bis-(diphenylamino)stilbene (BDPAS), identified by **CREOL**, deposited by thermal evaporation;

Spectroscopic ellipsometry measurements were performed on evaporated TPD films as shown in Figure 20, and similar measurements are being performed on BDPAS films to assist in the analysis of the optical and nonlinear optical properties of the plasmonic enhancement test structures.
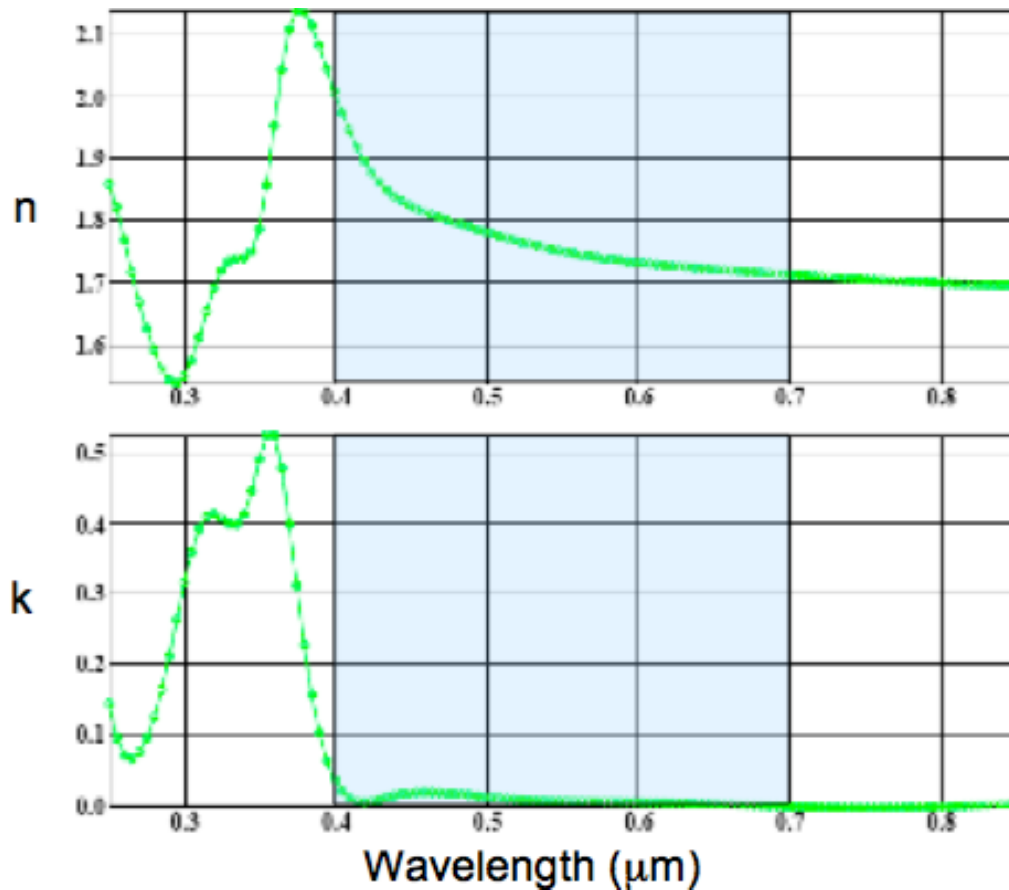
Figure 20. n and k for TPD obtained by spectroscopic ellipsometry measurements

Nanoimprinted plasmonic structures

We have recently developed a new technique for nanoimprinting nanostructures onto melt-processible polymers. In this technique, a mold fabricated by high resolution e-beam lithograph is made to incorporate the nanostructured features of interest. To date the mold has been fabricated in silicon, which is adequate for molding about 50 devices, but we are looking to base future molds on materials that can withstand hundreds of printing process without breaking.

The largest mold that has been made is 3mm × 3 mm, which is adequate for the purposes of the current program. This technique can be used to make well-defined metal-coated nanostructures, and thus complements other metal nanoparticle and fractal nanoparticle clusters. Figure 21 shows an initial structure that was made by molding polycarbonate. The posts are 30nm in diameter and 60nm high, typical dimensions for plasmonic structures. A 15nm silver film was subsequently deposited, and preliminary measurements indicate the presence of plasmonic features in the spectrum. We will work closely with the plasmonics experts throughout the MURI to determine how to best exploit this novel nanoimprinting technology which can allow for the systematic creation of nearly arbitrary test structures.
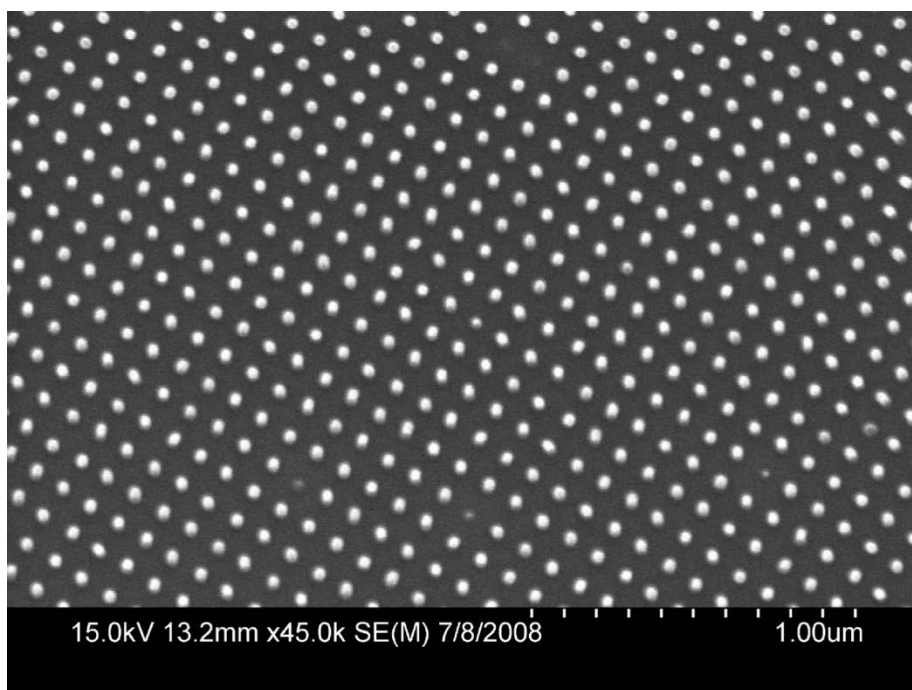
Figure 21. Nanoimprinted amorphous polycarbonate nanoposts; the posts 30nm are diameter and approximately 60nm high.

Nonlinear mirror based cobalt oxide composite

We demonstrated a nonlinear mirror that consists of a multilayer of PVK and Co_3O_4 doped PVA; the Co_3O_4 nanoparticles were identified as materials with exceptionally large nonlinear refractive indices. 24 layer nonlinear mirrors were fabricated, with individual layer thicknesses of 90nm, and the mirror demonstrated approximately 40% transmission at 532nm in the "off"state" and less than 5% transmission when "on"(Figure 22). The transmission drops to 50% of its "off state" value at approximately 90mJ/cm^2. Many nonlinear mirrors were made with similar performance, and the PVA:Co_3O_4 composite shows exceptionally high damage threshold (>1J/cm^2@ 523nm, 5 nsec pulses).

Novel quasiperiodic dielectric mirrors

The unique properties of one-dimensional (1D) Fibonacci chains of dielectric layers were experimentally demonstrated and exploited for the design of new mirrors with multiple reflection spectral windows (Figure 23). The new mirror structures are simple, straightforward to make and enable a wide variety of multiple spectral window device performance to be achieved. By changing the thickness of the layers or the order of the Fibonacci chain, tens or even hundreds of windows can be obtained with the same approximate reflectivity over a very broad spectral region. These mirrors have numerous applications in photonics and optoelectronics.

Novel nonlinear switching device concepts based on nonlinear Fibonacci mirrors were developed. In this approach a multiple window linear Fibonacci mirror is put together in an etalon configuration with a nonlinear Fibonacci (Figure 24). At low intensities the two mirrors are designed to have identical reflectivities and windows.
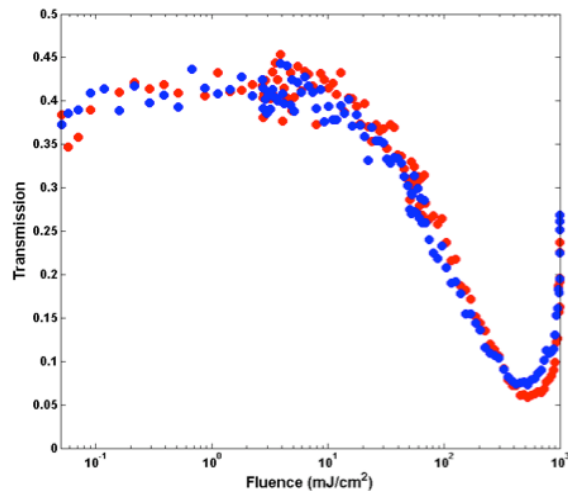
Figure 22. Transmission through 24 layer nonlinear mirror made from PVK and Co$_3$O$_4$-doped PVA
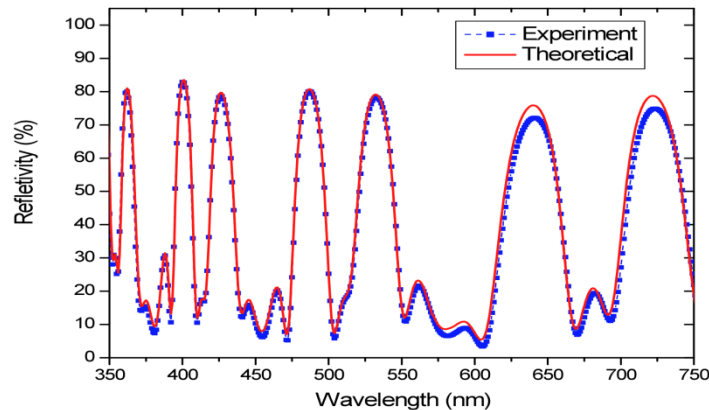

Figure 13. Multiple window Fibonacci mirror spectrum and agreement with theory

At high intensities, the spectrum of the nonlinear Fibonacci shifts in such a way that it blocks the windows of the linear mirror, leading to a broadband limiter.
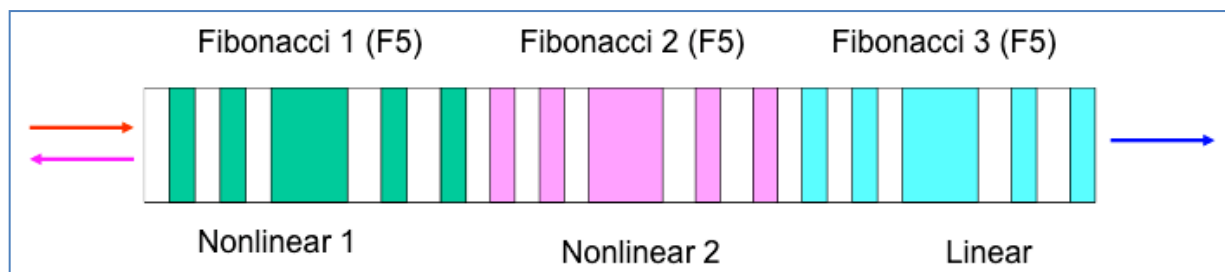

Figure 24. Nonlinear Fibonacci solid etalon

Lead phthalocyanine liquid crystal composite limiter

We have formulated composites of lead (II) tetrakis (4-cumylphenoxy) phthalocyanine (PbTCPc) doped into nematic liquid crystal (LC), 40 -pentyl-4-biphenylcarbonitrile (5-CB) (Figure 25) that has received a 90° twisted alignment and investigated the nonlinear transmission properties using both pulsed (Nd:YLF 52 nm, 5 ns) and cw (532 nm) lasers. In the nanosecond regime, this compound is a reverse saturable absorber performing similarly to low-concentration solutions of PbTCPc. Under cw conditions, we observe optically self-activated polarization switching with low threshold input energy. Our results suggest the potential for an all-optical switch working from the nanosecond time scale to cw.
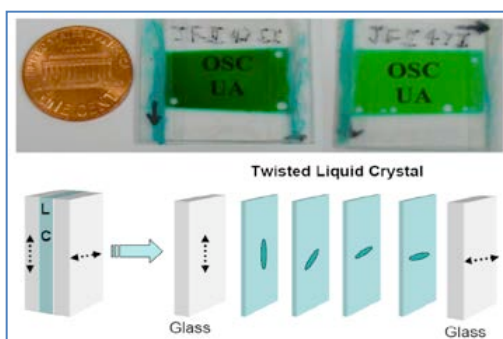

Figure 25. Lead phthalocyanine/liquid crystal based optical limiter

Porphyrin complexes containing rhenium selenide clusters

Organic macromolecules, such as phthalocyanines (Pc), porphyrin (Pph) and their metal complexes have been widely studied because their potential applications for nonlinear optical absorbers in the nanosecond (ns) regime, especially when heavy metal atoms are substituted at the center, as this increases the population of molecules in the triplet excited state. As a rule, an

essential condition for achieving preferable nonlinear transmission properties is that the molecules in the system should not be aggregated or only have slight aggregation. However, most unmodified porphyrins and phthalocyanines easily aggregate and have poor solubility in common solvents because of strong interactions between the planar molecules. The aggregation not only results in low solubility, but also adds relaxation pathways, shortens the excited-state lifetime, and reduces the effective nonlinear absorption. Chemically modified porphyrins or phthalocyanines can be made by introducing bulky groups on the periphery of the macrocycle to reduce the intermolecular interactions and to tailor the nonlinear response, and thus control the physical and chemical properties of these molecules. In the present case, a bulky rhenium selenide cluster $Re_6(m_3\text{-}Se)_8(PEt_3)_5$ has been coordinated to four periphery functional pyridyl groups on 5, 10, 15, 20-tetra(4-pyridyl) porphyrin (H_2TPyP) and its copper complex CuTPyP. The nonlinear transmittance of these compounds was measured and compared. The nonlinear transmission experiments were performed with a frequency doubled Nd:YLF laser (523 nm), which provides 10 ns width pulses with a repetition rate of 1 Hz.
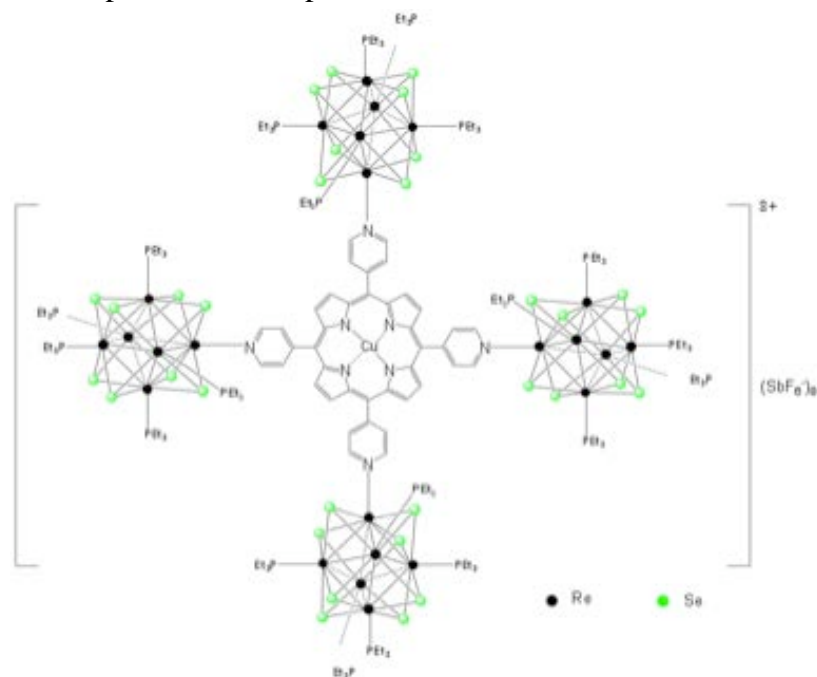

Figure 26. CuP5TPyP structure

5,10,15,20-Tetra(4-pyridyl)-porphyrin (H_2TPyP), and all solvents were of commercial origin and were used as received. The cluster solvate $[Re_6(\mu_3\text{-}Se)_8(PEt_3)_5(CH_3CN)]\text{-}(SbF_6)_2$ and cluster modified complexes of H_2TPyP and CuTPyP were prepared according to published procedures. The cluster $Re_6(\mu_3\text{-}Se)_8(PEt_3)_5$ is abbreviated as P5. The clusters were attached to the porphyrin macrocycle ligand by coordinating Re to four peripheral functional pyridyl groups. The detailed structure of $[Re_6(m_3\text{-}Se)_8(PEt_3)_5]_4$ CuTPyP(SbF_6)$_8$ (CuP5TPyP) is shown in Figure 26.
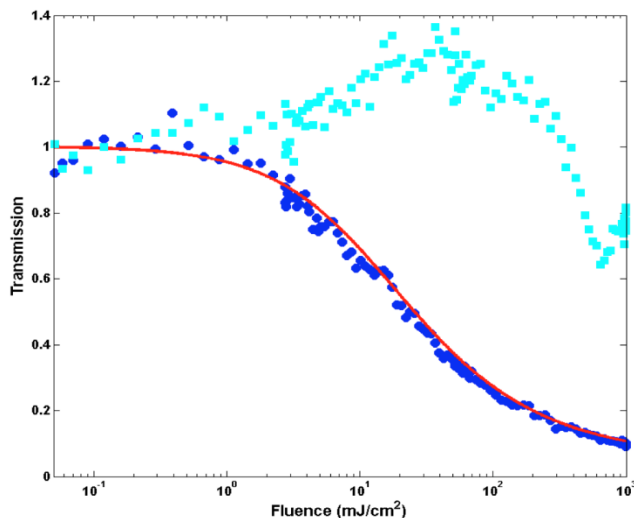
Figure 27. Nonlinear transmission of P5H$_2$TPyP and CuP5TPyP

The nonlinear transmission of P5H$_2$TPyP and CuP5TPyP solutions are shown in Figure 27. The compound CuP5TPyP has very strong nonlinear absorption. The nonlinear transmission threshold, I$_{th}$, which is defined as the input laser power strength when the nonlinear transmittance has reached 50% of its low intensity value, is 20 mJ/cm^2. The sample P5H$_2$TPyP has weak bleaching behavior when the input fluence is between 0.1 to 1 mJ/cm^2 and has a stronger photonic bleaching when the input fluence further increases from 1 mJ/cm2 to 400 mJ/cm^2. The strongest Q band absorption peak of P5TPyP is located exactly at 523 nm, which is the wavelength for our measurement laser. Although P5H$_2$TPyP has shown nonlinear absorption when the input power increases beyond 400 mJ/cm^2, only very weak nonlinear effect is observed, a conclusion that is supported by other work.

Figure 28. Nonlinear transmission of CuTPyP and CuP5TPyP


72
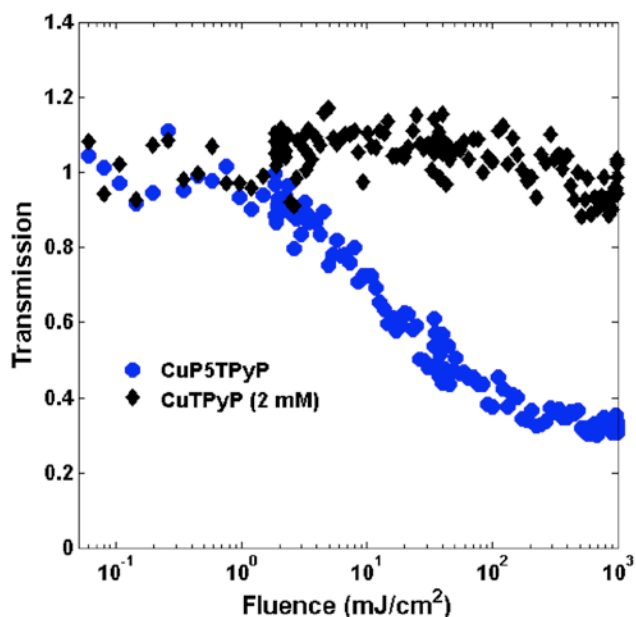
Figure 28 clearly shows the effect of the metal cluster on the nonlinear absorption of the copper porphyrin (CuTPyP). Without the cluster, there is very little nonlinear absorption, while the CuP5TPyP sample shows low fluence optical limiting. Together with the data of Figure 27, this demonstrates that it is the combination of the copper porphyrin with the rhenium selenide clusters that leads to strong nonlinear absorption. We further note that there is evidence that the metal clusters significantly reduce the tendency for the copper porphyrin molecules to aggregate, such that even at the same nominal concentrations of copper porphyrin, stronger nonlinear absorption is observed in the CuP5TPyP owing to both peripheral heavy metal atom effects and reduced aggregation.

Detailed characterization of Co_3O_4 composite

Co_3O_4, as the most stable phase in the Co-O system, is a mixed valence compound with a normal spinel structure $Co^{2+}(Co^{3+})_2O_4$ with Co^{2+} and Co^{3+} placed at tetrahedral and octahedral sites, respectively. Single-layer thin films of Co_3O_4 nanoparticles have large optical nonlinearity and the refractive index changes significantly with laser irradiation. The nonlinear refractive index has been previously found to be 1.0×10^{-10} m^2/W at 405 nm and -5.5×10^{-10} m^2/W at 650 nm. Various methods have been proposed to prepare Co_3O_4 thin films, such as sputtering, sol-gel, spray pyrolysis, and chemical vapor deposition. We have focused on making polymers filled with Co_3O_4 nanoparticles as a new composite system, since polymers are potentially useful materials for PBG structures being less sensitive to fracture, compatible with non-planar, flexible substrates, and suitable for large scale film processing.

In order to achieve equal refractive indices for the two adjacent layers at low light intensities, Co_3O_4 doped poly(vinyl alcohol) (PVA) with a volume fraction of 10% and poly(9-vinylcarbazole) (PVK) were used. The periodic PVA:Co_3O_4-PVK structure was fabricated by the method of spin coating. The linear transmission of the PBG structures was measure with a Cary 5000 UV-Vis-IR (Varian, Inc.). In our experiment, both 12-layer and 24-layer PBG structure with a target thickness of 85 nm for each layer were prepared. In order to confirm the advantages of the PBG structure, a single-layer PVA:Co_3O_4 film with a thickness of 500 nm was also fabricated. The linear transmissions of these three samples are shown in Fig. 29. The linear transmission of the 500 nm single-layer PVA:Co_3O_4 film is larger than 75% over the entire visible region. Due to thickness nonuniformities, surface roughness, and the effect of the PVK layer, the linear transmission of the 12-layer PBG structure is much smaller than that of the single-layer PVA:Co_3O_4 film, although the two samples have nearly the same amount of PVA:Co_3O_4. Nevertheless, the linear transmission of the 12-layer PBG is still larger than 45% over the entire visible. For the 24-layer PBG structure, the linear transmission is larger than 30% over the visible, and due to deviations in the layer thickness and the imperfectly matched linear refractive indices, there is a small band gap forming around 560 nm as shown by a local minimum in the transmission spectrum.
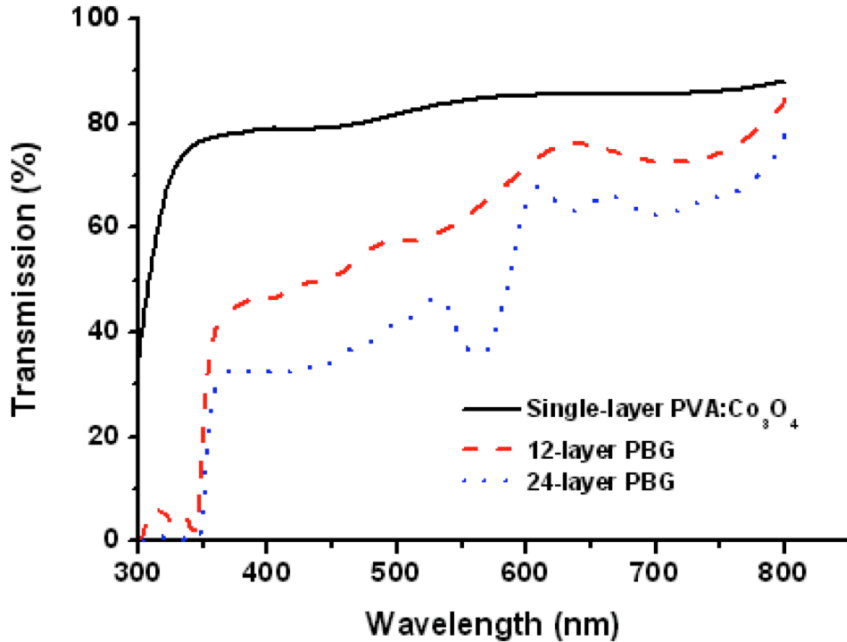
Figure 29. Linear transmission for single layer PVA/Co$_3$O$_4$ composite, 12 layer PBG and 24 layer PBG

The nonlinear transmission and reflection were measured using a frequency-doubled Q-switched Nd:YLF laser (TFR 523Q, Spectra-Physics) that has a wavelength of 523.5 nm and a pulse width of about 10 ns. Two polarizers were used to adjust the input energy. The laser beam was focused on the sample with a 5 cm focal length lens. The transmitted beam, the reflected beam, and a reference beam were measured with high-speed silicon detectors (DET10A, Thorlabs). Our initial experiments on these PBG devices focused on measuring only the nonlinear transmission, but the observation of increased reflection as the cause for reduced transmission is a true indication that the device is working principally as designed. Figure 5 shows that the actual situation is a bit more complicated than the design. At low fluences, less than 30 mJ/cm^2 for the 24 layer device and less than 80 mJ/cm^2 for the 12 layer device, there is indeed an increase in the reflection from the low intensity value. Above these fluences, there is a sudden drop in the relative reflection coefficient, indicative of either a better refractive index match or increased absorption. The measurements on the single layer PVA/Co$_3$O$_4$ film in fact shows that the system does exhibit nonlinear absorption at high fluences, suggesting that the cause for the change in behavior of the reflection coefficient is the onset of NLA. We have hypothesized that, in fact, the observed behavior comes from the presence of two distinct forms of cobalt oxide in the composite that have different optical properties. Furthermore, we speculate that there is an optically induced transition from one state to the other. Nonlinear spectroscopy at nanosecond time scales is needed to further elucidate the behavior of this intriguing composite.

Figure 30. Relative reflection of single layer film, 12-layer PBG, and 24-layer PBG as function of fluence
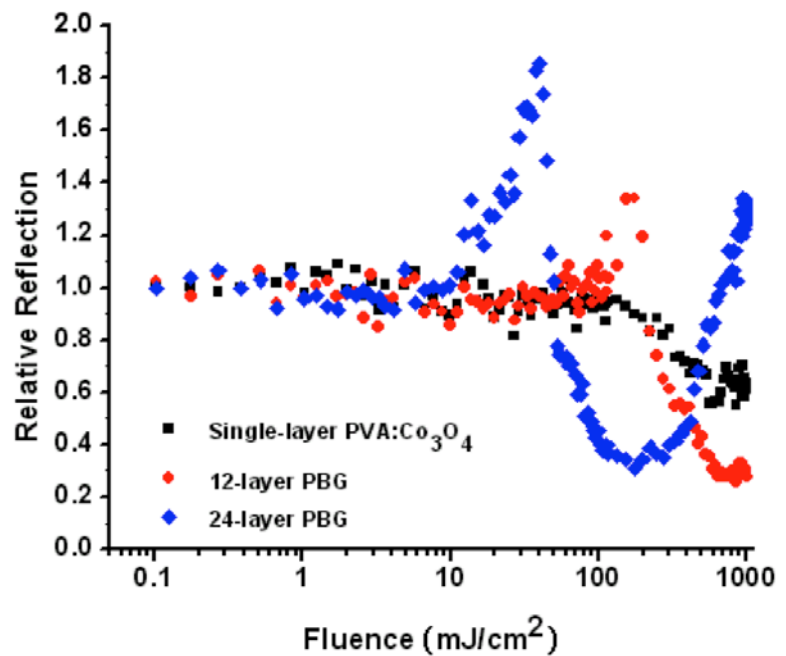
Fibonacci mirrors for multiple window Fabry-Perot devices

Our initial development of a new approach to nonlinear devices based on Fibonacci structures was reported last year. The long-term goal is to fabricate Fibonacci mirrors that incorporate a nonlinear material as one of the mirror layers. By making two identical nonlinear Fibonacci mirrors, it is then possible to make an air space etalon that will exhibit broadband optical limiting if the material nonlinear material used has a sufficiently large refractive nonlinearity. Since this is quite challenging fabrication, we have now focused on an initial demonstration Fibonacci device that is based on two linear Fibonacci mirrors that constitute an etalon that is filled with an appropriate nonlinear material (Figure 31). Figure 32 shows the modeled performance of the multiple window Fibonacci mirror that we have recently fabricated. Candidate nonlinear materials included relatively broadband two-photon absorbers (TPD, BDPAS,..) and reverse saturable absorbers (e.g., ZnPc).
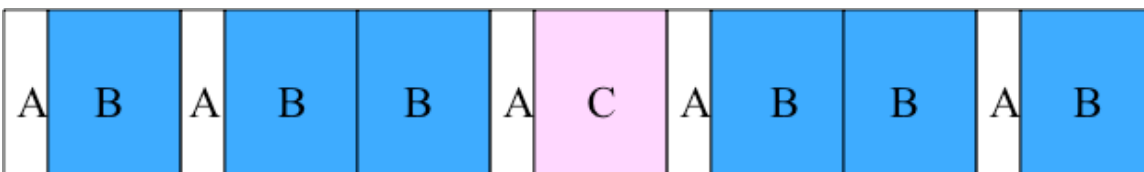

**Figure 31.** Fibonacci etalon surrounding a nonlinear material (C)

75
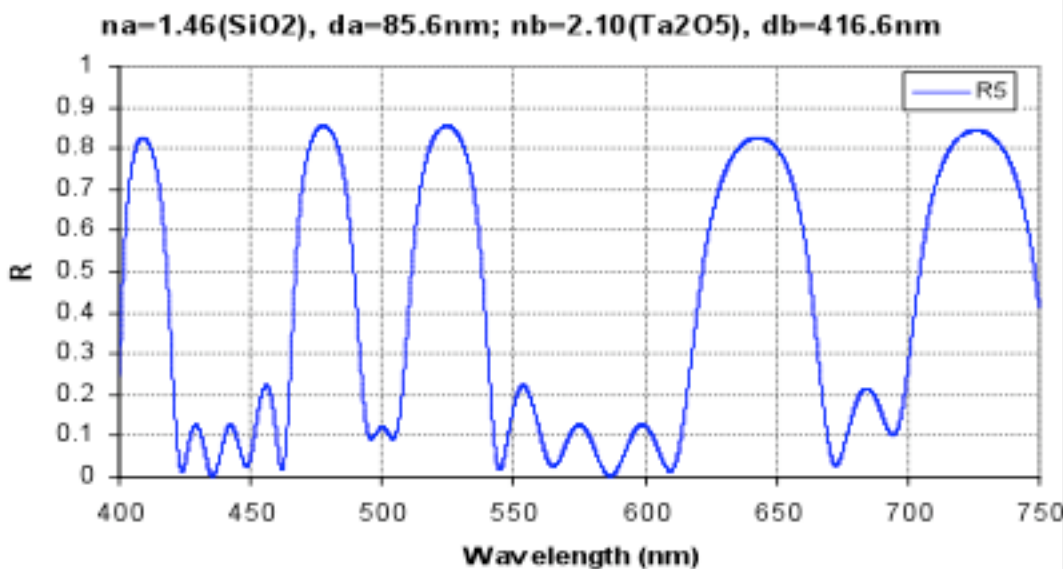
Figure 32. Designed spectral performance of multiple window Fibonacci mirror

Linear and nonlinear optical properties of the Co_3O_4 composite

We have shown that polymer/Co_3O_4 nanocomposites have compelling optical limiting properties in the 400-700nm range for nanosecond pulses and we performed experiments to further study these materials. In our experiments, mixtures of the commercial optical polymer polyvinyl alcohol (PVA) and Co_3O_4 nanoparticles (American Elements) were first made with a volume ratio of approximately 9:1. Three PVA:Co_3O_4 thin films with thicknesses of 500 nm, 570 nm, and 720 nm were then fabricated from the mixture by spin coating. A PVA thin film with a thickness of 500 nm was also fabricated as a reference. Linear transmission of these thin films was measured with a Cary 5000 UV-Vis-IR (Varian, Inc.). In Fig. 33, the transmission spectra of the four thin films are plotted in a wavelength range of 350 – 800 nm. Clearly, the PVA:Co_3O_4 films have two absorption bands centered at 420 nm and 740 nm. The absorption coefficient of the composite (shown by the magenta short dashed curve) is obtained by averaging the absorption coefficients of the three PVA:Co_3O_4 films. Based on the absorption coefficient of the PVA:Co_3O_4 film, the band gap energy can be obtained from the plot of $(\alpha h\nu)^2$ versus photon energy ($h\nu$) shown in Fig. 2 by using the relation $(\alpha h\nu)^2 = c(h\nu - E_g)$, where α is the absorption coefficient, $h\nu$ is the photon energy, c is a constant, and E_g is the band gap energy. Direct band gaps of 1.38 eV and 2.0 eV were obtained by fitting the linear regions of the curve shown in Fig. 34. The first band gap is assigned to the charge transfer process $Co^{3+}(\pi t_2) \rightarrow Co^{2+}(\sigma^* t_2)$ and the second one is $O(\pi^* \Gamma) \rightarrow Co^{2+}(\sigma^* t_2)$.
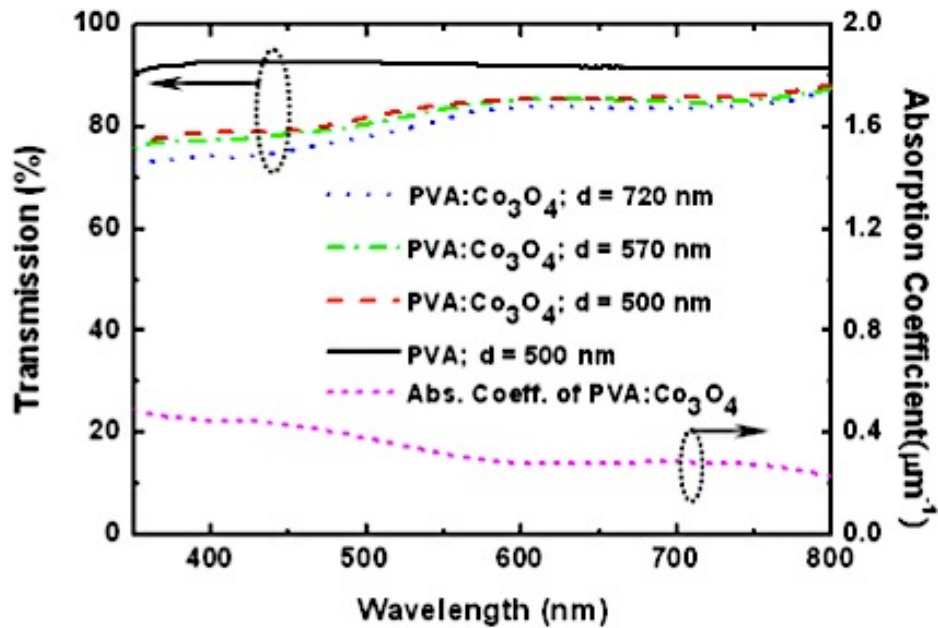
Fig. 33. The transmission spectra of the PVA (black solid curve) and the three PVA:Co$_3$O$_4$ films [d = 500 nm, (red curve); d = 570 nm (green curve); d = 720 nm (blue curve)] and the absorption coefficient of PVA:Co$_3$O$_4$ composite (magenta short dashed curve).

For the measurement of the refractive index of the composite, a thin film with a thickness of about 60 nm was prepared on silicon substrate. The refractive indices of the composite and the PVA were measured by spectroscopic ellipsometry (SopraLab) and are shown in Fig. 34. The refractive index of thicker films of the composite measured by the technique of prism coupling is also included in Fig. 35. The refractive index of the composite is much larger than that of the PVA in the wavelength range of 400 nm – 800 nm due to the large index of Co$_3$O$_4$.
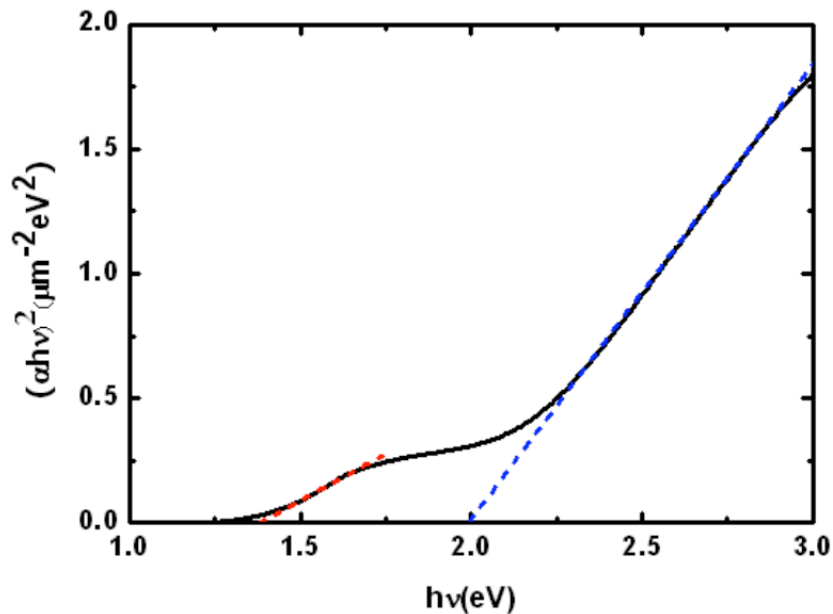

Fig. 34. Plot of $(\alpha h\nu)^2$ versus photon energy ($h\nu$) for the PVA:Co3O4 film. Band gaps of 1.38 eV and 2.0 eV are estimated by fitting the linear regions of the curve.
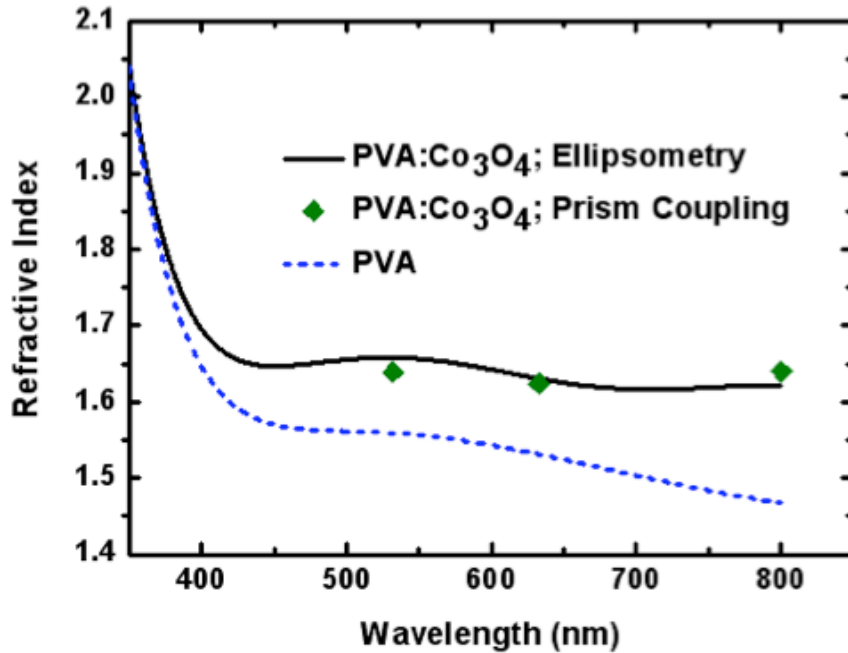
Fig. 35. Refractive indices of the PVA (blue dashed curve) and PVA:Co_3O_4 films (black solid cure) obtained by ellipsometric measurement. Diamonds show results measured by the technique of prism coupling at wavelengths of 532 nm, 632.8 nm, and 800 nm.

.

The nonlinear transmission characteristics of the three PVA:Co_3O_4 films were measured with the experimental setup shown as an inset in Fig. 36. The laser source was a frequency-doubled Q-switched Nd:YLF laser (TFR 523Q, Spectra-Physics) that has a wavelength of 523.5 nm and a pulse width of about 10 ns. Two polarizers were used to adjust the input energy. The laser beam was focused on the sample with a 5 cm focal length lens, while the transmitted beam and a reference beam were measured with high-speed silicon detectors (DET10A, Thorlabs). The nonlinear transmissions of the three samples as a function of the illuminating fluence are plotted in Fig. 36; the transmission of the PVA:Co_3O_4 films decreases with the increasing laser intensity and reaches a minimum value at an illuminating fluence of about 600 mJ/cm^2. The transmission then increases with illuminating fluence at higher light intensities due to saturable absorption of Co_3O_4 caused by the band filling effect. The reverse-saturable absorption of the single-layer PVA: Co_3O_4 film at moderate light intensities may due to two-photon absorption or other charge transfer processes. The distinct performances may be ascribed to the different response times and nonlinearities of the two nonlinear processes occurring in the Co_3O_4 material. Saturable absorption is a slow process and the reversed-saturable absorption is a fast process. When the pulse duration is 100 nsec, saturable absorption is dominant, while reverse saturable absorption is more dominant when the pulse duration is 35 ps. In our experiment, reverse saturable absorption occurs first because the threshold of the reversed saturable absorption is smaller than that of the saturable absorption when the pulse duration is 10 ns. However, the magnitude of the saturable absorption is much larger than that of the reverse saturable absorption. Therefore, the absorption decreases with increasing fluence for fluences larger than 600 mJ/cm^2.

78
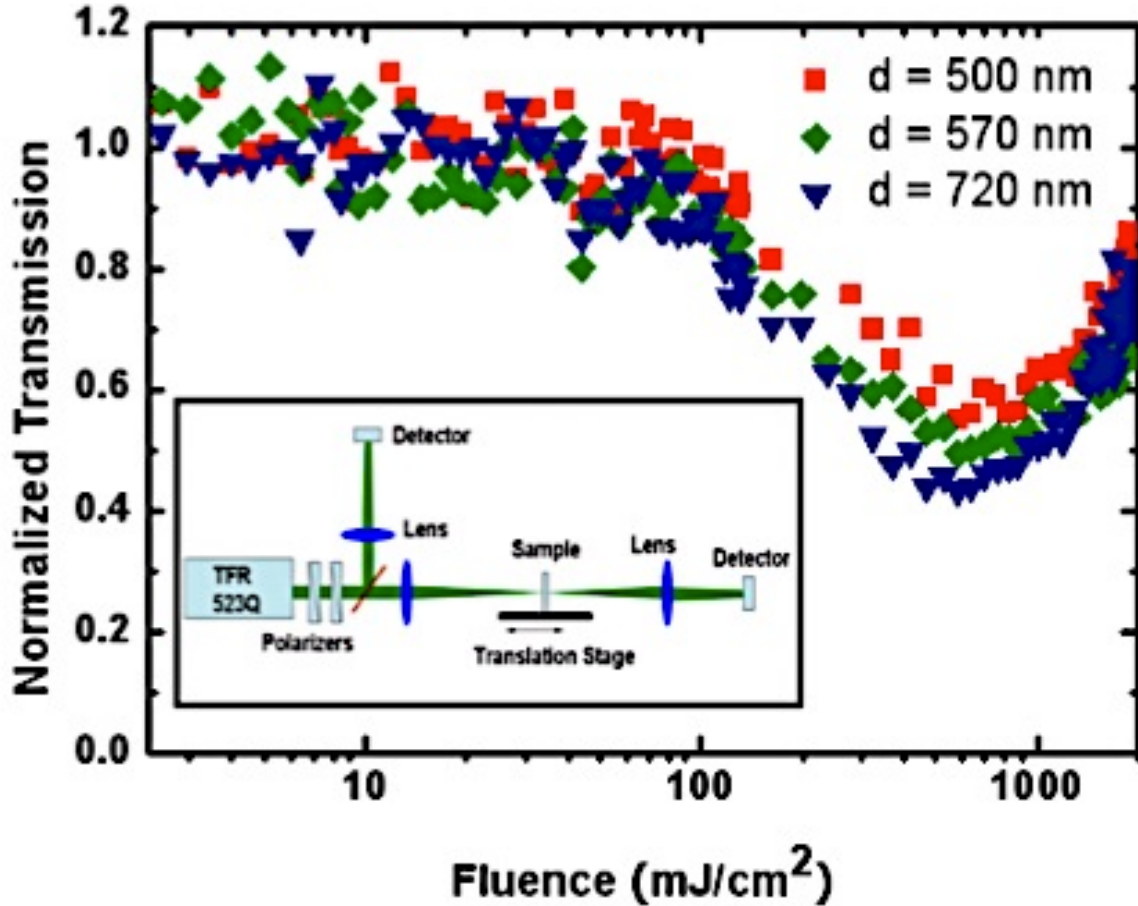
Fig. 36. Nonlinear transmission of the three PVA:Co$_3$O$_4$ films. Thickness d = 500 nm (red squares); thickness d = 570 nm (green diamonds); thickness d = 720 nm (blue triangles). Inset shows the experimental setup.

In order to evaluate the nonlinearity of the reverse saturable absorption, a Z-scan measurement was conducted on the setup (inset in Fig. 36) with a fluence of 500 mJ/cm^2. Open aperture and the closed aperture Z-scan measurement results are shown in Fig. 37(a) and (b), respectively. Using the method of Gaussian decomposition, we can determine the nonlinear absorption coefficient (β) and the nonlinear refractive index (n_2) by fitting the experimental results shown in Fig. 5. A nonlinear absorption coefficient $\beta = 6.2 \times 10^{-5}$ cm/W and the nonlinear refractive index $n_2 = -1.08 \times 10^{-9}$ cm^2/W are obtained. Clearly the optical and nonlinear optical properties of the composite can be further tailored by simply changing the volume fraction of cobalt oxide, providing a pathway to fabricate materials with desired linear and nonlinear properties. Such control of optical properties is essential for nanophotonics and nanoelectronics applications.
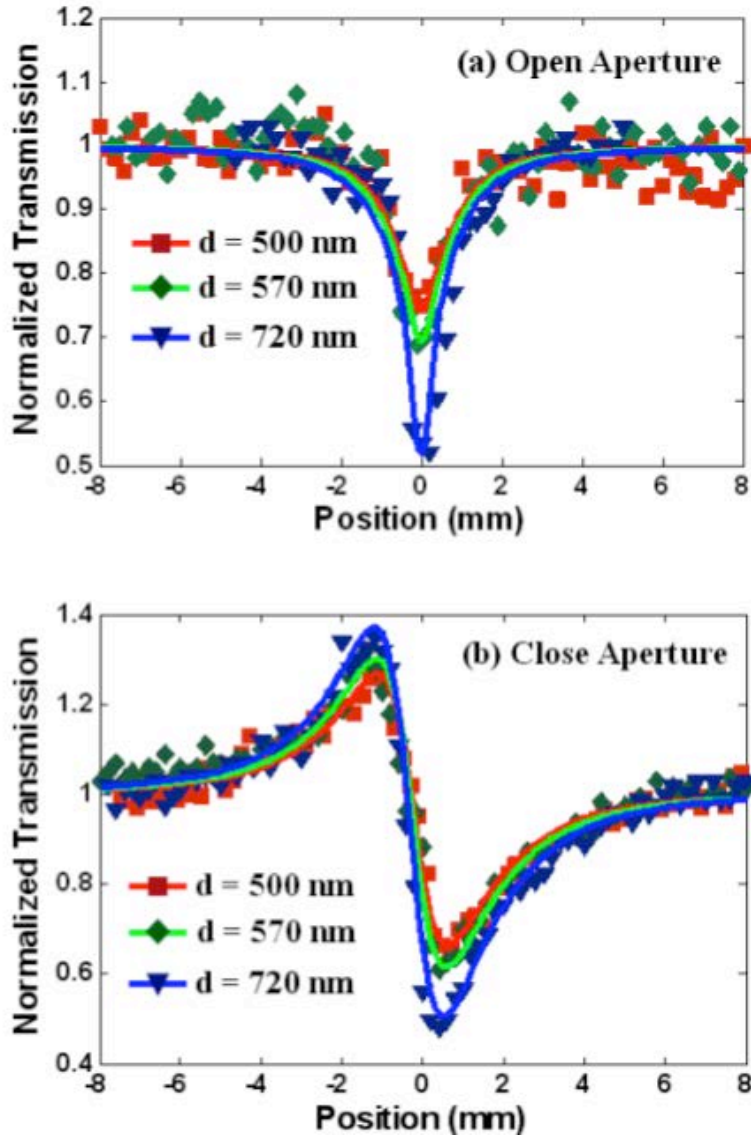
Fig. 37. (a) Open aperture and (b)close aperture Z-scan measurement results of the three PVA:Co$_3$O$_4$ films. Thickness d = 500 nm (red curve and squares); thickness d = 570 nm (green curve and diamonds); thickness d = 720 nm (blue curve and triangles).

Thue-Morse mirrors for multiple window Fabry-Perot devices

Throughout the program we have experimented with new multilayer structures for simultaneously achieving resonant behavior and broadband coverage through multiple window operation. The Fibonacci mirror and etalon device is one notable development that has been reported in previous years and has been the subject of several publications and presentations. In the past year we have investigated the properties of a new multiple window mirror system, based on the Thue-Morse sequence as opposed to the Fibonacci sequence.   Figure 38 shows the S_4

Thue-Morse sequence for two materials, *A* and *B,* where the two materials generally have a big difference in index, such as silica (1.45) and tantalum pentoxide (2.1). Each "sub-layer" in the Thue-Morse sequence is either a quarter-wave thick (material A) or a multiple *m* of the quarter-wave thickness (material B), so that we can fully describe a Thue-Morse mirror with the nomenclature $S_n(1,m)$ where *n* is the level of the Thue-Morse sequence. Figure 39 shows the reflection and transmission of a $S_4(1,4)$ Thue-Morse mirror where we see that multiple windows with moderate reflectivities are obtained. An advantage of the Thue-Morse approach is that the overall device thickness required for a given number of windows and reflectivity is reduced compared to the equivalent Fibonacci device.
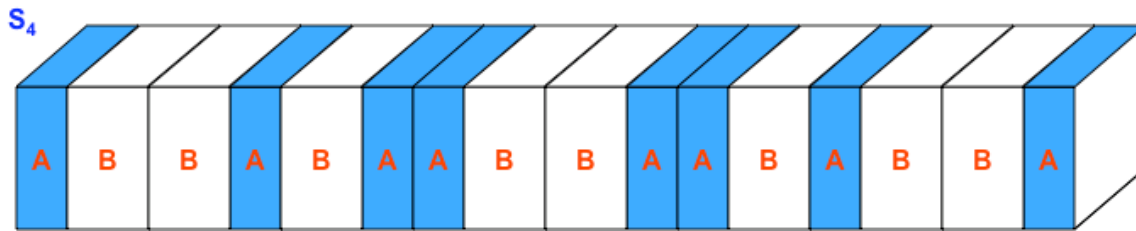

**Figure 38.** Thue-Morse mirror sequence for S_4 sequence device
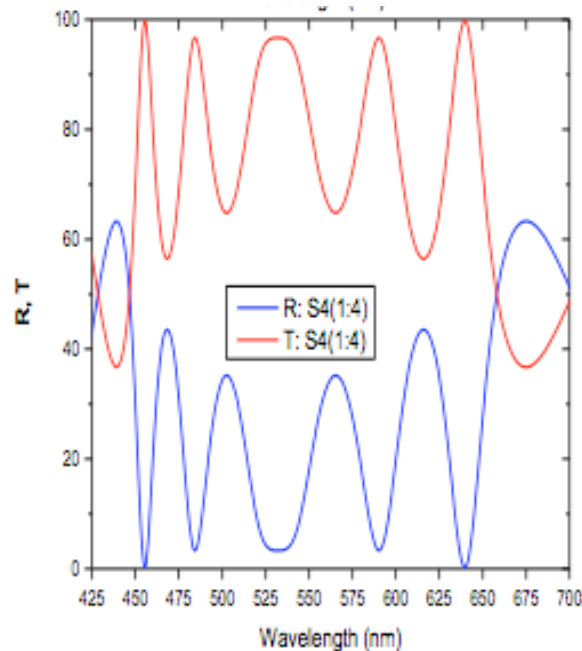
Figure 39. Designed spectral performance of $S_4(1,4)$ Thue-Morse mirror

Publications

- D. T. Nguyen, C. Sheng, J. Thomas, R. Norwood, B. Kimball, D. M.. Steeves, and N. Peyghambarian, "Observation of nonlinear transmission enhancement in cavities filled with nonlinear organic materials," *Applied Optics* **47**, 5777 (2008).
- C. Sheng, R. A. Norwood, J. Wang, J. Thomas, Y. Wu, Z. Zheng, N. Tabirian, D. M. Steeves, B. R. Kimball, and N. Peyghambarian, " Time resolved studies of photoinduced birefringence in azobenzene dye doped polymer films," *Applied Optics* **47**, 5074 (2008).
- X. Zhu, J. Wang, P. Lau, D. Nguyen, R. A. Norwood, and N. Peyghambarian, "Nonlinear optical performance of periodic structures made from composites of polymers and Co_3O_4 nanoparticles," *Appl. Phys. Lett.* **97**, 093503 (2010).
- D. T. Nguyen, R. A. Norwood, and N. Peyghambarian, "Multiple spectral window mirrors based on Fibonacci chains of dielectric layers," *Opt. Comm.* **283**, 4199 (2010).
- Y. Wu, J. Wang, X. Kong, C. Sheng, R. Wang, N. Peyghambarian, R. A. Norwood, and Z. Zheng, "A dinuclear europium(III) complex with thenoyltrifluoroacetonato and 1-(2-pyriylzao)-2-naphtholato ligands and its optical properties," *Inorganic Chimica Acta* **370**, 346 (2011).
- C. Sheng, Q. Chen, R. A. Norwood, J. Wang, J. Thomas, and N. Peyghambarian, "Simple way for achieving passive all-optical switching for continuous wave lasers using pure nematic liquid crystal," *Appl. Optics* **50**, 5788 (2011).
- X. Zhu, J. Wang, D. Nguyen, J. Thomas, R. A. Norwood, and N. Peyghambarian, "Linear and nonlinear optical properties of Co_3O_4 nanoparticle-doped polyvinyl-alcohol thin films," *Optical Materials Express* **2**, 103 (2012).

Presentations

- J. Wang, X. Tu, Z. Zheng, R. Norwood, D. Steeves, B. Kimball and N. Peyghambarian, "Novel nonlinear transmission of porphyrin complexes containing rhenium selenide clusters," presented at *SPIE Photonics West 2010* (January 23-28, 2010, San Francisco, CA).
- X. Zhu, J. Wang, P. Lau, D. Nguyen, R. A. Norwood, D. Steeves, B. Kimball, and N. Peyghambarian, "Nonlinear transmission using highly nonlinear Bragg mirrors," presented at *SPIE Photonics West 2010* (January 23-28, 2010, San Francisco, CA).
- D. T. Nguyen, R. A. Norwood, and N. Peyghambarian, "Multiple photonic band gaps in 1d Fibonacci system," *Integrated Photonics Research OSA Topical Meeting* (July 25-29, 2010, Monterey, CA).
- D. T. Nguyen, R. A. Norwood, and N. Peyghambarian, "Multiple spectral window mirrors based on Fibonacci chains of dielectric layers and applications," *Proc. SPIE* **7781**, 77810B-1 (2010).
- R. A. Norwood, "Hybrid polymer optical materials and devices: The best of both worlds," invited talk at *SPIE Photonics West* (January 23 – 28, 2011, San Francisco, CA).

Plasmonic Nanoantenna Arrays for Enhanced Nonlinear Absorption

<u>Goals:</u>
- Develop nanoantennae arrays for enhanced nonlinear absorption

The major task of this effort was to optimize plasmonic nanoantennae appropriate for enhanced nonlinear absorption of the selected molecules.

The main results include:
- the measurements of the dielectric function of metal in the nanostructure like nano-antennas, which is typically very different from bulk values;
- an annealing, improving the resonance quality of the nanoantennas, is shown to be a particle-shape dependent;
- methods of the nano-antennas modeling have been developed taking into account a real sample roughness as well as the methods of the dyes modeling;
- enhanced nonlinear absorption by gold nanoantennas have been demonstrated with an exemplary 2P commercial absorber BDPAS, and synthesized by Georgia Tech group.

The results have been published in the following papers. Section 5 and 6 present the results on the enhancement effect of gold nanoantennas on the nonlinear absorption of the selected molecules. The manuscript preparation is in progress.

1. Kildishev, A.V.; Borneman, J.D.; Chen, K.-P.; Drachev, V.P. Numerical Modeling of Plasmonic Nanoantennas with Realistic 3D Roughness and Distortion. Sensors 2011, 11, 7178-7187.
Nanostructured plasmonic metamaterials, including optical nanoantenna arrays, are important for advanced optical sensing and imaging applications including surface-enhanced fluorescence, chemiluminescence, and Raman scattering. Although designs typically use ideally smooth geometries, realistic nanoantennas have nonzero roughness, which typically results in a modified enhancement factor that should be involved in their design. Herein we aim to treat roughness by introducing a realistic roughened geometry into the finite element (FE) model. Even if the roughness does not result in significant loss, it does result in a spectral shift and inhomogeneous broadening of the resonance, which could be critical when fitting the FE simulations of plasmonic nanoantennas to experiments. Moreover, the proposed approach could be applied to any model, whether mechanical, acoustic, electromagnetic, thermal, etc, in order to simulate a given roughness-generated physical phenomenon.

2. M. D. Thoreson, J. Fang, A. V. Kildishev, L. J. Prokopeva, P. Nyga, U. K. Chettiar, V. M. Shalaev, and V. P. Drachev, "Fabrication and realistic modeling of three-dimensional metal-dielectric composites," J. Nanophoton. 5, 051513 (May 23, 2011); doi:10.1117/1.3590208
Historically, the methods used to describe the electromagnetic response of random, three-dimensional (3D), metal-dielectric composites (MDCs) have been limited to approximations

such as effective-medium theories that employ easily-obtained, macroscopic parameters. Full-wave numerical simulations such as finite-difference time domain (FDTD) calculations are difficult for random MDCs due to the fact that the nanoscale geometry of a random composite is generally difficult to ascertain after fabrication. We have developed a fabrication method for creating semicontinuous metal films with arbitrary thicknesses and a modeling technique for such films using realistic geometries. We extended our two-dimensional simulation method to obtain realistic geometries of 3D MDC samples, and we obtained the detailed near- and far-field electromagnetic responses of such composites using FDTD calculations. Our simulation results agree quantitatively well with the experimentally measured far-field spectra of the real samples.

3. K.P. Chen, V.P. Drachev, J.D. Borneman, A.V. Kildishev, and V.M. Shalaev, "Drude relaxation rate in grained gold nanoantennas," Nano Letters 10, 916-922 (2010).
We study the effect of grain boundaries on the electron relaxation rate, which is significant even for large area noble metal films and more so for plasmonic nanostructures. Optical spectroscopy and X-ray diffraction show a substantial improvement in plasmon resonance quality for square-particle nanoantennas after annealing due to an enlarged grain size from 22 to 40 nm and improved grain boundaries described by the electron reflection coefficient. The electron relaxation rate due to the grains is shown to decrease by a factor of 3.2.

4. J. Trieschmann,, S. Xiao, L. J. Prokopeva, V. P. Drachev, and A. V. Kildishev, "Experimental retrieval of the kinetic parameters of a dye in a solid film," Optics Express 19, 18253-18259 (2011).
Effects of a solid matrix on the dye kinetic parameters for Rh800 were experimentally studied. Saturation intensity dependencies were measured with a seeding pulse amplification method using a picosecond and a femtosecond white light super-continuum source. The kinetic parameters were obtained by fitting experimental dependencies with Yee's finite difference time-domain model coupled to the rate equations of the 4-level Rh800-system. The comparison of these parameters (Rh800-solid host) with liquid host parameters revealed a and a strong change of the non-radiative decay rate. This experimentally determined model enables predictive simulations of time-domain responses of active metamaterials.

5. V. Drachev, A. Kildishev, J. Borneman, K-P. Chen, V. Shalaev, N. Peyghambarian, R. Norwood, K. Yamnitskiy , S. Marder, D. Hagan, S. Webster, L. Padilha, and E. Van Stryland, "Engineered nonlinear materials using gold nanoantenna array" (in progress)
The effective third order susceptibility of a metal dielectric composite, in the simplest case, is a product of two complex values: the enhancement factor and the third order susceptibility of the component materials, which are both wavelength dependent. Therefore, one can engineer an effective nonlinear material by matching the nanoantenna resonance and the wavelength dependence of the susceptibility. In this section we describe the use of a gold nanoantenna array

to enhance both the nonlinear refractive index (n_2) and 2PA of the organic dye 4,4'-bis(diphenylamino)stilbene (BDPAS), which is known as a dye with a relatively large 2PA known from the literature. Experimental results show a 40× enhancement for the effective nonlinear absorption of the composite layer at 600 nm, as supported by 3D finite element method (FEM) numerical simulations.

BDPAS has a strong one-photon absorption cross-section, $2.02 \times 10^{-16} \text{cm}^2$, at 390 nm, and negligible linear absorption in the visible. BDPAS has 42 pi-conjugated bonds and exhibits

strong 2PA from 600 nm to 800 nm, with a peak 2PA cross section of δ=320 GM ($1 \, \text{GM} = 10^{-50} \, \text{cm}^4 \text{s/photon}$) in dichloromethane (DCM) at 670 nm. The dimensions of the gold nanoantennas shown in Fig. 5.1(a) were designed so that the resonance wavelength (λ_r) is close to the 2PA cross section peak of BDPAS.
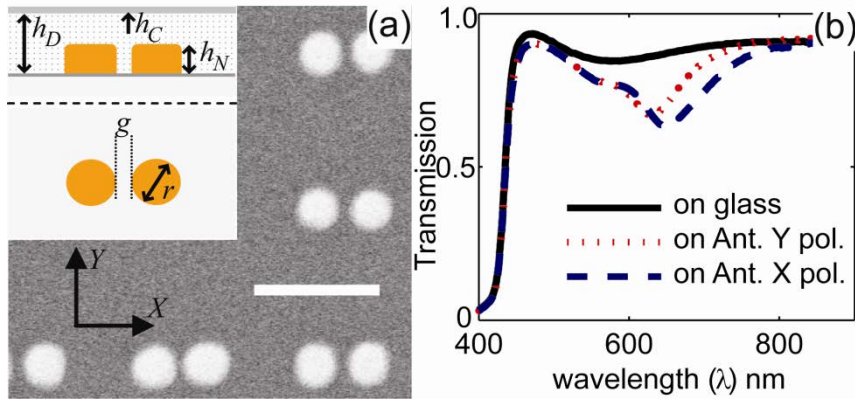

Fig.5.1 (a) A schematic, $h_D, h_N, h_C, g, r = 175, 60, 20, 14, 66$ nm respectively, and SEM image of the gold nanoantenna structure. (scale bar = 200 nm); (b) Experimental transmission spectra of 175 nm thick BDPAS film on and off the gold nanoantenna arrays.
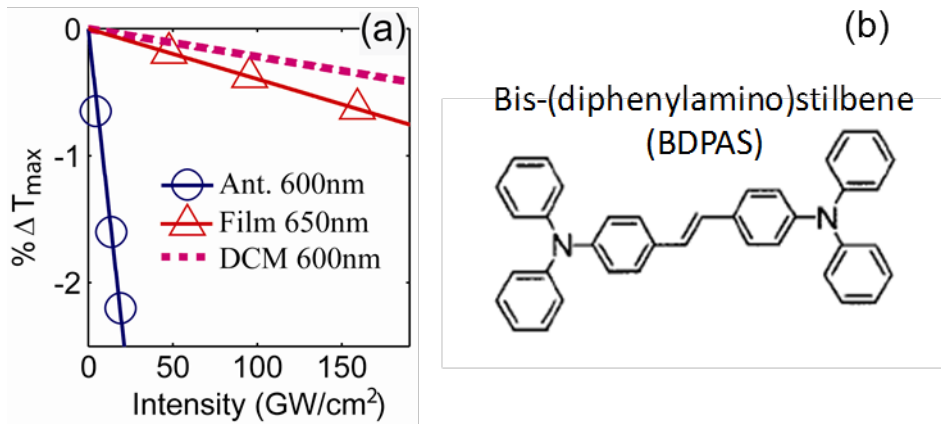

Fig.5.2. (a) %ΔT from Z-scans vs. incident intensity for BDPAS with nanoantennas, BDPAS film, and BDPAS solution with exponential fit lines; (b) BDPAS chemical structure.

Our FEM simulations show that the only thin layer near the nanoantennas has an enhanced nonlinear absorption. Figure 5.3 shows that the nonlinear changes in the reflection, transmission, absorption grow with the thickness of the nonlinear layer and then this dependence is saturated. The most significant grows is observed up to the thickness of about 60 nm, which corresponds to the nanoantennas height.
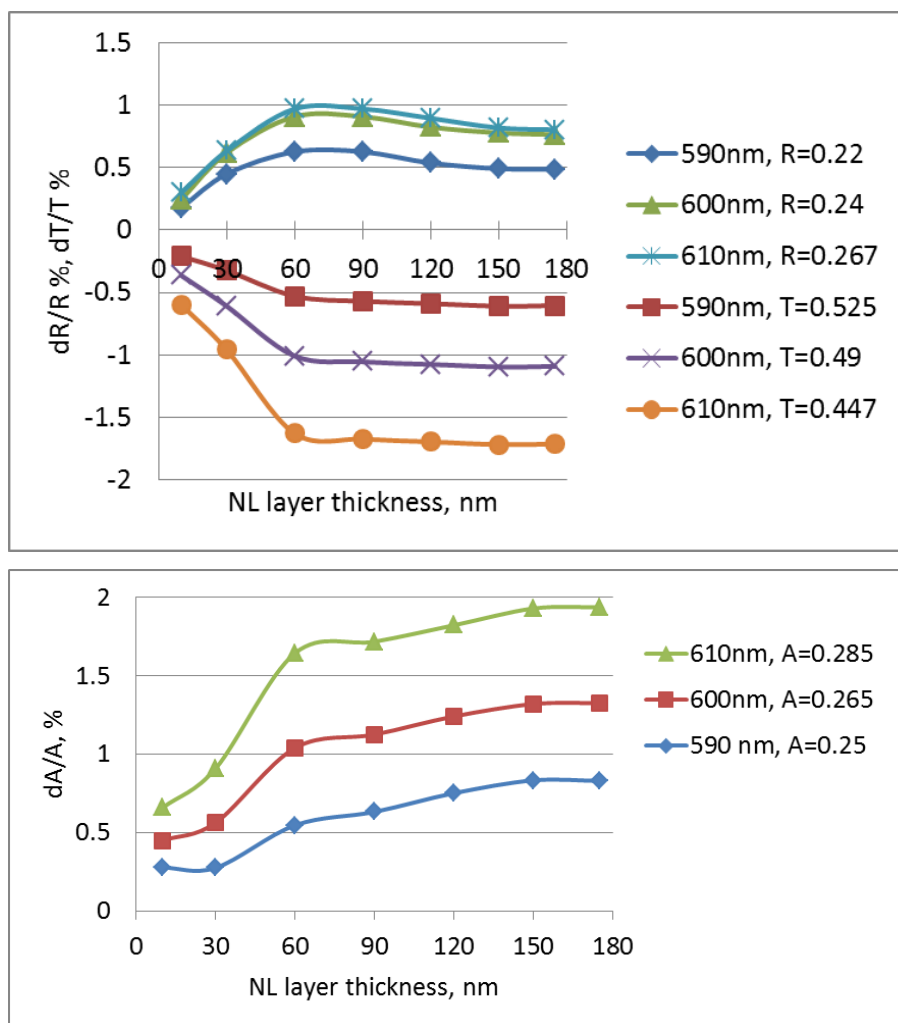
Fig. 5.3 Relative nonlinear changes (%) in transmission (dT/T), reflection (dR/R) (upper panel), and absorption (dA/A) at three wavelengths 610, 600, 590 nm; the linear values of T,R,A are shown in the legends as a fraction of unity.

6. The nanoantenna array effect on the nonlinear absorption of about factor 22-40 was demonstrated also in our experiments for GW-I-119B (Structure-Property Relationships for Two-Photon Absorbing Chromophores: Bis-Donor Diphenylpolyene and Bis(styryl)benzene Derivatives *J. Am. Chem. Soc.* 2000, 122, 9500-9510) provided by S. Marder group. The main advantages of this 2PA absorber is a good quality of the coated films as well as 2PA maximum is at 770 nm, which should match better to the nanoantenna resonance in our system. A relatively thick molecular layer (about 1.5 µm) was spin coated on the nanoantennas. Figure 6.1 shows the structural formula and transmission spectrum of the molecules.
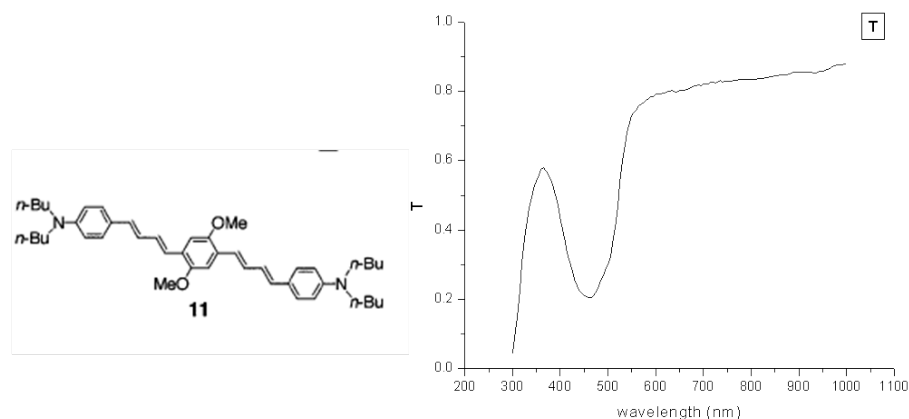
Fig. 6.1. The structure and transmission spectrum of the GW-I-119B.
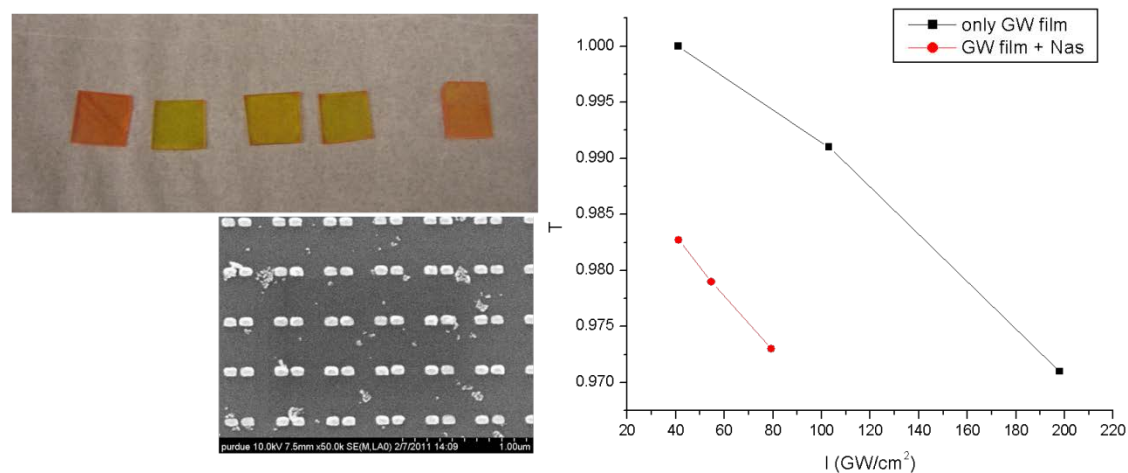
Fig. 6.2. Coated films of GW with different thickness (upper left), scanning electron microscopy image (SEM) 2.4x1.7 µm of the nanoantennas (bottom left), and intensity dependence of the transmission for GW film and GW film with nanoantennas made on the same substrate.

Figure 6.2 illustrates a good quality of the molecular films and the geometry of the Au nanoantennas. It shows also an enhancement in two-photon absorption by factor 2.5 due to nanoantennas even though only a very thin layer of 2PA near the nanoantennas can be involved in the enhancement. The upper bound of the thickness involved in the enhancement is about 60-100 nm as it can be estimated from the calculated thickness dependence. This gives an enhancement due to the nanoantennas array is about factor 22-40 in this case.